



January 2017

Lightcurve Study Of V-Type Asteroids

Matt Nowinski

Follow this and additional works at: <https://commons.und.edu/theses>

Recommended Citation

Nowinski, Matt, "Lightcurve Study Of V-Type Asteroids" (2017). *Theses and Dissertations*. 2301.
<https://commons.und.edu/theses/2301>

This Thesis is brought to you for free and open access by the Theses, Dissertations, and Senior Projects at UND Scholarly Commons. It has been accepted for inclusion in Theses and Dissertations by an authorized administrator of UND Scholarly Commons. For more information, please contact zeinebyousif@library.und.edu.

LIGHTCURVE STUDY OF V-TYPE ASTEROIDS

by

Matthew Clarke Nowinski
B.S. Aerospace Engineering, Virginia Tech, 1991
M.S. Mechanical Engineering, Virginia Tech, 1993
Ph.D. Mechanical Engineering, EPFL, 1999

A Thesis

Submitted to the Graduate Faculty

of the

University of North Dakota

in partial fulfillment of the requirements

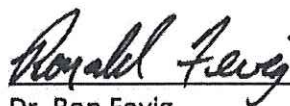
for the degree of

Master of Science

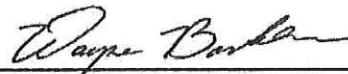
Grand Forks, North Dakota

December
2017

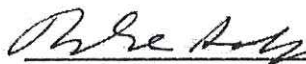
This thesis, submitted by Matt Nowinski in partial fulfillment of the requirements for the Degree of Master of Science from the University of North Dakota, has been read by the Faculty Advisory Committee under whom the work has been done and is hereby approved.



Dr. Ron Fevig



Dr. Wayne Barkhouse



Dr. Mike Gaffey



Dr. Paul Hardersen



Dr. Vishnu Reddy

This thesis meets the standards for appearance, conforms to the style and format requirements of the Graduate School of the University of North Dakota, and is hereby approved.



Dr. Grant McGimpsey
Dean of the School of Graduate Studies



Date

PERMISSION

Title: Lightcurve Study Of V-Type Asteroids

Department: Space Studies

Degree: Master of Science

In presenting this thesis in partial fulfillment of the requirements for a graduate degree from the University of North Dakota, I agree that the library of this University shall make it freely available for inspection. I further agree that permission for extensive copying for scholarly purposes may be granted by the professor who supervised my thesis work or in his absence, by the chairperson of the department or the dean of Graduate School. It is understood that any copying or publication or other use of this thesis or part thereof for financial gain shall not be allowed without my written permission. It is also understood that due recognition shall be given to me and to the University of North Dakota in any scholarly use which may be made of any material in my thesis.

Matt Nowinski
November 28, 2017

TABLE OF CONTENTS

LIST OF FIGURES.....	VII
LIST OF TABLES	X
ACKNOWLEDGEMENTS	XI
ABSTRACT.....	XIII
CHAPTER 1 INTRODUCTION	14
1.1 Asteroids.....	19
1.1.1 Vesta.....	24
1.2 Meteorites.....	25
1.2.1 HED Meteorites	27
1.3 Taxonomy.....	28
1.3.1 V-Type Taxonomy.....	30
1.4 Dynamics	33
1.4.1 Collisions and Asteroid Families.....	33
1.4.2 Resonances.....	35
1.4.3 Yarkovsky/YORP Effects.....	38
1.4.4 Rotation	42
1.4.5 Vesta Dynamical family (the “Vestoids”)	43
1.5 Current Study	44
CHAPTER 2 ASTEROID ROTATION AND LIGHTCURVES	46

2.1	Rotation	47
2.1.1	Principal Axis Rotation.....	48
2.1.2	Rotation Measurement	51
2.2	Lightcurve Photometry.....	51
2.2.1	Lightcurve Database (LCDB)	53
2.3	Asteroid Population.....	54
2.3.1	Spin Barrier	54
2.3.2	Maxwellian Distribution	57
2.4	Rotational Studies of Asteroid Families	60
CHAPTER 3 MEASUREMENTS AND DATA REDUCTION		63
3.1	Asteroid Observations.....	63
3.1.1	Telescopes	64
3.1.2	Target Selection.....	67
3.1.3	Observation Strategy.....	68
3.2	Data Reduction	72
3.2.1	Calibration	73
3.2.2	Plate-Solving (WCS)	74
3.2.3	Photometry.....	75
3.2.4	MPO Canopus.....	79
CHAPTER 4 RESULTS AND ANALYSIS		82
4.1	Target Asteroids	82
4.2	Asteroid Lightcurve Measurements.....	86

4.2.1 (3648) Raffinetti	87
4.2.2 (5235) Jean-Loup	88
4.2.3 (9223) Leifandersson	91
4.2.4 (11699) 1998 FL105	93
4.2.5 (12073) Larimer	94
4.2.6 (15121) 2000 EN14	95
4.2.7 (16452) Goldfinger	98
4.2.8 (20557) Davidkulka	99
4.2.9 (29796) 1999 CW	100
4.2.10 (35821) 1999 JW50	102
4.3 Rotational Characteristics of V/V _p -type Asteroids	104
4.3.1 Lightcurve Period vs. Diameter	107
4.3.2 Lightcurve Amplitude vs. Spin Rate	109
4.3.3 Maxwellian Distributions	111
CHAPTER 5 SUMMARY AND CONCLUSIONS	116
REFERENCES	121

LIST OF FIGURES

Figure 1. Pyramid Model of Planetary Exploration.....	15
Figure 2. Distribution of Minor Planets: Semimajor Axis	20
Figure 3. Distribution of Minor Planets: e vs. i	21
Figure 4. Cumulative Raw Size-Frequency Distribution of Asteroids	22
Figure 5. Heliocentric Distribution of Asteroid Types (Simplified)	23
Figure 6. Heliocentric Distribution of Asteroid Types.....	24
Figure 7. V_p -Type Asteroid Radial Distribution	32
Figure 8. Dynamic Asteroid Families.....	35
Figure 9. The Kirkwood Gaps	36
Figure 10. Diurnal Yarkovsky Effect	40
Figure 11. Yarkovsky Seasonal Effect.....	41
Figure 12. Vesta Dynamical family of Asteroids	44
Figure 13. Non-Principal-Axis Rotation of (4179) Toutatis.....	49
Figure 14. Principal Axis Rotation of a Typical Triaxial Ellipsoid-Shaped Asteroid	50
Figure 15. (25143) Itokawa Lightcurve	53
Figure 16. Asteroid Rotational Period vs. Diameter	56
Figure 17. Asteroid Lightcurve Amplitude vs. Rotational Period.....	57
Figure 18. Asteroid Spin Distribution (MB and NEA)	59

Figure 19. Asteroid Spin Distribution ($D \geq 40\text{km}$)	60
Figure 20. Aster-Gantt Observation Planning Chart (CTIO)	70
Figure 21. Daily Observation Planning Tool (June 1, 2017 @ CTIO)	71
Figure 22. Aperture Photometry Method	78
Figure 23. MPO Canopus Period Search	81
Figure 24. Target Asteroids: Inclination Angle (i) vs. Semimajor Axis (a)	85
Figure 25. Target Asteroids: Eccentricity (e) vs. Semimajor Axis (a)	85
Figure 26. (3648) Raffinetti Lightcurve	88
Figure 27. Flora Asteroid Family	90
Figure 28. Near-Infrared Reflectance Spectrum of (5235) Jean-Loup	90
Figure 29. (5235) Jean-Loup Lightcurve	91
Figure 30. (9223) Leifandersson Lightcurve	93
Figure 31. (11699) 1998 FL105 Lightcurve	94
Figure 32. (12073) Larimer Lightcurve	95
Figure 33. (15121) 2000 EN14 Lightcurve	97
Figure 34. Synchronous Binary Asteroid Lightcurve	98
Figure 35. (16452) Goldfinger Lightcurve	99
Figure 36. (20557) Davidkulka Lightcurve	100
Figure 37. Near-Infrared Reflectance Spectrum of (29796) 1999 CW77	101
Figure 38. (29796) 1999 CW77 Lightcurve	102
Figure 39. (35821) 1999 JW50 Lightcurve	103
Figure 40. V/V_p -Type Absolute Magnitude (H) Histogram	105

Figure 41. V/V _p -Type Asteroid Diameter (D) Histogram.....	106
Figure 42. Asteroid Lightcurve Period vs. Diameter	109
Figure 43. Lightcurve Amplitude vs. Spin Rate	111
Figure 44. Spin Frequency Distribution: V-Type Asteroids.....	114
Figure 45. Spin Frequency Distribution: All V/V _p -Type Asteroids.....	115

LIST OF TABLES

Table 1. Stone Edge Observatory (SEO).....	65
Table 2. PROMPT 6 (CTIO)	65
Table 3. PROMPT 1/PROMPT 3 (CTIO).....	66
Table 4. Yerkes-41 (Yerkes Observatory).....	66
Table 5. Summary of V_p -Type Target Asteroids.....	83
Table 6. Summary of V_p -Type Target Lightcurve Measurements.....	86

ACKNOWLEDGEMENTS

I wish to express my sincere appreciation to the members of my thesis committee for their guidance and support. Special thanks are extended to my thesis advisors, Dr. Paul Hardersen and Dr. Ron Fevig. When I started this program, Dr. Hardersen invited me to accompany him during an observing session at the Infrared Telescope Facility on Mauna Kea, HI. This ignited a passion for asteroids and planetary science which fueled my efforts for the three years that followed. After Dr. Hardersen departed UND for warmer environs, Dr. Fevig bravely stepped up and helped me “bring this thing home”. I look forward to collaborating with them both in the future.

I would also like to thank my many new “astronomy” friends. Tyler Linder and Gordon Gartrelle are fellow UND peers (and mentors) who have always been available and eager to “talk asteroids”. In addition, the observations which underpin this investigation would not have been possible without Tyler’s generous contribution of telescope time on the PROMPT 1, 3, and 6 telescopes at CTIO. Amanda Pagul, Vivian Hoette, and Kate Meredith, members of the SEO and Yerkes support teams, consistently expressed interest and provided encouragement during my studies. My involvement with the University of Chicago’s astronomy education outreach programs (Skynet Junior Scholars, McQuown Scholars, etc.) has truly been one of the highlights of my volunteer activities in STEM education. I would like to send a special “shout out” to Amanda, who

makes sure that I stay current with a wide range of topics, including the Hubble Frontier Fields, dark energy, gravitational lensing, and also things that she think will help me stay cool and hip with the “young people” (as much as possible, that is).

Finally, I would like to thank my family for their support over these past three-and-a-half years. My children, Hannah, Claire, and Jack certainly have had their fill of asteroids and meteorites at home. And if that wasn’t enough, they had to hear it in their schools too (from elementary school through college, there is no escape!). My wife, Mary, had it even worse perhaps, as asteroids routinely invaded the bedroom too. All shooting star jokes aside, there were many late nights spent with the glow of the laptop screen filling the bedroom and the “sounds” of the telescope (Slack’s “knock brush” clarion call) when the slit closed unexpectedly or the telescope stopped tracking after a meridian flip. During the day, Mary stepped up and did much more than her fair share around the house when I had to study, to write, and just “to think”. Mary, a veteran of my two previous graduate school endeavors, showed the same grace and patience she has throughout our marriage. Mary, I couldn’t have done it without you...and yes, I *think* this is going to be the last one.

ABSTRACT

A massive impact event on (4) Vesta is believed to have created the Vesta family of asteroids (Asphaug, 1997). The rotational characteristics of the Vesta family provide important clues about this event, including its timing, the make-up of the resulting debris, the subsequent migration of members of the family into Earth-crossing orbits, and the deposition of the Howardite-Eucrite-Diogenite meteorites on the Earth's surface. This study conducted lightcurve measurements of ten V_p -type asteroids, drawn from an asteroid taxonomy defined by Carvano et al. (2010) and based on the Sloan Digital Sky Survey (SDSS) Moving Object Catalogue (MOC4). These measurements identified a range of asteroid rotation periods from approximately 2.5 to 9.5 hours, as well as a potential synchronous binary system, (15121) 2000 EN14. The lightcurve results were combined with those of other V/V_p -type asteroids available in LightCurve Database (LCDB; Warner et al., 2009), and matched with both WISE diameter/albedo (J. Masiero et al., 2011) and near-infrared spectroscopic (Hardersen et al., 2014-2018) data. This integrated approach identified a set of Vesta family asteroids with relatively fast spin rates, nearly spherical shapes, and loose aggregate compositions. These findings, combined with the non-Maxwellian shape of this population's spin rate distribution, highlighted the importance of thermal Yarkovsky-YORP effects on the evolution of the Vesta family.

CHAPTER 1

INTRODUCTION

Approximately two centuries after the discovery of (1) Ceres in 1801, the study of asteroids has entered an era of unprecedented exploration, discovery, and insight. For evidence of this, one needs look no further than the NASA Dawn space probe. At the time of this writing, Dawn is orbiting and conducting *in situ* measurements of Ceres, after spending fourteen months studying the asteroid (4) Vesta. Planetary scientist, Richard Binzel, hailed the Dawn mission as a “golden spike for planetary science” (Binzel, 2012), depicting the planetary exploration process as a pyramid (refer to Figure 1). Binzel explains, “Planetary exploration begins with discovery, often in the course of surveys. Physical measurements, with increasing precision, bring to focus particularly tantalizing objects. Science questions become refined through both observation and theory, often to their limit. Spacecraft exploration capable of delivering consequential breakthroughs forms the capstone” (Binzel, 2012).

Binzel’s pyramid can also be viewed in terms of the historical evolution of planetary science. In the case of asteroids, the discovery phase has been, until very recently, accomplished using ground-based telescopes, beginning with the discovery of the first four asteroids: (1) Ceres, (2) Pallas, (3) Juno, and (4) Vesta, in the first decade of the nineteenth century. In the nearly one hundred and fifty years that followed, asteroids

were, as their name suggests, simply star-like points. Physical measurements during this time were essentially restricted to orbital determinations. While this provided sufficient evidence to establish the existence of a large population of asteroids in a main belt between the orbits of Mars and Jupiter, as well as the existence of dynamically related asteroid “families”, little was known about their true nature or origin. Several theories were proposed, including the possibility that the asteroids were fragments of a disrupted “missing” planet or perhaps the orphaned remnants of the solar system’s planet formation process.

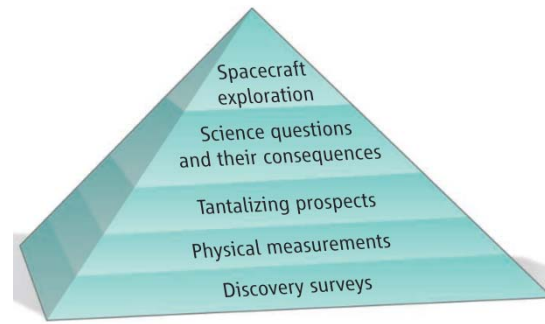


Figure 1. Pyramid Model of Planetary Exploration (Binzel, 2012)

Beginning in the 1950’s, with the advent of instrumental photometry, asteroids finally began to be resolved as three-dimensional, planetary bodies. Photometric light curves were used to estimate asteroid sizes, shapes, and rotational characteristics. In the 1970’s, researchers began to use spectrophotometric and spectroscopic analysis of reflected light to group asteroids by type and to infer asteroid surface composition. During this time, the asteroid (4) Vesta was identified as a particularly “tantalizing prospect” (Binzel, 2012) due to its Earth-like basaltic surface composition and the fact that its reflectance spectra closely matched that of meteorites belonging to the HED

(Howardite-Eucrite-Diogenite) group. The emergence of the CCD (charge-coupled device) in the 1980's vastly improved the sensitivity of telescopic observations, and also facilitated the development of spaceborne instruments. The Hubble Space Telescope, launched in 1990, and Spitzer Space Telescope, launched in 2003, have both been used to study asteroids (Thomas and Binzel, 1997; Mueller et al., 2011). The NEOWISE (Near Earth Object Wide-Field Infrared Survey Explorer), first launched as WISE (Wide-Field Infrared Survey Explorer) in 2009, has been employed in both the measurement of known asteroids, as well as the discovery of new ones (Mainzer et al., 2011a).

The exploration of asteroids by space probes began with the 1991 Galileo flyby of (951) Gaspra. Several other space missions followed, including the 2000 NEAR Shoemaker rendezvous with (433) Eros, as well as the aforementioned Dawn mission to Vesta and Ceres. Sample return missions to asteroids, an important next step in quantifying their mineralogical composition, include the 2005 Hayabusa mission to (25143) Itokawa, the Hayabusa 2 mission to (162173) Ryugu (launched on December 3, 2014), as well as the OSIRIS-Rex mission to near-Earth asteroid (101955) Bennu (launched on September 8, 2016).

As the science of asteroids has evolved, so too have the reasons for studying them. The discovery of (1) Ceres in 1801 by Giuseppe Piazzi generated substantial interest from astronomers who hoped that it might be the “missing planet” predicted by the Titius–Bode law. Piazzi, writing to a fellow astronomer soon after the discovery, hinted “I have announced this star as a comet, but... I surmise that it could be something better than a comet [presumably a planet]” (Serio et al., 2003). In the ensuing decade, with the

discovery of three other similar objects, it became clear that asteroids were too small and numerous to be considered as "real" planets, and their perceived importance dwindled. For many years, asteroids were considered merely a nuisance, a source of unwanted streaks on otherwise valuable stellar images.

Today, however, the scientific importance of asteroids as enduring records of our solar system's evolution is widely acknowledged. Asteroids are remnants of the primitive materials that constituted the solar nebula and early solar system. In addition, asteroids contain evidence of thermal and chemical changes which, in combination with laboratory measurements of meteorites, can provide important clues about the formation of the planets. The current population of asteroids includes a mixture of primordial material that never fully coalesced into a planetary body, collisional fragments of early planet embryos, as well as some enduring planetesimals, including (1) Ceres and (4) Vesta.

Asteroids are also closely tied to the evolution of our own planet. Researchers believe that asteroid impacts on the early Earth are responsible for depositing a "veneer" of water and carbon-based organic molecules on its surface (Bottke, 2002). As such, asteroids may have played a critical role in "seeding" life on our planet. By contrast, asteroid impacts have also produced catastrophic damage and "extinction" events on the Earth. As an example, it is believed that a 10 km diameter asteroid which impacted the Earth approximately 66 million years ago was primarily responsible for the extinction of the dinosaurs (Alvarez and Asaro, 1990).

In recent years, the tracking of asteroids to predict and avoid a future asteroid-Earth impact has become an important priority. The NASA Planetary Defense Coordination Office (PDCO) is responsible for detecting, tracking, and characterizing potentially hazardous objects (PHO), defined as asteroids or comets of at least 30-50 meters in diameter which pass within 0.05 AU of the Earth's orbit (<https://www.nasa.gov/planetarydefense/overview>). The presence of near-Earth asteroids has also garnered the attention of the emerging commercial space industry. The potential of near-Earth asteroids as source of valuable natural resources may one day result in these objects being mined for their precious metals, or being used as refueling stops for solar system exploration.

Both scientific and commercial activities related to asteroids require a detailed understanding of their physical properties, including their size and shape, composition, orbits, and rotational characteristics. In this chapter, a general overview of the asteroid population is provided. The chapter begins with a discussion of the main asteroid belt and meteorites. Dynamic interactions, such as collisions, orbital resonances, and the Yarkovsky/YORP effect, are also described. The importance of the rotational characteristics of asteroids for providing insight into these interactions is highlighted. In addition, a specific emphasis is placed on (1) the asteroid (4) Vesta, (2) its dynamical family, commonly referred to as the "Vestoids", and (3) its associated meteorite types, the HED group. The chapter closes with a statement of the specific objectives of this study.

1.1 Asteroids

There are three primary populations of asteroids in the solar system: (1) the main belt asteroids, which are located between the orbits of Mars and Jupiter; (2) the Trojans, which are grouped along Jupiter's orbital path at its L4 and L5 Lagrangian points, and (3) the near-Earth asteroids, which are defined by a perihelion of 1.3 AU or less. The largest collection of asteroids in the inner solar system is contained in the main belt located from approximately 1.8 AU to 3.3 AU.

The origins of the main belt are closely tied to the process which formed the terrestrial planets. This process started with the accretion of dust in the solar nebula into small bodies, called planetesimals. As the planetesimals grew in size, gravitational effects became significant and they coalesced to form the rocky planets. In the region of the main asteroid belt, however, this process was interrupted by the newly-formed Jupiter. Jupiter's substantial gravity perturbed the orbits of the planetesimals, favoring collisions over coalescence, and preventing the formation of planetary bodies in this region. This perturbative effect continues to the present day, and Jupiter is responsible for altering the orbits of asteroids in the main belt, sending them inward toward the sun and terrestrial planets, or outward into the Kuiper belt.

An understanding of the orbital characteristics of the main belt asteroids and the distribution of their physical properties can provide valuable clues to the origins and evolution of the solar system. The radial distribution of asteroids in the main belt is illustrated in Figure 2. It is marked by several narrow radial "gaps" where relatively few asteroids exist. These regions are the so-called mean motion resonances, where the

orbits of objects inside are destabilized by the gravitational influence of Jupiter. Resonances are described in more detail in Section 1.4.1. The radial distances of the 3:1 (2.5 AU), 5:2 (2.8 AU), and 2:1 (3.3 AU) mean motion resonances have also traditionally been used to divide the main belt into three sections: the inner (2 – 2.5 AU), middle (2.5 - 2.8 AU), and outer main belts (2.8 – 3.3 AU).

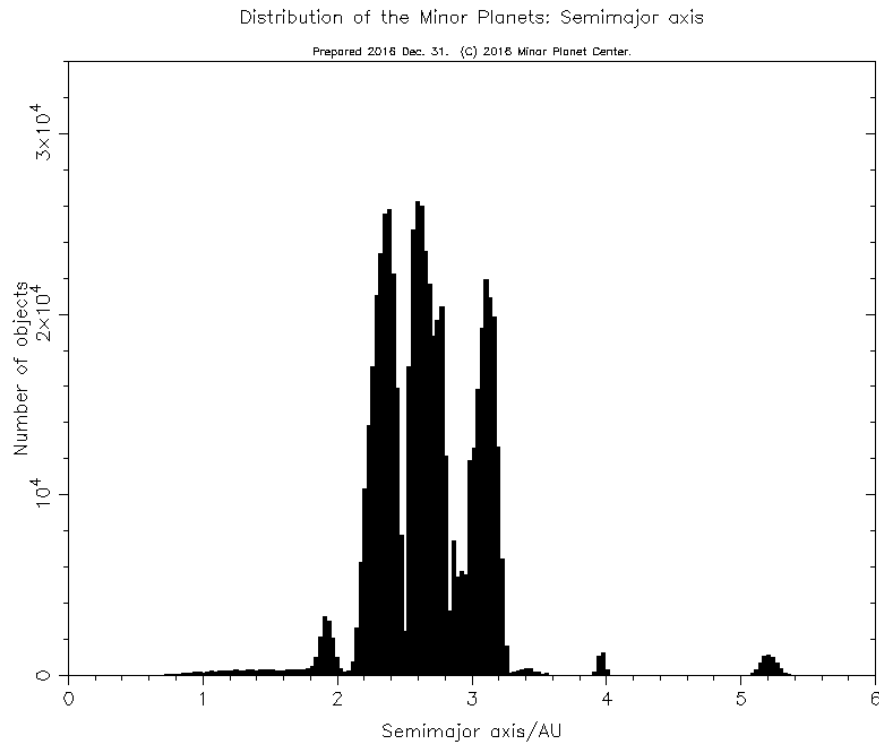


Figure 2. Distribution of Minor Planets: Semimajor Axis (Minor Planet Center, 2016a)

The orbits of the asteroids in the main belt are generally more inclined and eccentric than those of the planets. This is likely the result of the gravitational influence of Jupiter, and to a lesser extent, Saturn; and it provides additional evidence that these planets experienced an orbital migration after their initial formation (Morbidelli et al., 2010). As shown in Figure 3, the majority of main belt asteroids have orbital eccentricities between 0 and 0.35 and inclinations between 0 and 20 degrees.

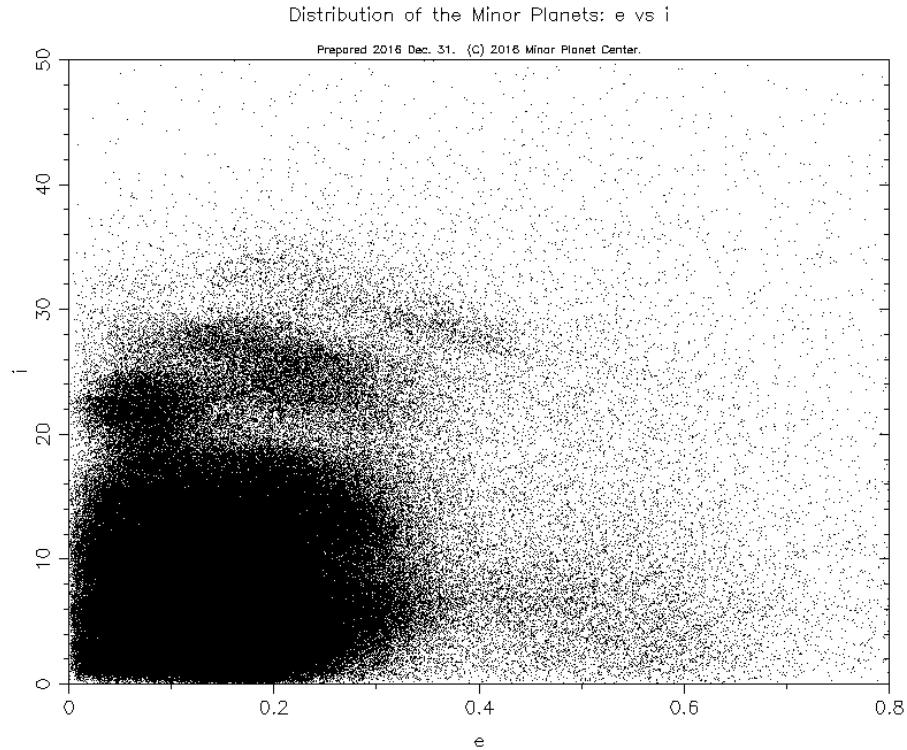


Figure 3. Distribution of Minor Planets: e vs. i (Minor Planet Center, 2016b)

The sizes of asteroids in the main belt are described by the size frequency distribution provided in Figure 4. The cumulative number of main belt asteroids rises dramatically with decreasing diameter. This trend indicates a persistence of the larger (> 100 km) asteroids from primordial times, but a progressive comminution of smaller asteroids (<10 km) due to collisions (Gladman et al., 2009). Currently, there are an estimated one million asteroids in the main belt with a diameter of 1 km or more (Tedesco and Desert, 2002). Larger diameter asteroids are much less numerous, and only approximately 200 main belt asteroids have a diameter of 100 km or larger (Yeomans, 2015), with Ceres (952 km), Pallas (545 km), and Vesta (530 km) being the largest three.

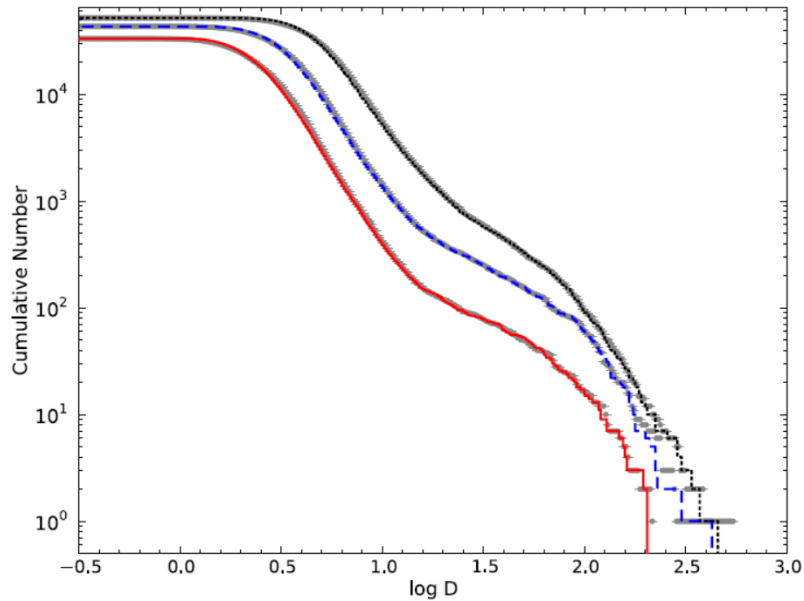


Figure 4. Cumulative Raw Size-Frequency Distribution of Asteroids in the inner-(red), middle-(blue), and outer-Main Belt (black) from NEOWISE (J. R. Masiero et al., 2011). The $\log D$ term is the logarithm of the asteroid diameter in kilometers.

The distribution of material (e.g., minerals, metals, and volatiles) in the asteroid belt is an important basis for understanding the composition of the solar nebula and the evolution of the early solar system. Figure 5 presents a simplified view of the heliocentric distribution of asteroid types in the main asteroid belt (Gradie and Tedesco, 1982). This set of asteroid types, commonly referred to as a taxonomy, is defined by asteroid albedo and reflected “color”. The S-type asteroids, marked by moderate albedo and a spectral absorption feature near $1.0 \mu\text{m}$, are predominant in the inner main belt. The S-types make up approximately 17% of all asteroids and are generally thought to be dry, mafic-silicate assemblages which have undergone some level of melting. In the middle main belt, the C-type asteroids dominate. C-type asteroids compose approximately 75% of all asteroids and have low albedo and mostly flat, featureless spectral shapes. C-type asteroids are thought to have an essentially primordial

composition with significant water (ice) content and the presence of other volatiles, including organic materials. In the outer main belt, even darker (and “icier”) asteroid types prevail. The D-type asteroids, for instance, are characterized by very low albedos, reddish spectral slopes, and are thought to be similar in composition to the Kuiper belt objects. In addition to the C, S, and D-types several other asteroid groups exist, including the M, V, and E, and P-type asteroids. The V-type asteroids are commonly associated with Vesta and its dynamical family.

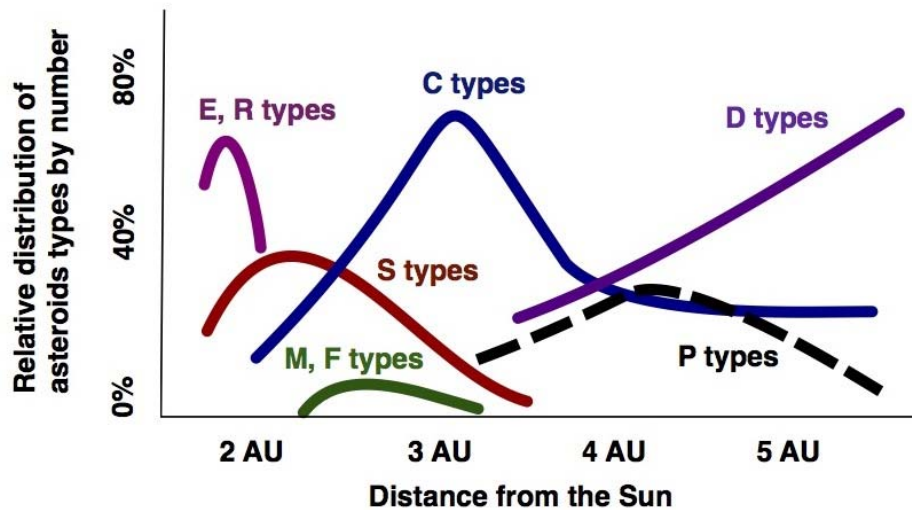


Figure 5. Heliocentric Distribution of Asteroid Types (Simplified) (Gradie and Tedesco, 1982; Newton, 2014)

The implications of this early work by Gradie and Tedesco (1982) was that: (1) the distribution of asteroid types in the main asteroid belt was primarily influenced by the heat gradient associated with distance from the Sun, and (2) the asteroids remained more or less in the same heliocentric locations where they were formed. More recent studies using a larger sampling of asteroids (DeMeo and Carry, 2014), have demonstrated that while this basic distribution remains mostly applicable to the largest

diameter asteroids (> 100 km), there is substantially more radial mixing of smaller asteroids in the main asteroid belt than first thought (refer to Figure 6). These results imply the presence of radial inhomogeneities in the solar nebula, as well as the influence of gravitational interactions which produced enhanced mixing.

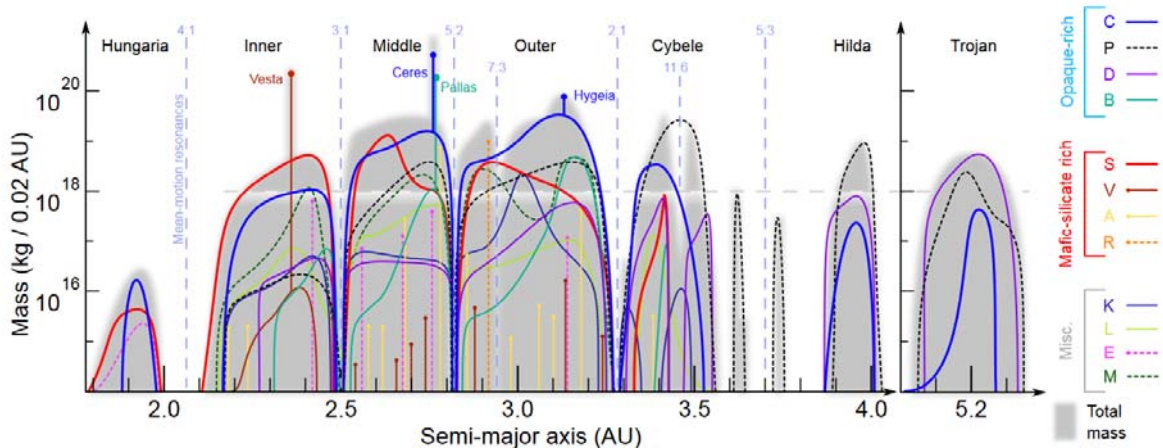


Figure 6. Heliocentric Distribution of Asteroid Types (DeMeo and Carry, 2014)

1.1.1 Vesta

The asteroid Vesta was discovered on March 27, 1807 by German astronomer Heinrich Wilhelm Olbers. Vesta, a name given to it by German mathematician, Carl Friedrich Gauss, refers to the virgin goddess of home, hearth, and family in Roman mythology. The goddess Vesta is probably best known for the Vestal Virgins, a select group of Roman priestesses responsible for maintaining Rome’s “sacred fire”, symbolic of the empire’s security and endurance.

Since its discovery, Vesta has been perhaps the most closely studied of all of the asteroids. Earth, space-based (e.g. the Hubble Space Telescope), and in situ measurements (the Dawn spacecraft) have revealed an object of unusual brightness variations, complex geology and morphology, and an Earth-like basaltic surface, mantle,

and metallic core. Vesta is located in the inner main belt (refer to Figure 6), and has an orbital semi-major axis of 2.36 AU and eccentricity of 0.097. It is the third largest asteroid, with a diameter of 524 km, and is the second most massive, with a mass of 2.59×10^{20} kg. Vesta has a density of 3.46 g/cm^3 and a rotational period of 5.34 hours.

Years of observations hinted that the surface of Vesta bore the marks of a long and varied collisional history. Gaffey (1997) observed surface spectral variations and suspected that they were caused by impacts which exposed the lower crust and mantle. Subsequent Hubble observations indicated a flattened south polar region, likely created by an impact (Thomas et al., 1997; Thomas and Binzel, 1997). Dawn confirmed two large impact basins on Vesta's southern pole, the younger Rheasilvia (500 km) and the older Veneneia (400 km). It is suspected that these impacts exposed lower crustal, diogenitic material, and likely generated ejecta that resulted in the Vesta dynamic asteroid family, as well as the HED meteorites (Marchi et al., 2012).

Visible and near infrared (VNIR) reflectance spectroscopy of Vesta have revealed surface absorptions characteristic of basaltic minerals (Gaffey, 1983, 1997). Spectra were comparable to those obtained in the laboratory for the HED meteorites (McCord et al., 1970). Spectral data obtained by the Dawn space probe has further supported this linkage (De Sanctis et al., 2012; Prettyman et al., 2012; Reddy et al., 2012).

1.2 Meteorites

For much of human history, meteorites were regarded as religious artifacts, often buried in ancient tombs or displayed and worshipped in churches. The scientific study

of meteorites, known as meteoritics, did not begin until the late 1700's. In 1794, E. F. Chaldni, a German physicist now regarded as the "father of meteoritics", published a book which proposed that meteorites were of extraterrestrial origin. This statement was controversial and initially received substantial ridicule. The common belief at that time was that meteorites were of terrestrial origin, related to atmospheric or geologic (e.g. volcano) events.

The controversy over the origin and nature of meteorites even entered the political arena. Thomas Jefferson, responding to a report by two Yale professors about a meteorite fall, was quoted (perhaps apocryphally) as saying, "Gentlemen, I would rather believe that two Yankee professors would lie than believe that stones fall from heaven" (McSween, 1999). Despite Jefferson's contradictions however, the idea that meteorites had an extraterrestrial origin became more or less universally accepted within a decade of the publication of Chaldni's book.

There are three fundamental groupings of meteorites: stony, irons, and stony-irons. The stony meteorites are primarily composed of silicate minerals, and also commonly contain small metal grains. The iron meteorites are predominantly composed of iron/nickel alloys, and are likely derived from the remnant cores of larger differentiated bodies. The stony-iron meteorites are a combination of the two, and are potentially associated the mantle-core transition of a differentiated parent asteroid (e.g., pallasites) or impact mixing (e.g., mesosiderites).

The stony meteorites are further delineated into chondrite and achondrite meteorite groups. The chondrite meteorites are a mix of dusts and grains from the

primordial solar system, and have undergone only limited thermochemical modification due to heating. The achondrites are composed primarily of igneous rock caused by melting of its original constituents and subsequent recrystallization. The HED meteorites, a part of achondrite group, are believed to be derived from the crust of (4) Vesta, a differentiated body.

Meteorites are a critical component in the study of asteroids. Laboratory measurements of meteorites can provide important clues about the timing of thermal events in the forming solar nebula and planetary system. Furthermore, if a particular asteroid can be identified as the parent body of a meteorite group, for instance by remote or in situ spectroscopic observations of the asteroid surface, these early solar system formation events can also be spatially resolved. This type of information provides the basis for theories and models of how our solar system was formed.

1.2.1 HED Meteorites

The HED meteorites are a subset of the achondrite stony meteorites. They include the howardite, eucrite, and diogenite types. The HED meteorites account for about 5% of all meteorite falls, which is about 60% of all achondrites falls (“Meteoritical Bulletin Database,” 2015).

HED meteorites have been mineralogically linked to Vesta by comparing the reflectance spectra of Vesta, obtained both remotely (McCord et al., 1970) and in situ by Dawn (De Sanctis et al., 2012), with that of meteorite spectra obtained in the laboratory. It is believed that the HED meteorites are originally derived from the south pole Rheasilvia impact, approximately 1 billion years ago (Marchi et al., 2012).

Fragments from this impact were injected toward the 3:1 mean motion resonance at 2.5 AU, where they were launched on Earth-crossing orbits (Migliorini et al., 1997).

The three types of HED meteorites are associated with different layers of Vesta's surface. The eucrite meteorites are the result of lava flows and believed to come from the outer crust of Vesta. The diogenite meteorites are likely extracted from a deeper crustal layer, such as that exposed at the bottom of the Rheasilvia basin. The howardite meteorites are breccias of the eucrite and diogenite types, believed to be the result of surface material mixing generated by impacts on Vesta's surface.

1.3 Taxonomy

As introduced in Section 1.1, an asteroid taxonomy is a grouping of asteroid types based on a set of observed properties, such as color, albedo, and spectral absorption features. Over the years, several different taxonomies have been created, modified and extended. While taxonomic classifications suggest groupings with similar physical properties, they do not necessarily imply similar mineralogy or genetic linkages (Gaffey et al., 2002). Asteroid taxonomy is nevertheless an important way to make broad characterizations and also to identify targets for more detailed measurements.

The earliest asteroid taxonomy was developed by Chapman et al. (1975) based on spectrophotometric, radiometric, and polarimetric measurements. Chapman et al. (1975) classified 110 asteroids using two primary types: (1) C(carbonaceous), and (2) S(tony or iliceous). The carbonaceous asteroid class is typically characterized by little or no color variation and low albedo. The siliceous asteroid class is characterized by a

reddish color and higher albedo. Any asteroids that did not fit in either the C or S classes were assigned to the U(known) type. The Chapman et al. (1975) taxonomy was refined, extended, and applied to a larger set of asteroids (~500) by Bowell et al. (1978) and Gradie and Tedesco (1982).

Tholen (1984) developed an improved taxonomy based on the Eight-Color Asteroid Survey (ECAS) spectra (0.3-1.1 μm) (Zellner et al., 1985) and albedo measurements of approximately 589 asteroids. Tholen (1984) used Principal Component Analysis (PCA) techniques to reduce the observed spectral quantities into two key absorption features, one in the ultraviolet spectral range and one in the near-infrared range. Combining this data with albedo measurements, Tholen (1984) developed a taxonomy that consisted of a total fourteen spectral classes: A, B, C, D, E, F, G, M, P, Q, R, S, T, and V. The Tholen (1984) taxonomy, with some minor refinements over the years, has remained the basis of asteroid taxonomies in use today.

Over the years, researchers have applied the Tholen taxonomy to other sets of asteroid data for the purposes of verifying or extending the taxonomy, as well as highlighting asteroids trends or distributions. Bell et al. (1995) conducted a 52-color asteroid survey (0.8-2.5 μm) with the objective of outlining the basic mineralogy of the Tholen taxonomic types. Xu et al. (1995) applied the Tholen taxonomy to 316 asteroids obtained as part of the Small Main-Belt Asteroid Spectrographic Survey (SMASS) (0.435–0.925 μm). New spectral features revealed by SMASS, and its follow-on SMASS II (Bus and Binzel, 2002b), lead to refinements to the original Tholen scheme, and ultimately the proposal of a new scheme (Bus and Binzel, 2002a). Bus and Binzel (2002a) identified

a total of 26 classes, including one new class (L) and several intermediate classes (e.g., Cb, Cg, Sa, etc.) not in the original Tholen taxonomy. Subsequently, DeMeo et al. (2009) extended the (Bus and Binzel, 2002a) taxonomy into the near-infrared range (0.45 to 2.45 μm). The resulting taxonomy identified a total of 24 classes, eliminating the Sl, Sk, Ld classes, and adding a new one, Sv.

Of particular importance to this study, Carvano et al. (2010) developed a taxonomy based on the Sloan Digital Sky Survey (SDSS) five color (u' , 0.354 μm ; g' , 0.477 μm ; r' , 0.6230 μm ; i' , 0.7630 μm ; z' , 0.913 μm) photometric survey with the primary goal of identifying “...interesting targets for NIR spectroscopic follow-up observations and to study the distribution of taxonomies in families and in the main belt as a whole” (Carvano et al., 2010). Using data for approximately 63,000 asteroids from the fourth release of the SDSS Moving Object Catalogue (MOC4) (Ivezić et al., 2010) and meteorite spectra from the RELAB database, Carvano created a taxonomy that was compatible with the (Bus and Binzel, 2002a) scheme, and added a subscript p to indicate its reliance on photometric data, e.g. C_p , V_p , S_p , etc.

1.3.1 V-Type Taxonomy

For approximately a decade after the development of the first asteroid taxonomy by Chapman et al. (1975), the Vesta or V-type taxonomic class included only one known asteroid, Vesta itself. Chapman et al. (1975) specifically noted the absence of any other objects like Vesta and implied that they may have long since been ejected from the main belt, stating “The apparent absence of additional Vesta-type may raise a challenge for those who claim that Vesta is in the kind of orbit from which fragments cannot readily

reach the Earth". Similarly, Bowell et al. (1978), Gradie and Tedesco (1982), and Tholen (1984) also identified Vesta as unique. Tholen (1984) did nevertheless, and perhaps optimistically, create a separate V-type class.

The Bell et al. (1988) 52-color survey identified an "Earth-crosser...of basaltic composition", hinting that it could be the second known member of the V-type class. In a follow-up effort, Bell (1988) more boldly (and poetically) stated, "While the goddess Vesta had no offspring, the asteroid Vesta almost certainly does." Bell (1988) identified the asteroid (3551) 1983 RD as a likely V-type object based on the presence of two major spectral absorption bands (near 1 μm and 2 μm) characteristic of the presence of the mineral pyroxene. This asteroid was also studied along with two other likely basaltic objects, (3908) 1980 PA and (4055) 1985 DO₂, by Cruikshank et al. (1991).

Binzel and Xu (1993), using observations from the SMASS (Xu et al., 1995) effort, specifically targeted 15 potential V-Type asteroids dynamically linked to Vesta, as well as more than 80 other asteroids near the orbit of Vesta. A total of 20 objects were found to be of basaltic origin, characterized by a strong absorption feature around 0.9 μm . Of these, 14 asteroids were classified as Vesta-like eucritic bodies, with absorption band centers near 0.94 μm . The other 6 asteroids were characterized by a deeper and less broad absorption peak closer to 0.9 μm , indicative of a diogenite surface. Binzel and Xu (1993) also proposed a new class for these objects, J (mnemonic for the Johnstown diogenite meteorite). From an asteroid dynamics perspective, 12 of the 20 proposed V-type asteroids had been previously linked to the Vesta asteroid family. Interestingly, the other 8 asteroids had orbits which suggested a "bridge" between Vesta and the 3:1

mean motion resonance. Binzel and Xu (1993) suggested that this bridge could be evidence of a dynamical pathway for V-type asteroids to enter near-Earth orbit, and ultimately be responsible for the HED meteorites.

SMASS II (Bus and Binzel, 2002a; Bus and Binzel, 2002b) included a specific focus on the dynamical Vesta family of asteroids. This study substantially added to the number of identified V-type asteroids (30+ additional objects). DeMeo et al. (2009) added an additional 15 V-type asteroids discovered in the inner belt, and were the first to identify a V-type asteroid in the outer main belt, (1904) Masevitch.

Carvano, J. M. et al. (2010), using data from the fourth release (MOC4) of the Sloan Digital Sky Survey, identified a total of 2,818 V_p -type asteroids. The V_p class is defined by the sharpest $1\ \mu\text{m}$ absorption feature (filter z' ; $0.913\ \mu\text{m}$) among all classes. As shown in Figure 7, most of these asteroids were located in the vicinity of Vesta, but a number were also discovered in the middle and outer main belts.

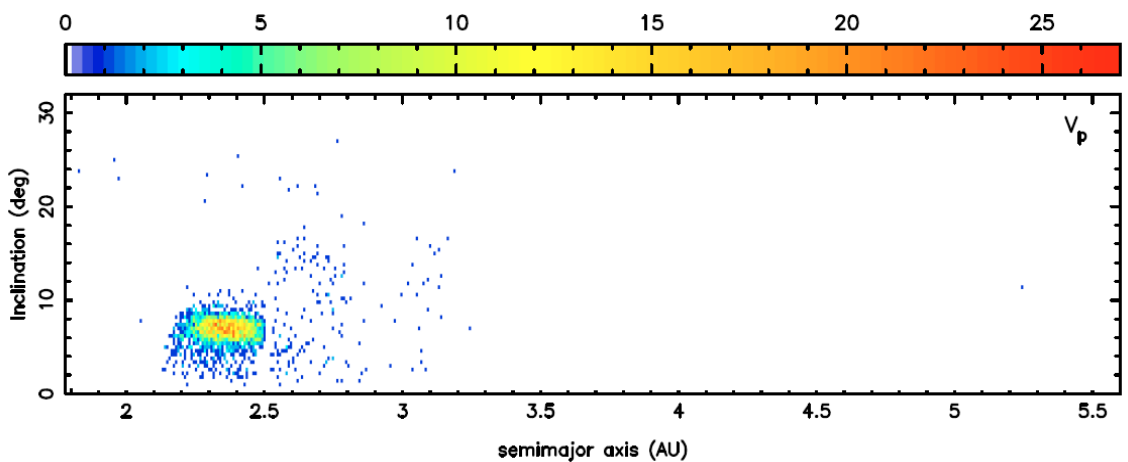


Figure 7. V_p -Type Asteroid Radial Distribution (Carvano et al., 2010). The color legend indicates the number of asteroid present in a square region measuring 0.008 AU in semimajor axis and 0.4° in inclination.

1.4 Dynamics

Asteroids dynamics encompasses all of the processes which affect an asteroid's orbital and rotational characteristics. These include collisions, mean motion and secular resonance effects, as well as thermally-induced motion, such as the Yarkovsky effect. These effects can combine to inject main belt asteroids into Earth-crossing orbits and ultimately produce the meteorites that fall on the Earth. Hence, an understanding of these mechanisms is key to linking meteorites with their parent bodies and understanding the evolution of the early solar system over time and space.

1.4.1 *Collisions and Asteroid Families*

Collisions represent perhaps the most fundamental interaction influencing the evolution of the main asteroid belt. As mentioned in Section 1.1, for instance, comminution due to collisions is the likely explanation for the abundance of “small” asteroids in the asteroid belt. In addition, impacts are responsible for changes in asteroid orbits, rotational characteristics, and their make-up (e.g., the formation of aggregated bodies or so-called “rubble pile” asteroids). Asteroid collisional dynamics have been studied using both laboratory experiments and numerical simulations (Jutzi et al., 2015; Paolicchi et al., 2002). In the laboratory, experiments analyze the impact of objects several orders of magnitude smaller than the asteroidal systems that they are trying to simulate (Ryan and Melosh, 1998; Holsapple et al., 2002). Hence, the experimental results must be extrapolated using a “scaling law” (Holsapple and Schmidt, 1982). Numerically, algorithms commonly referred to as “hydrocodes” (or “hydrodynamic codes”) have been applied to study asteroid impacts (Asphaug et al.,

2002). In addition, a number of numerical impact studies have been dedicated to studying collisions on Vesta (Asphaug, 1997; Jutzi et al., 2013; Ivanov and Melosh, 2013).

An important remnant of past asteroid collisions is the existence of asteroid families. Asteroid families, illustrated in Figure 8, are a dynamically related grouping of asteroids that represents the aftermath of one or more catastrophic collisions involving the parent body. Asteroid families were first observed and described by Japanese astronomer, Kiyotsugu Hirayama, in 1918 (Kozai, 1994). Hirayama based his analysis on the proper orbital elements: semi-major axis (a_p), inclination (i_p), and eccentricity (e_p). The proper orbital elements represent the average values of their "instantaneous" counterparts (i.e. a , i , and e) over astronomically long timescales. Hirayama proposed that asteroids which shared similar proper orbital elements likely shared a common collisional history. This approach has been refined over the years, and several numerical methods have been developed to more accurately identify asteroid family members (Zappalà et al., 1995; Nesvorný, 2010). The Vesta dynamic asteroid family is described in further detail in Section 1.4.5.

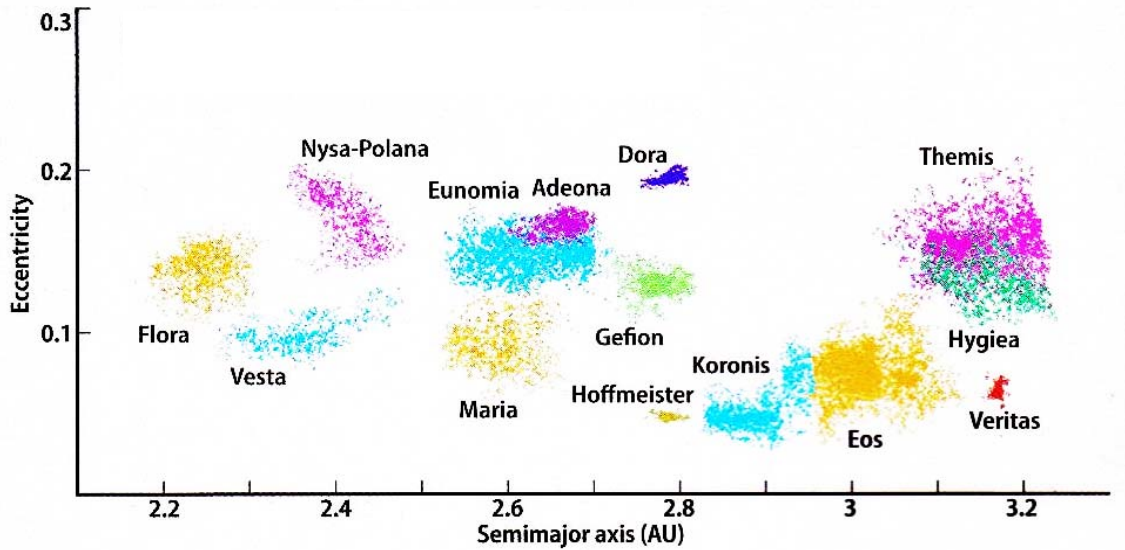


Figure 8. Dynamic Asteroid Families (Jedicke and Jedicke, 2006)

1.4.2 Resonances

The gravitational influence of the giant planets, Jupiter and Saturn, play a primary role in the shape and dynamic behavior of the asteroid belt. As described in Section 1.1, the radial distribution of the asteroids in the main belt is marked by “gaps”. These regions were first described by Kirkwood (1888), and in his honor are referred to as the Kirkwood Gaps. The Kirkwood Gaps reveal mean motion resonances with the planet Jupiter. As shown in Figure 9, the main asteroid belt is bounded on the inside by the 4:1 resonance (2 AU), and on the outside by the 2:1 resonance (3.3 AU). The intermediate resonances include 3:1, 5:2, and 7:3.

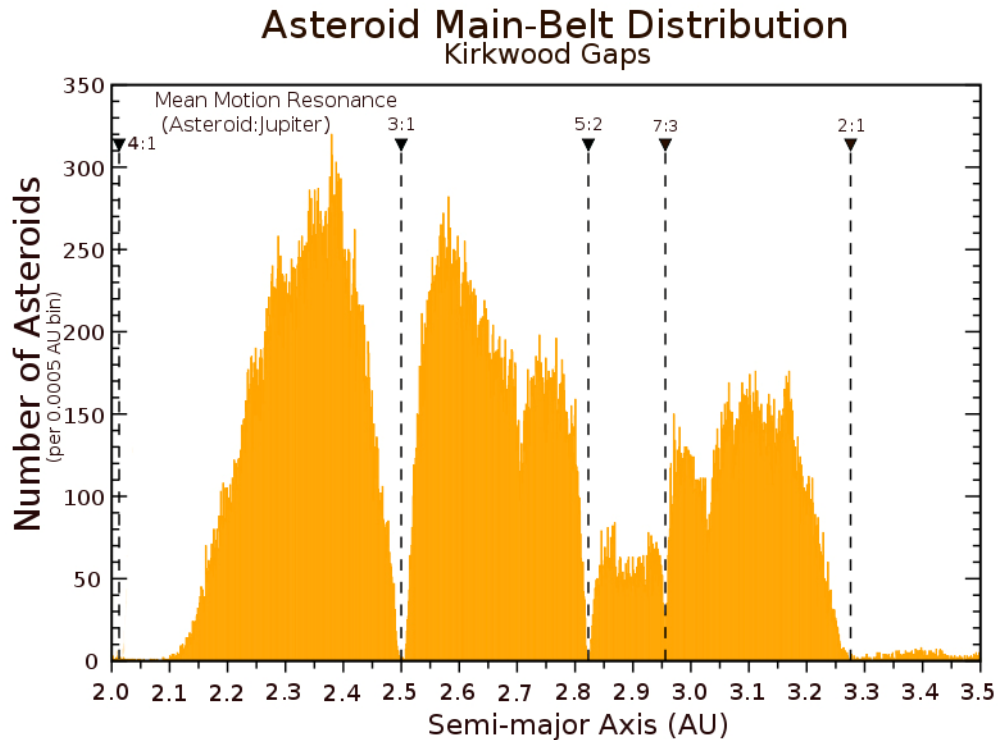


Figure 9. The Kirkwood Gaps (Chamberlain, 2007)

Objects within a mean motion resonance have orbital periods that are integer multiples of Jupiter’s orbital period. Hence, for example, an asteroid in the 3:1 mean motion resonance would orbit the sun three times for every one orbit by Jupiter. The mean motion resonances are chaotic, negatively-damped zones. Asteroids that enter these regions have their orbital eccentricities increased and enter planet-crossing orbits over relatively short time periods, typically on the order of 1-2 My (Gladman et al., 1997). These resonances are largely responsible for the tremendous amount of material that has been removed from the main asteroid belt since its formation approximately 4.6 Gy ago (Bottke. et al., 2005). The mean motion resonances act as “escape hatches” by which asteroids are ejected from the main asteroid belt and (potentially) land on the Earth as meteorites. Using Vesta as an example, observations by Binzel and Xu (1993)

have identified a migratory “tail” of related impact fragments from the location of Vesta (2.3 AU) to the 3:1 mean motion resonance (2.5 AU). It is believed that this dynamic mechanism is responsible for bringing the HED meteorites to the Earth.

Another type of resonance that is relevant to behavior of asteroids in the main belt is the secular resonance. A secular resonance is a synchronization of the precession of the perihelion of a planet, like Saturn, and the asteroids in these resonant regions. Secular resonances are generally less chaotic than mean motion resonances and cause the orbital eccentricities of the asteroids to periodically increase and decrease. In the case of the prominent ν_6 secular resonance with Saturn, asteroids are commonly injected into Mars-crossing orbits, and are often ejected from the asteroid belt by close passes with Mars. Secular resonances, unlike mean motion resonances, have complex, three-dimensional shapes. The ν_6 resonance forms an inner (2.1 AU) and upper (inclination of approximately 20 degrees) boundary on the asteroid belt.

Of particular interest for this study is the 3:1 mean motion resonance (2.5 AU) and the ν_6 secular resonance (2.1 AU) because of their relative proximity to Vesta (2.3 AU) and the Vesta asteroid family. Using numerical simulations, Gladman et al. (1997) demonstrated that asteroids entering these resonances will have their eccentricities increased substantially over one million year time scales. Most asteroids will enter Jupiter-crossing orbits or be flung into the sun. Some, however, will be extracted from the resonance by close passes with the terrestrial planets, and could be delivered to the planet surface as meteorites.

Migliorini et al. (1997) used similar numerical models to look at the effect of the 3:1 and ν_6 resonances on the orbit of Vesta and its family members, including an attempt to link objects entering these resonances with known V(esta)-type asteroids in near-Earth orbit. They were able to show that the orbits of known V-type near-Earth asteroids (NEA) were compatible with Vesta fragments delivered from both the 3:1 and the ν_6 resonances. However, estimates of the (older) ages of the V-type NEA's were incompatible with the time scale (shorter) predicted to deliver Vesta family members to near-Earth orbits. Migliorini et al. (1997) hypothesized that there could be a physical mechanism that allowed Vesta fragments to "loiter" near the mean motion resonances before entering these regions. Alternatively, it has been proposed that Vesta fragments are not being directly injected into the resonances by the initial impact, but rather by a slower process that moves the impact fragments towards the resonances (Bottke et al., 2006). Such a process, the Yarkovsky effect, is discussed in the next section.

1.4.3 Yarkovsky/YORP Effects

The Yarkovsky effect is a force that acts on rotating, solar system objects that results from the emission of thermal energy from the object's surface. This effect was introduced in 1900 by the Polish engineer, Ivan Osipovich Yarkovsky. Writing in a pamphlet, Yarkovsky explained that the periodic heating by the sun of a rotating object in space would produce a small force that, over time, could significantly modify that object's orbital properties (Öpik, 1951). This effect is particularly applicable to relatively small bodies, like asteroids.

The Yarkovsky effect is composed of two components: a diurnal effect, in which the spin axis of the asteroid is nominally perpendicular to its orbital plane; and a seasonal effect, in which the spin axis of the asteroid is nominally parallel to its orbital plane. A key physical property intrinsic to both effects is the delay between the absorption and emission of thermal energy from the sun, called thermal inertia.

Figure 10 illustrates the diurnal Yarkovsky effect. When an asteroid orbits around the sun, its sun-facing side is warmed by the sun. As this side rotates away from the sun, its temperature naturally decreases to approach the temperature of its surroundings. The asteroid's thermal inertia, however, delays the emission of this thermal energy into space. This effect is equivalent to that which, all other factors aside, causes the afternoon to be the warmest time of the day on the Earth. As a result of thermal inertia, the reactionary force exerted by the emitted photons is biased toward a given direction, which depends on whether the asteroid is rotating in a prograde or retrograde direction. For prograde rotation, the Yarkovsky force has a component in the same direction as the orbital motion. This added force will cause an increase in the semi-major axis, and to some extent, the orbital eccentricity. Over long periods of time, this can result in substantial changes to the asteroid's orbit. For an asteroid in retrograde rotation, the Yarkovsky force will have a component in the opposite direction as the orbital motion. This force will cause a decrease in the semi-major axis and eccentricity.

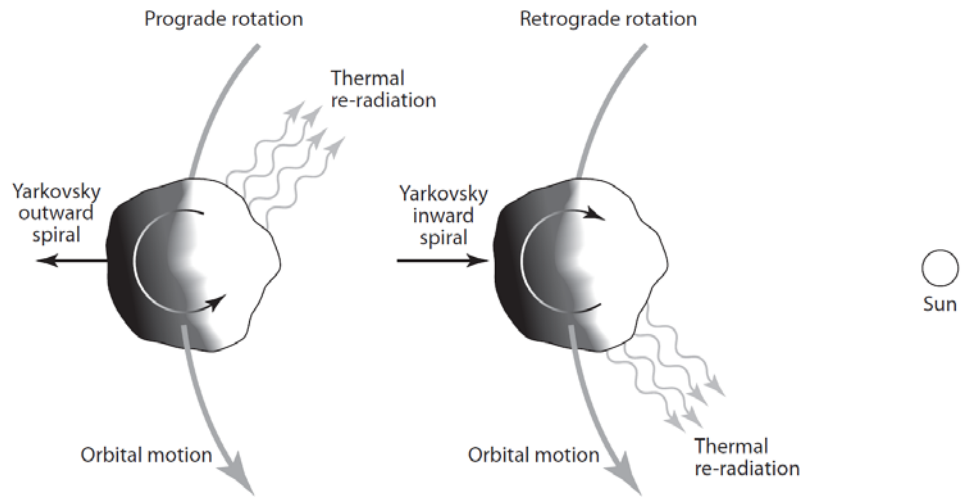


Figure 10. Diurnal Yarkovsky Effect (Yeomans, 2013)

The seasonal Yarkovsky effect is illustrated in Figure 11. As the asteroid orbits the sun, its northern (A) and southern sides (C) are alternatively heated over the period of an asteroid “year”. Similar to the diurnal effect, the re-emission of absorbed thermal energy is delayed, depending on the thermal properties of the asteroid. As a result, a related force is applied at B (northern hemisphere heating) and D (southern hemisphere heating) in a direction that opposes the orbital motion. Hence, the seasonal Yarkovsky effect causes the asteroid to spiral inward towards the sun. Unlike the diurnal effect, the asteroid spin direction does not alter the sense of this effect.

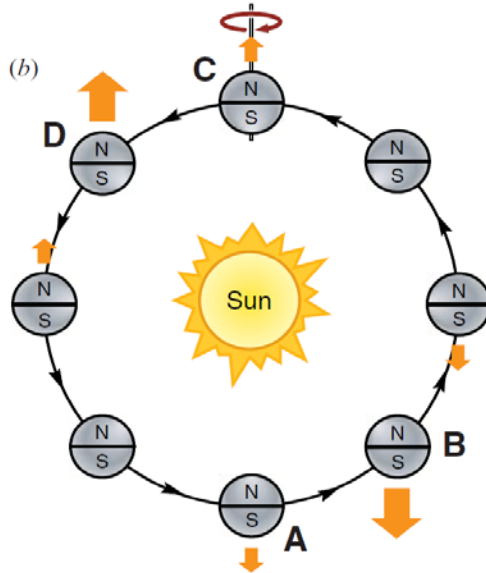


Figure 11. Yarkovsky Seasonal Effect (Bottke et al., 2006)

The importance of the Yarkovsky effect for asteroids is its ability to deliver asteroid impact fragments into the mean motion and secular resonances where some enter Earth-crossing orbits and potentially land as meteorites. Bottke et al. (2002) states that the Yarkovsky effect exerts an important influence on the orbits of asteroids of diameters 20 km or less. Numerical models (Bottke et al., 2002; Farinella et al., 1998) have shown that the average semi-major axis change resulting from the Yarkovsky effect is approximately 0.1 AU. In the case of Vesta, for example, this could be sufficient to move its family members inward toward the ν_6 resonance or outward toward the 3:1 resonance. In rare cases (Roig et al., 2008), the Yarkovsky effect could also result in Vesta fragments being transported across the 3:1 resonance into the middle main belt.

The Yarkovsky–O'Keefe–Radzievskii–Paddack (YORP) effect is variation of the Yarkovsky effect that influences an asteroid's rotation rate (Scheeres, 2007). The YORP effect, like the Yarkovsky effect, is driven by the heating and subsequent re-emission of

thermal energy from the asteroid surface. In the case of the YORP effect, non-symmetries in the asteroid shape can lead to a net torque being applied. Depending on the sense of the asteroid's rotation, this torque can work to increase or decrease the asteroid's rotational rate. While the YORP effect is not directly responsible for altering the orbits of asteroids, its effect on the asteroid's rotation influences the Yarkovsky effect. For instance, if the YORP effect increases the rotational rate of a given asteroid sufficiently, the Yarkovsky effects will be minimized (there is no Yarkovsky effect on an asteroid with infinite spin rate).

1.4.4 Rotation

An asteroid's rotational characteristics are one of its most fundamental properties and provide a wealth of information about its origin, make-up, and dynamic interactions (collisions, gravitational, Yarkovsky-YORP, etc.). Asteroid rotational data has been obtained using a wide-range of techniques, including ground-based optical telescopes (Warner et al., 2009), ground-based radar (Pater et al., 1994), space telescopes (Thomas et al., 1997), and in situ space missions (Cheng, 2002; Russell et al., 2012). Analyses of these data (Pravec et al., 2002; Paolicchi et al., 2002) have revealed important information about the asteroid population. These findings include the presence of a spin rate "barrier" (~11 rev/day) for "rubble pile" asteroids, the prevalence of binary asteroid systems, and the importance of YORP effects to alter the primordial Maxwellian distribution of asteroid spin rates. Asteroid rotation and lightcurve photometry, an important technique for measuring asteroid spin rates, are discussed in additional detail in Chapter 2.

1.4.5 Vesta Dynamical family (the "Vestoids")

As mentioned in Section 1.4.1, a significant outcome of asteroid collisions is the creation of dynamical families. The Vesta family of asteroids, the target of the current study, is one of the largest in the main asteroid belt (refer to Figure 12). It consists of 16,136 asteroids (Nesvorný, 2012), including Vesta itself. The family is bounded in orbital space by the proper element ranges: $2.26 \text{ AU} < a_p < 2.48 \text{ AU}$, $0.075 < e_p < 0.122$, and $5.6 \text{ deg} < i_p < 8.3 \text{ deg}$. The highest density of family members is centered on the location of Vesta (2.36 AU), but is somewhat "stretched" in the radial direction toward the ν_6 secular and 3:1 mean motion resonances.

It is believed that the Vesta dynamical family is primarily the result of a tremendous impact at Vesta's south pole approximately 1 Gy ago (Marchi et al., 2012). This impact created the 500 km Rheasilvia basin, and ejected material into the region of space around Vesta. The volume of material removed by the Rheasilvia impact, however, is significantly more than that represented by the Vesta dynamical family (Nesvorný et al., 2008), indicating that much of the impact material was likely lost to the neighboring resonances.

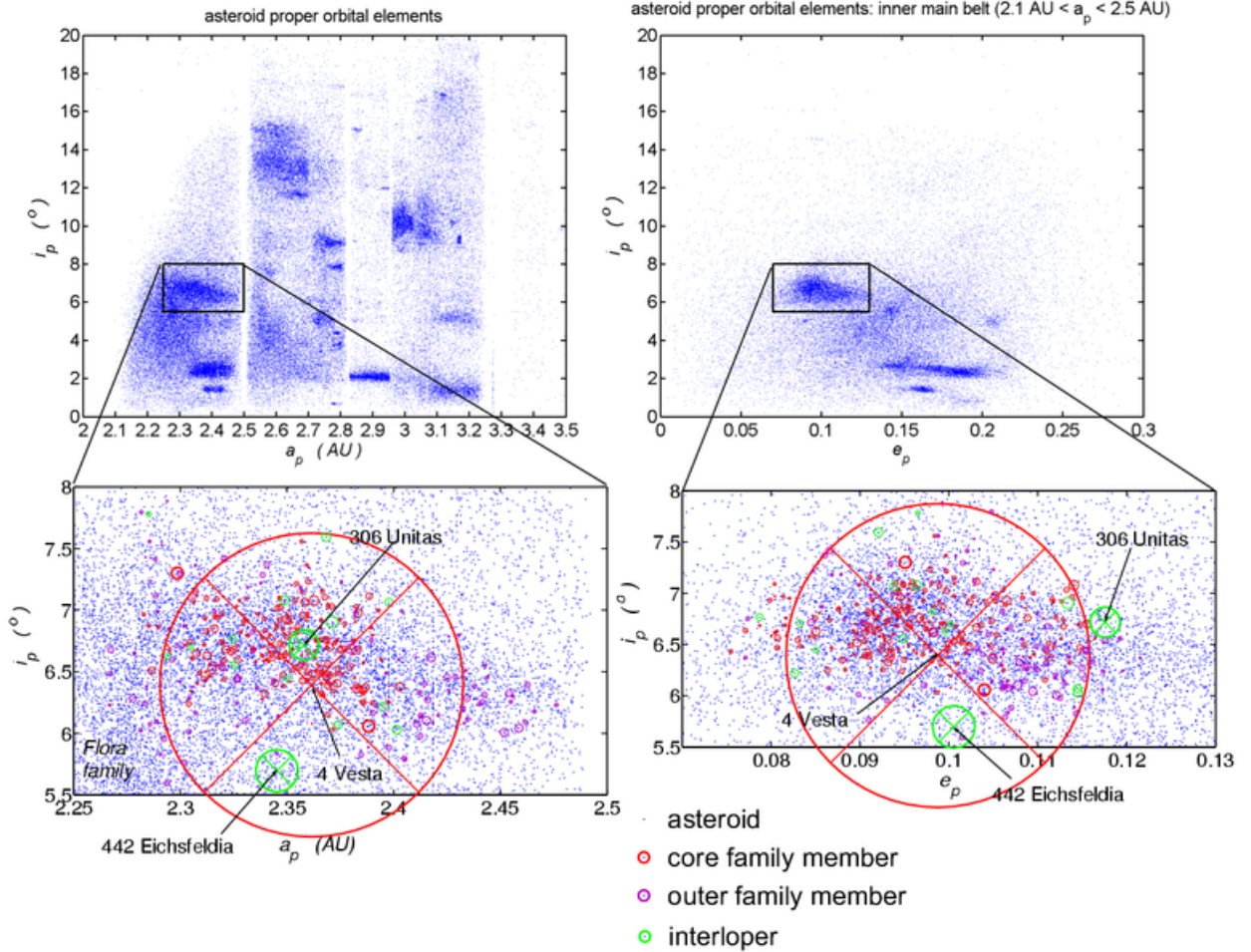


Figure 12. Vesta Dynamical family of Asteroids (Deuar, 2006)

1.5 Current Study

The objective of this investigation was to better constrain the rotational characteristics of the Vesta asteroid family (“the Vestoids”). This study measured the spin rates of several V_p -type asteroids using lightcurve photometry. This information can be used to improve our understanding of the collisional event which created the Vestoids, as well as the mechanisms that have likely delivered members of this family into Earth-crossing orbits and ultimately meteorites (e.g., the HED group) to the Earth’s surface.

Targets for this study were selected using the Carvano et al. (2010) V_p -type asteroid taxonomic classification, which is based on the SDSS MOC4. The V_p -type sub-population has generally not been well-represented in past V-type rotational studies (Hasegawa et al., 2014; Ryan et al., 2004) and represents a set of asteroids which is generally smaller in diameter than those studied previously. The final targets were determined primarily by observability from the telescopes employed during this study: (1) Stone Edge Observatory (G52) in Sonoma, CA; (2) Yerkes Observatory (754) in Williams Bay, WI; and (3) Cerro Tololo Inter-American Observatory (807) in La Serena, Chile. Targets were also restricted to those for which the rotation rate was unknown or had been previously estimated with high levels of uncertainty (Warner et al., 2009). Finally, to the extent possible, priority was given to those objects which had been included in a previous asteroid compositional survey of V_p -type asteroids (Hardersen et al., 2013, 2014a, 2015b; Hardersen, 2016; Hardersen, 2016).

Combining the data obtained from this effort with that available in the literature, this study searches for trends among the rotational characteristics of the Vesta family of asteroids. In addition, a preliminary statistical analysis is applied to identify potential correlations between rotational period, lightcurve amplitude, and asteroid diameter. The results of these analyses are compared with the existing, extensive, multi-disciplinary knowledge of Vesta's origin and collisional history to see what new information can be obtained. It is expected that this study will highlight the importance of the Yarkovsky and YORP effects, which are more pronounced for the smaller diameter asteroid population addressed here.

CHAPTER 2

ASTEROID ROTATION AND LIGHTCURVES

The rotational characteristics of an asteroid provide important clues into its collisional history, dynamic evolution, make-up, shape, and size. As described in Section 1.4.4, several different techniques are employed to measure an asteroid's rotation, including ground-based lightcurve photometry and radar, as well imaging performed by spaceborne telescopes and in situ spacecraft. Lightcurve photometry is perhaps the most common method applied to rotational studies of asteroids, and was the one used in this investigation.

In this chapter, a review of important concepts governing asteroid rotation is provided. The lightcurve photometry technique is described and its application to asteroid rotational studies is summarized, including the compilation of the asteroid LightCurve DataBase (LCDB; Warner et al., 2009). Using data from the LCDB, the rotational characteristics of the asteroid population are examined. Finally, the results of previous lightcurve studies of asteroid families are presented, with particular emphasis on those dedicated to the Vesta family (Hasegawa et al., 2014; Ryan et al., 2004).

2.1 Rotation

An asteroid's rotation is fundamentally described by the angular momentum vector, \vec{L} , as defined below:

$$\vec{L} = \hat{I} \vec{\omega} \quad (1)$$

In this equation, $\vec{\omega}$ is the asteroid spin vector, which describes the instantaneous speed and axis of rotation; and \hat{I} is the moment of inertia tensor, which is defined as follows:

$$\hat{I} = \begin{bmatrix} I_{XX} & I_{XY} & I_{XZ} \\ I_{YX} & I_{YY} & I_{YZ} \\ I_{ZX} & I_{ZY} & I_{ZZ} \end{bmatrix} \quad (2)$$

In Equation 2, the terms I_{XX} , I_{YY} , and I_{ZZ} are the moments of inertia around their respective axes, and the remaining terms are referred to as the products of inertia.

Overall, the moment of inertia tensor describes how the mass of an asteroid is distributed around its instantaneous axis of rotation. For a given asteroid shape, there exists a unique xyz-coordinate system such that all non-diagonal members of the moment of inertia tensor will be zero:

$$\hat{I} = \begin{bmatrix} I_{XX} & \mathbf{0} & \mathbf{0} \\ \mathbf{0} & I_{YY} & \mathbf{0} \\ \mathbf{0} & \mathbf{0} & I_{ZZ} \end{bmatrix} \quad (3)$$

In this case, the terms I_{XX} , I_{YY} , and I_{ZZ} are called the principal moments of inertia, and are typically defined such that $I_{XX} \leq I_{YY} \leq I_{ZZ}$. The corresponding xyz-axes are called the principal axes of inertia. The principal axes of inertia represent an important concept in the rotation of asteroids over long time periods (Pravec et al., 2002), as described in the following section.

2.1.1 *Principal Axis Rotation*

In a general state of rotation, such as that resulting from a collision, the asteroid spin vector, $\vec{\omega}$, varies in time due to changes in the moment of inertia about the instantaneous axis of rotation. For such asteroids, commonly referred to non-principal axis rotators or “tumblers”, the spin vector, $\vec{\omega}$, and angular momentum vector, \vec{L} , are not aligned. As a result, the asteroids experience complex, non-periodic rotation. A well known example of such a “tumbler” is the near-Earth asteroid is (4179) Toutatis (Hudson and Ostro, 1995). Derived from radar imagery, Figure 13 shows a computer model of the asteroid spin state over a duration of nine days. The principal axes are represented in red, green, and blue. Toutatis rotates about its long axis (blue) every 5.41 days, and the rotation axis (yellow) precesses around the angular momentum vector (magenta) on the average of every 7.35 days.

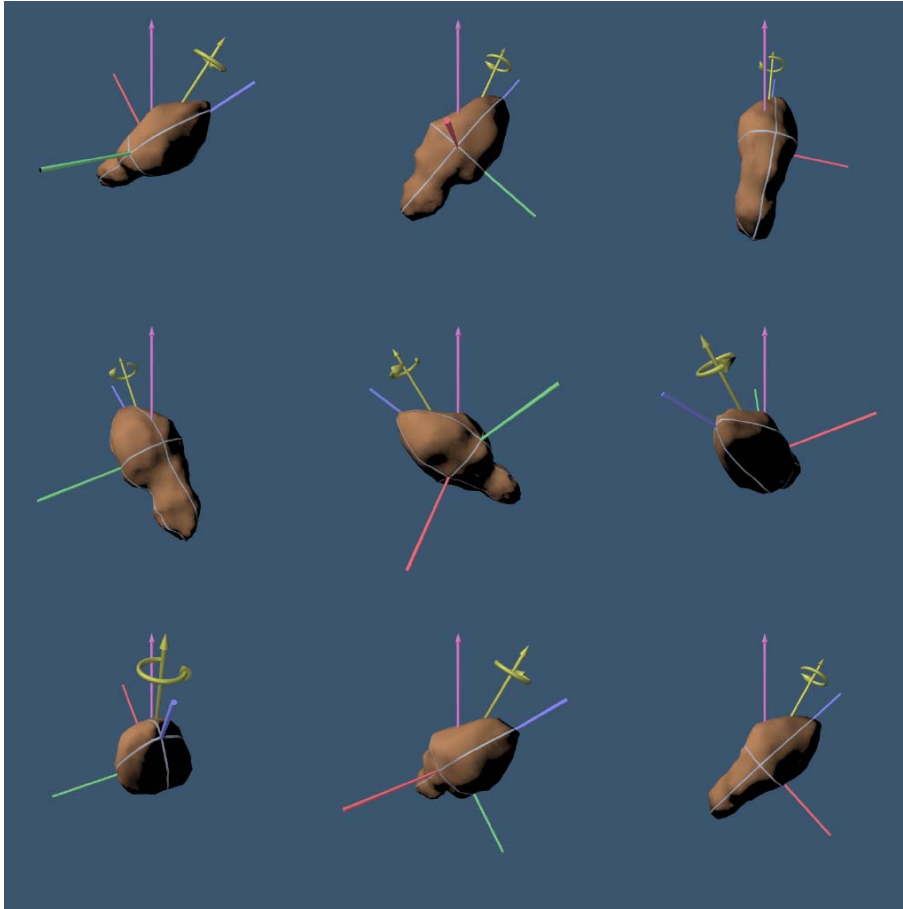


Figure 13. Non-Principal-Axis Rotation of (4179) Toutatis. Computer models of the asteroid are shown at one-day intervals (from left to right, top to bottom). The red, green, and blue axes are the principal axes of inertia. The magenta axis is the angular momentum vector. The yellow axis is the spin vector. (Hudson and Hamilton, 2013)

An asteroid in non-principal axis rotation can be considered in an “excited” rotational state. This motion produces cyclical stresses/strains across the asteroid body. However, because asteroids are not truly rigid bodies and instead are composed of elastic and often loosely assembled material, this rotational energy is dissipated within the asteroid interior. Over time, the asteroid’s rotation approaches a state of minimal rotational energy, resulting in rotation about the principal axis with the largest moment of inertia, I_{ZZ} . For a typical asteroid, modeled as a triaxial ellipsoid (“flattened potato”),

this state is described by rotation about the shortest axial dimension (Z_1), as shown in Figure 14.

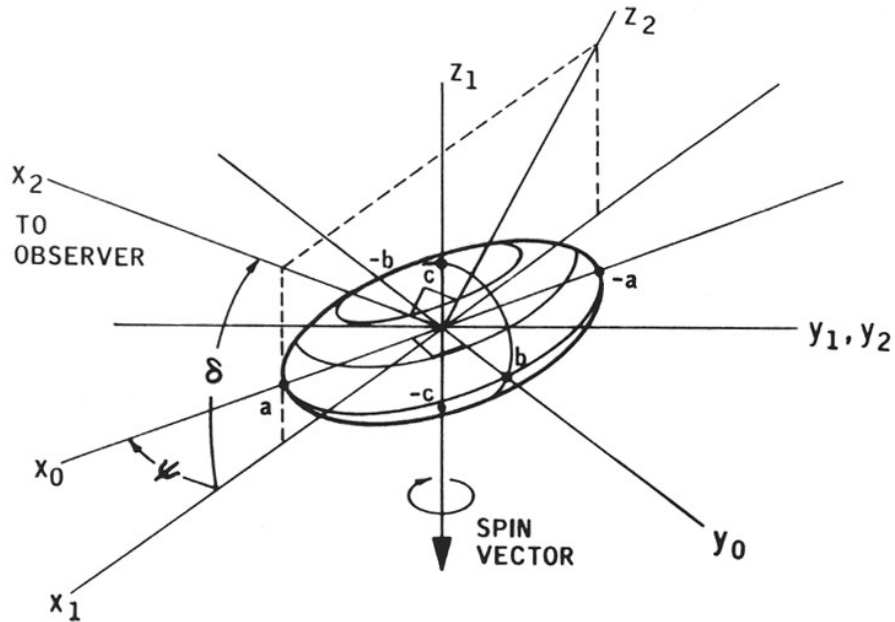


Figure 14. Principal Axis Rotation of a Typical Triaxial Ellipsoid-Shaped Asteroid

The damping timescale of excited, non-principal axis asteroid rotation has been estimated using several different techniques (Paolicchi et al., 2002; Pravec et al., 2002). Harris (1994) expresses the damping timescale, τ , as follows:

$$\tau = \frac{P^3}{C^3 D^2} \quad (4)$$

Where $P = 2\pi/\omega$ is the rotation period in hours, D is the mean diameter in kilometers, C is a constant (approximately 17), and τ is in billions of years. For a typical asteroid with a diameter of 10 km and a rotational period of 5 hours, the damping timescale, τ , is approximately 250,000 years. For most asteroids, therefore, the rotational damping time is significantly smaller than the events (e.g., collisions) causing their excitation. As a result, the vast majority of asteroids rotate in principal axis rotation states. This fact

facilitates the measurement of asteroid rotational period by lightcurve photometry, as described in the following sections.

2.1.2 Rotation Measurement

The angular momentum, \vec{L} , of a spinning asteroid cannot be measured directly from ground-based observations. Instead, such observations are aimed at measuring the spin vector, $\vec{\omega}$. The angular momentum of a given asteroid can then be calculated using this value and an estimate of its moment of inertia, based on the asteroid size, shape, and density. However, an accurate estimation of the moment of inertia typically requires in situ (space mission) measurements.

As mentioned in Section 1.4.4, both radar and optical, ground-based techniques are being applied in the characterization of an asteroid's spin vector. For nearby objects, or those particularly reflective in the radio part of the spectrum, radar imagery can be used to obtain detailed information about both the rotation vector, as well as the shape of the asteroid. The most commonly applied observation technique for this purpose, however, is lightcurve photometry. The lightcurve photometry technique, and a review of its application to asteroid rotational studies, is described in the following section.

2.2 Lightcurve Photometry

The lightcurve photometry technique uses optical observations of an asteroid, obtained over time, to characterize the asteroid's rotational properties. In its most basic form, lightcurve photometry can be applied to measure an asteroid's rotational period. Using more advanced variations of this technique, an asteroid's shape, spin vector, or

even the presence of one or more “companions” can be detected. This type of data can provide invaluable clues about an asteroid’s origin, evolution, and physical properties.

A typical example of an asteroid lightcurve is shown in Figure 15 for (25143) Itokawa (Fujiwara et al., 2006). Itokawa has an elongated shape and rotates around its principal axis with a period of approximately 12 hours. As can be seen in Figure 15, Itokawa’s brightness reaches a maximum when sunlight is reflected from its broad side towards the Earth (Figure 15 A and B). Similarly, Itokawa’s brightness is at a minimum when its narrow end faces the Earth (Figure 15 C and D). The resulting lightcurve has two “lobes” and is typical of most asteroid lightcurves (Warner et al., 2009).

The lightcurve period is equivalent to the rotational period of the asteroid. The lightcurve amplitude also provides useful information. Assuming no significant asteroid surface variegations or geometric scattering effects, the lightcurve can be used to approximate the general shape of the asteroid (Harris et al., 2014), as follows:

$$A = -2.5 \log \left(\frac{CS_{min}}{CS_{max}} \right) \quad (5)$$

where A is the lightcurve amplitude, CS_{min} is the minimum cross-sectional area of the asteroid, and CS_{max} is the maximum cross-sectional area of the asteroid. In addition, in cases where the amplitude minima or maxima of a dual-lobed lightcurve are asymmetric (refer to the minimum amplitudes defined by Figure 15 C and D), the difference in these amplitudes can be used to approximate the surface area differences of the opposing sides. More quantitative characterizations of an asteroid’s shape using lightcurves, a technique called inversion, require that such data to be obtained over long periods of time (e.g., multiple apparitions) (Kaasalainen, 2001a, 2001b).

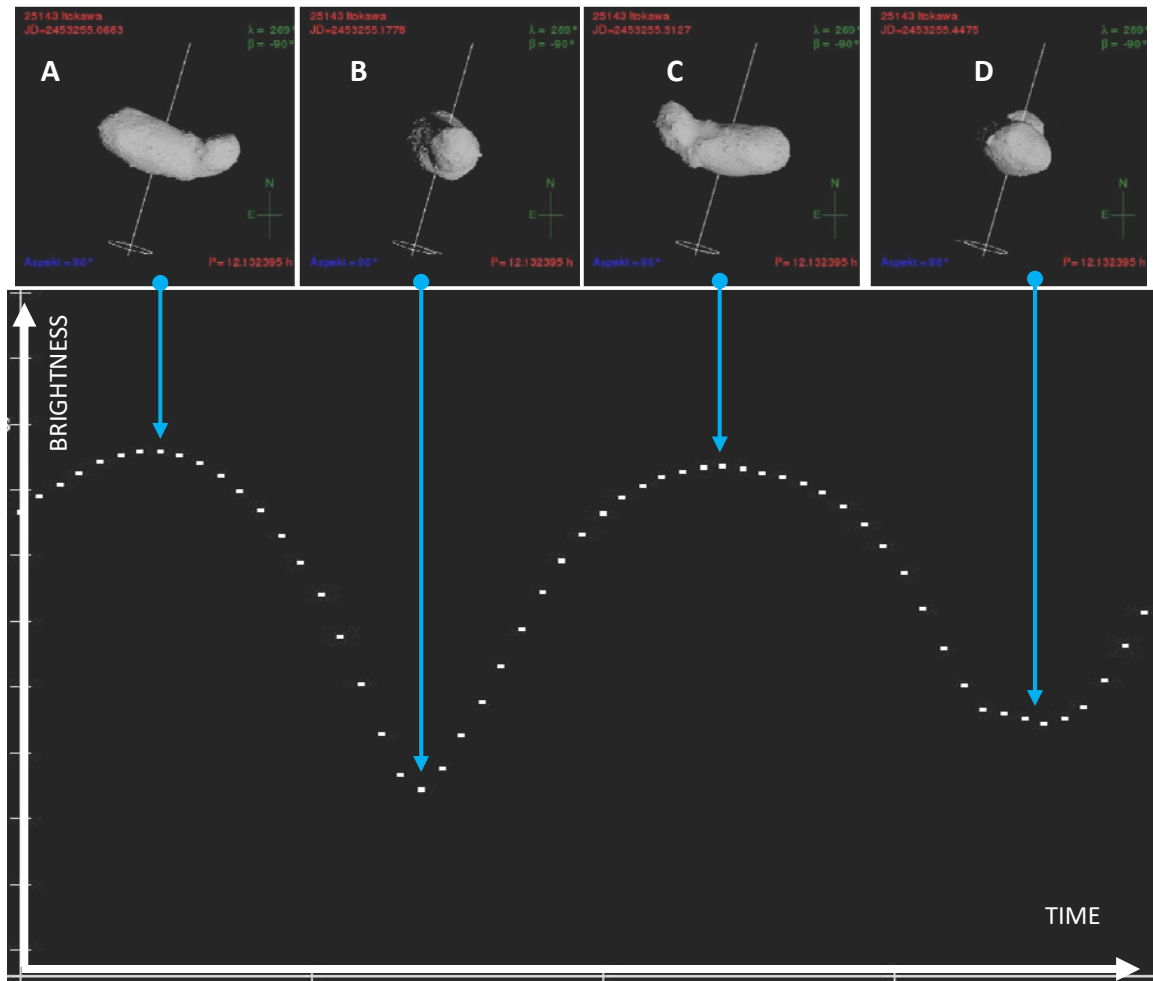


Figure 15. (25143) Itokawa Lightcurve is shown for four rotational positions of the asteroid. Blue lines indicate the part of the lightcurve corresponding to each asteroid orientation.

2.2.1 Lightcurve Database (LCDB)

Lightcurve measurements can be conducted with relatively inexpensive equipment, but typically require significant amounts of observing time. For this reason, much of the work is done by the amateur astronomy community. There do exist, however, several major initiatives dedicated to asteroid lightcurve studies that are sponsored by various private and educational research groups (Behrend, 2017; Chang et al., 2015; Pravec, 2017; Warner et al., 2009). Together, the lightcurve measurements of these individuals

and groups is compiled in a central repository called the LightCurve Database (LCDB; Warner et al., 2009).

The LCDB contains asteroid lightcurve data, including rotation rate and amplitude, along with other asteroid properties (e.g., diameter, albedo, taxonomic type, etc.) for more than 16,000 asteroids (at last count). The LCDB facilitates collaboration amongst the global community of asteroid lightcurve investigators and provides an invaluable resource on which to base statistical analyses of the rotational characteristics of asteroids. In the following section, current data from the LCDB is used to discuss the distribution of lightcurve-derived spin rates and amplitudes of the asteroid population.

2.3 Asteroid Population

An analysis of the distribution of rotational properties within the asteroid population can reveal important information about its collisional history, dynamic evolution, and make-up. In the following sections, the asteroid spin rate distributions are used to discuss the so-called “spin barrier” and its implications for asteroid make-up. In addition, the similarities between these distributions and a standard Maxwellian (also called Maxwell-Boltzmann) distribution are used to aid in understanding asteroid collisional dynamics, as well as the role of thermal effects like YORP.

2.3.1 *Spin Barrier*

The distribution of asteroid spin rates has a strong dependence on diameter. Figure 16 shows a graph of asteroid rotational period/spin rate as a function of asteroid diameter. The data in this plot are based on over 10,500 main belt and near-Earth

asteroids drawn from the LCDB in June 2017. The variation of the average spin rate can be roughly estimated by dividing the asteroids into three groups: (1) large ($D = 40$ km or greater); (2) medium ($D = 0.1$ to 40 km), and (4) small ($D < 0.1$ km). Using the data from Figure 16, the average spin rate is approximately 2 rev/day (12 hours) for the large group and 4 rev/day (6 hours) for the medium group. These averages are in good agreement with those cited by Pravec et al. (2002). The small diameter group is dominated by near-Earth asteroids and is characterized by a large number of very fast (> 100 rev/day).

Perhaps the most obvious feature in Figure 16 is an apparent limit on the maximum spin rate for asteroids within the medium group ($D = 0.1$ to 10 km). This so-called “spin barrier”, approximately 11 rev/day, is represented in Figure 16 with a dotted red line. This limit corresponds closely to the maximum spin rate that a strengthless body (i.e. held together only by gravity) of density 2.0 g/cm^3 could sustain before starting to break apart (Pravec and Harris, 2000). Hence, the presence of this limit implies that most asteroids in this size range are in fact loosely bound, gravitationally-assembled aggregates with little tensile strength (Pravec et al., 2002). Such so-called “rubble pile” asteroids were likely formed by debris which was gravitationally reassembled soon after a collision. The loose aggregate nature of these asteroids is important for understanding their bulk density, shape, susceptibility to tidal effects, cratering mechanics, and other physical and dynamic properties.

If asteroids governed by the “spin barrier” are “rubble piles”, then it is likely that those which exist beyond it are, by contrast, predominantly intact bodies. Hence, the

small asteroid group ($D < 0.1$ km), with a predominance of very fast rotators, is likely composed of monolithic collisional debris.

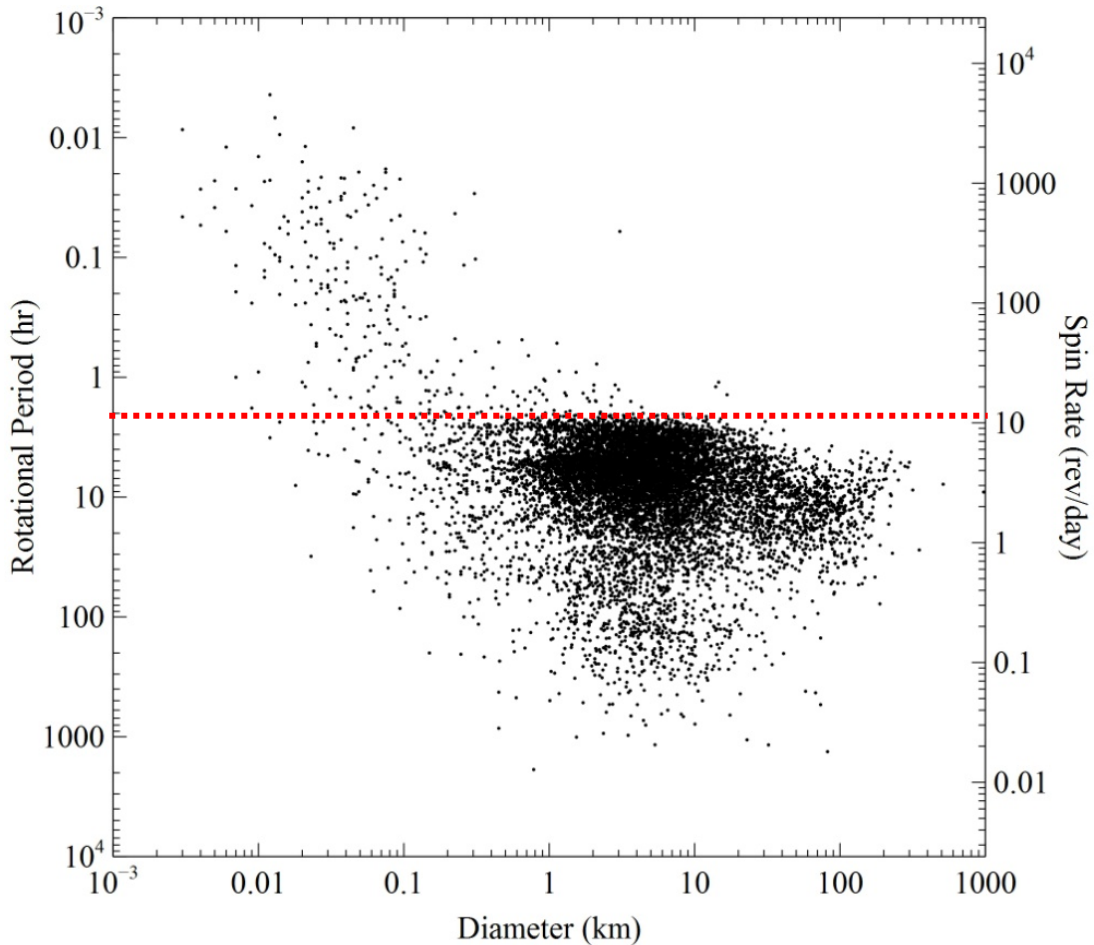


Figure 16. Asteroid Rotational Period vs. Diameter. Data represents 10,588 main belt and near-Earth asteroids taken from the LCDB (June 2017). The red dotted line represents the “spin barrier” for larger asteroids at a spin rate of approximately 11 rev/day.

The asteroid “spin barrier” can also be visualized in terms of the lightcurve amplitude, a rough indicator of overall shape. Figure 17 shows the lightcurve amplitude as a function of spin rate for the same data set presented Figure 16. The red dotted line in Figure 17 represents the “spin barrier” of a spherical body with a bulk density of 2 g/cm^3 (Pravec and Harris, 2000). From this plot, it can be seen that the majority of

asteroids closest to the “spin barrier” tend to have small lightcurve amplitudes. Smaller lightcurve amplitudes typically imply more symmetric asteroid shapes. This behavior is consistent with the “rubble pile” nature of these asteroids, which would assume increasingly spherical shapes as their rotation rates increased.

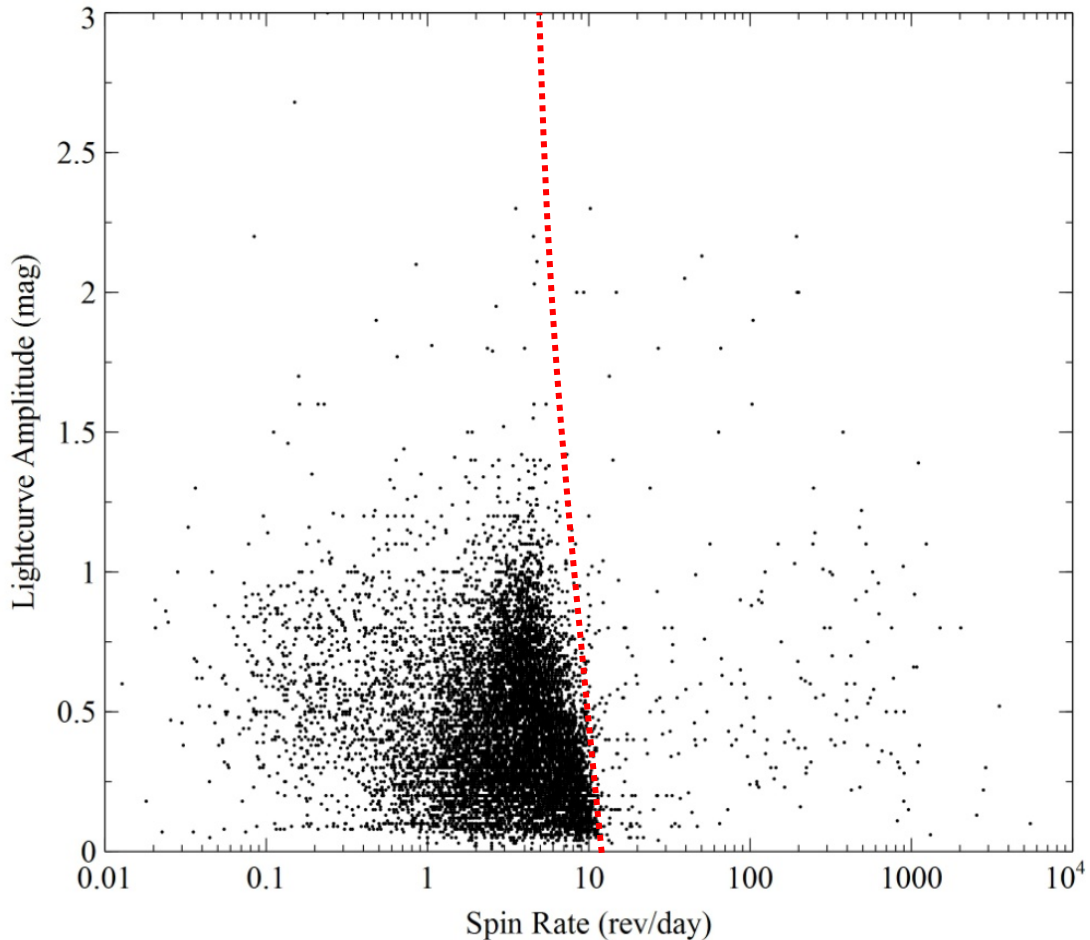


Figure 17. Asteroid Lightcurve Amplitude vs. Rotational Period. Data represents 10,588 main belt and near-Earth asteroids taken from the LCDB (June 2017). The red dotted line represents the upper spin rate limit of a body with a bulk density of 2 g/cm^3 which can held together by gravitational forces alone (Pravec and Harris, 2000).

2.3.2 Maxwellian Distribution

By analyzing the distribution of asteroid spin rates, an understanding of their dynamic evolution can also be obtained. One approach to this analysis is to compare the

spin rate distribution of a group of asteroids to a Maxwell-Boltzmann distribution, also called a Maxwellian distribution. The Maxwell-Boltzmann distribution was originally derived to describe the statistical particle dynamics in an ideal gas. As applied to asteroids, Pravec et al. (2002) states that “...the distribution of spin rates of asteroids is Maxwellian if all the three components of $\vec{\omega}$ are distributed according to a Gaussian with zero mean values and equal dispersions”. This technique was initially applied to asteroid rotational rates by Harris and Burns (1979). In this study and others (Binzel et al., 1989; Farinella et al., 1981; Fulchignoni et al., 1995), asteroid spin rate distributions close to the Maxwellian distribution were considered to be “collisionally relaxed” (Pravec et al., 2002). In other words, the rotational characteristics of the given asteroid population are considered to be primarily determined by the collision(s) from which they were formed (Salo, 1987). For asteroid spin rate distributions which were not Maxwellian, other effects (e.g., YORP) are considered important.

Figure 18 shows a histogram of the normalized spin rate for the main belt and near-Earth asteroid populations. The data in this plot are based on over 10,500 main belt and near-Earth asteroids drawn from the LCDB in June 2017. The black dotted line shown in Figure 18 represents the Maxwellian distribution which would describe this population. It is clear from this plot that the asteroid population as a whole is not Maxwellian. This is not surprising as the importance of non-collisionally derived dynamics, including Yarkovsky/YORP and resonances, is well known.

However, an important finding of the asteroid spin rate studies cited previously is that the spin rate distribution of the large group of asteroids ($D \geq 40$ km) is Maxwellian.

Figure 19 shows a histogram of the normalized spin rate for the asteroids with $D \geq 40$ km. The data in this plot are based on the same data set as Figure 18. The black dotted line shown in Figure 19 represents the Maxwellian distribution which would describe this population. It can be seen from this plot that the spin rate distribution of the large asteroid group is indeed closer to Maxwellian, although there are some excesses for faster rotators. This trend indicates that the rotational dynamics of the larger asteroids continue to be dominated by the collisions from which they were formed. In this case, effects like Yarkovsky/YORP play a significantly diminished role.

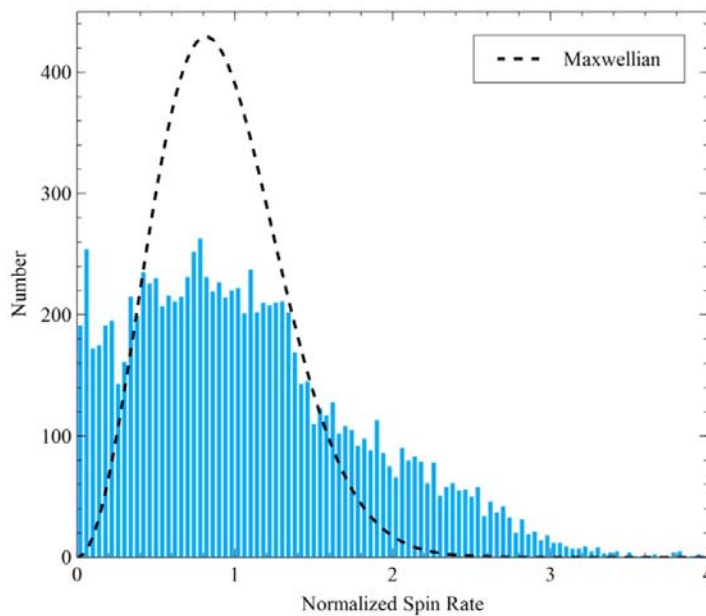


Figure 18. Asteroid Spin Distribution (MB and NEA) Data represents 10,588 main belt and near-Earth asteroids taken from the LCDB (June 2017). The dotted black line represents a corresponding Maxwellian distribution.

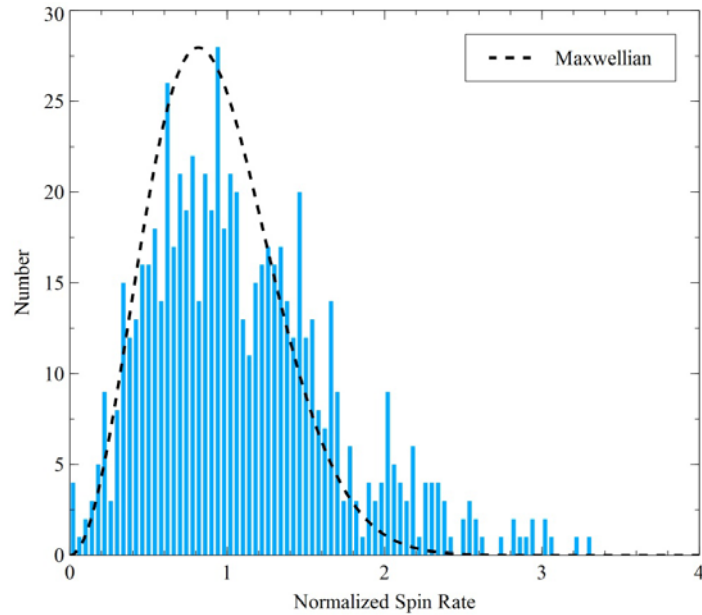


Figure 19. Asteroid Spin Distribution ($D \geq 40\text{km}$). Data represents 10,588 main belt and near-Earth asteroids taken from the LCDB (June 2017). The dotted black line represents a corresponding Maxwellian distribution.

2.4 Rotational Studies of Asteroid Families

The current study is focused on improving understanding of the rotational characteristics of the Vesta family. In the literature, there are a few previous studies which have been devoted to understanding the rotational properties of different asteroid families. Perhaps the most well known of these is the work conducted by Binzel (1988) and Binzel et al. (1989) to study the Koronis and Eos families. These studies found that the distribution of rotational rates in the Eos family approximated a Maxwellian distribution, indicating that they were primarily collisionally derived. The Koronis family did not show a similar Maxwellian distribution, but instead was marked by unusually large lightcurve amplitudes and a potential alignment of spin axes.

This alignment of spin axes was confirmed by Slivan et al. (2003) and Vokrouhlicky et al. (2003) who showed that of the spin axes of some members of the Koronis were

aligned due to a dynamical mechanism, called the Slivan effect. The Slivan effect locks the spin axis of the 20–40 km-diameter asteroids in a preferential direction when the precessional rate of the axis matches that of Saturn’s longitude of nodes. Kryszczyńska (2013) and Kryszczyńska et al. (2012) found evidence of the Slivan effect in the Flora family as well.

Alvarez-Candal et al. (2004) performed a rotation study of the Themis, Maria, and Eos families. Using existing data in the literature, combined with newly measured lightcurves from 17 asteroids in the aforementioned families, the authors performed a statistical analysis aimed at detecting possible correlations between rotational periods, overall lightcurve amplitudes, and object diameters. No significant correlations were found, but a weak anti-correlation was identified between asteroid diameter and rotational period.

Finally, there are two rotational studies in the literature focused specifically on the Vesta family. Ryan et al. (2007, 2004) conducted a lightcurve survey of Vesta family members analyzing both asteroid rotational rate and shape. In total, 34 Vesta family asteroids were observed and 22 rotational periods were derived. Of these, 10 asteroids were observed over multiple apparitions and phase angles. After the discovery of a binary asteroid (3782 Celle) amongst this group (Ryan et al., 2004), much of subsequent published work was dedicated to studying the existence of multiple asteroid systems in the Vesta family (Ryan et al., 2004). No rotational analysis of the asteroids as a group was conducted.

Hasegawa et al. (2014) also performed a lightcurve study of the Vesta family. The authors observed 13 V-type asteroids. Rotational periods were derived for 11 of these asteroids. Combining these measurements with rotational data for Vesta family members available in the literature, the authors demonstrated that the spin rate distribution of this group was not consistent with a Maxwellian distribution. They cited thermal radiation effects (i.e. YORP) as the likely cause of this discrepancy.

CHAPTER 3

MEASUREMENTS AND DATA REDUCTION

This chapter describes the hardware, software, and methods used to obtain, calibrate, reduce, and analyze the data for this study. The first section describes the process of performing asteroid observations, including the telescopes and cameras used in this study, how targets were selected, and the overall observing strategy. The next section explains how the resulting data was calibrated and reduced to produce asteroid lightcurves. The final section details how the asteroid lightcurves were analyzed to extract their amplitude and period.

3.1 Asteroid Observations

The observations supporting this study were performed over the course of approximately eight months (November 2016 to June 2017). This effort was made possible by spreading the observations among five different telescopes. Furthermore, a target selection and observation strategy which maximized the amount of good quality data during this time period was key. In this section, these observational components of the study are described.

3.1.1 Telescopes

Asteroid observations were obtained using five telescopes located in both North and South America. These facilities included: (1) Stone Edge Observatory (SEO) in Sonoma, CA (refer to Table 1), (2) PROMPT 1, 3, and 6 at the Cerro Tololo Inter-American Observatory (CTIO) in La Serena, Chile (refer to Table 3 and Table 2, respectively), and (3) Yerkes-41 at the Yerkes Observatory in Williams Bay, WI (refer to Table 4). All of the aforementioned telescopes are remotely controlled. The PROMPT and Yerkes telescopes are members of the Skynet Robotic Telescope Network (<https://skynet.unc.edu>). The Skynet network provides web-based access to its telescopes which supports the queuing of targets, selection of imaging parameters, bias/dark/flat image calibration, World Coordinate System (WCS) plate-solving, and image storage and retrieval services. The Skynet telescopes, when not devoted to their primary scientific missions (e.g., gamma ray burst follow-up, near-Earth asteroid astrometry, etc.) are available to observers for educational purposes. The Stone Edge Observatory is not a member of Skynet, but provides similar web-based (<https://stoneedgeobservatory.com>) and command line remote functionality.

The individual observatory and telescope specifications are provided in Table 1 to Table 4. This information includes observatory locations and designations, telescope parameters (aperture, focal length, filters, etc.), as well as the associated CCD specifications. All of the telescopes are of the basic Cassegrain reflector design, with SEO and P6 using the Ritchey-Chretien variant, and P1 and P3 using the Dall-Kirkham type. Each of the telescopes is equipped with a full complement of filters. However, for

this study, only the clear filter or open setting (i.e. no filter) was used. This was done in order to maximize the light received from the relatively faint targets. The average absolute magnitude for the V_p -type asteroids is approximately 15.7. Similarly, a CCD binning of 2x2 was used for all SEO and PROMPT observations in order to maximize the target flux and better match the typical seeing at the given observatory.

Table 1. Stone Edge Observatory (SEO)

Location / Code	Sonoma, CA, USA / G52
Latitude / Longitude	38.259° / -122.440°
Altitude	8 m
Type	Ritchey-Chretien
Aperture	0.51 m (20 in.)
Focal Length / Ratio	4115 mm (162 in) / f8.1
Filters	u', g', r', i', z', H-alpha, ¹ Clear
Field Of View	23.7 x 15.8 arcmin (STXL-6303E), 25.6 x 25.6 arcmin (CG230)
CCD:	
<i>Model</i>	FLI CG230
<i>Resolution</i>	2048 x 2048 pixels
<i>Pixel Size</i>	15 μ m
<i>Image Scale</i>	0.75 arcsec/pixel
<i>A/D Resolution</i>	16-bit
<i>A/D Gain</i>	1.85e-/ADU
<i>Binning</i>	1x1, ¹ 2x2... 8x2048
<i>Operational Temp.</i>	-20° C

¹Filter/Binning setting used for observations.

Table 2. PROMPT 6 (CTIO)

Location / Code	La Serena, Chile / 807
Latitude / Longitude	-30.172° / -70.801°
Altitude	2304 m
Type	Ritchey-Chretien
Aperture	0.41 m (16 in.)
Focal Length / Ratio	7081 mm (278.8 in) / f17.3
Filters	U, B, V, R, I, Red, Green, Blue, Lum, H-alpha, ¹ Open, Clear
Field Of View	14.9 x 14.9 arcmin
CCD:	
<i>Model</i>	Andor Aspen CG230
<i>Resolution</i>	2048 x 2048 pixels
<i>Pixel Size</i>	15 μ m
<i>Image Scale</i>	0.437 arcsec/pixel
<i>A/D Resolution</i>	16-bit
<i>A/D Gain</i>	2.79e-/ADU
<i>Binning</i>	1x1, ¹ 2x2...8x2048
<i>Operational Temp.</i>	-35° C

¹Filter/Binning setting used for observations.

Table 3. PROMPT 1/PROMPT 3 (CTIO)

Location / Code	La Serena, Chile / 807
Latitude / Longitude	-30.172° / -70.801°
Altitude	2304 m
Type	Dall-Kirkham
Aperture	0.6 m (24 in.)
Focal Length / Ratio	4000 mm (157.5 in) / f6.6
Filters (P1)	U, B, V, R, I, Red, Green, Blue, Lum, H-alpha, OIII, ¹ Clear
Filters (P3)	u', g', r', i', z', Red, Green, Blue, Lum, SII, *Clear
Field Of View	11.4 x 11.4 arcmin
CCD:	
<i>Model</i>	Apogee Alta F47
<i>Resolution</i>	1024 x 1024 pixels
<i>Pixel Size</i>	13 μm
<i>Image Scale</i>	0.668 arcsec/pixel
<i>A/D Resolution</i>	16-bit
<i>A/D Gain</i>	1.17e-/ADU
<i>Binning</i>	1x1, ¹ 2x2...8x2048
<i>Operational Temp.</i>	-20° C

¹Filter/Binning setting used for observations.

Table 4. Yerkes-41 (Yerkes Observatory)

Location / Code	Williams Bay, WI, USA / 754
Latitude / Longitude	42.578° / -88.5410°
Altitude	267 m
Type	Cassegrain
Aperture	1.0 m (40 in.)
Focal Length / Ratio	8200 mm (322.8 in) / f8.2
Filters	u', g', r', i', z', B, H-alpha, ¹ Clear
Field Of View	10.3 x 10.3 arcmin
CCD:	
<i>Model</i>	SBIG STL-1001E
<i>Resolution</i>	1024 x 1024 pixels
<i>Pixel Size</i>	24 μm
<i>Image Scale</i>	0.607 arcsec/pixel
<i>A/D Resolution</i>	16-bit
<i>A/D Gain</i>	1.97e-/ADU
<i>Binning</i>	¹ 1x1, 2x2, 3x3, 9x9, 1xN
<i>Operational Temp.</i>	-20° C

¹Filter/Binning setting used for observations.

3.1.2 Target Selection

The targets for this study were selected from the V_p -type asteroids identified by Carvano et al. (2010). The complete set of asteroids classified in this study are available on the NASA Planetary Data System (PDS) (Hasselmann et al., 2012). The Carvano et al. (2010) database classifies 107,466 SDSS MOC4 observations of 63,468 unique asteroids. Of these, 2,855 asteroids are classified as V_p -type.

The rotational properties of this population of asteroids are poorly constrained, with only approximately 6% of V_p -type asteroids having rotational period estimates available in the LCDB. In a step towards addressing this deficit, this study focused on target asteroids which were either not present in the LCDB or had rotational period estimates with high levels of uncertainty. This group was defined by a LCDB quality code rating (U) of 2 or less.

The quality code rating system for asteroid lightcurves is defined in Warner et al. (2009) and has values that range from 1 (highest uncertainty) to 3 (lowest uncertainty), with “+” and “-” designations used to indicate intermediate scores. According to Warner et al. (2009), a rating of 1 is defined by a “result based on fragmentary lightcurve(s)...[and] may be completely wrong.” A rating of 2 is defined by a “result based on less than full coverage, so that the period may be wrong by 30% or so...[or] may be wrong by an integer ratio”, and a rating of 3 “denotes a secure result with no ambiguity and full lightcurve coverage.” By filtering out all V_p -type asteroids with existing, high quality period estimates ($U > 2$), a total of 2,815 V_p -type asteroids were

identified as potential targets. Of these, 2,694 asteroids had no available rotational information, and 121 asteroids had rotational period estimates with $U \leq 2$.

In the next step, the asteroids were evaluated based on their “observability” during the period from November 2016 to June 2017. The following “observability” criteria were applied:

- Elevation of 30° or greater
- Apparent magnitude (m) of 17 or brighter
- Nightly availability of 5 hours or more

The minimum elevation (30°) was chosen to minimize atmospheric effects, as the airmass changes rapidly below that value. The minimum brightness ($m \leq 17$) was defined by the limiting magnitudes of the available telescopes. The minimum nightly availability was selected based on the mean rotational period of small asteroids (~ 5 hours) and the desire to capture full rotational periods in a single observing session, when possible. After applying these criteria, a final list of 99 target asteroids was identified, 72 without rotational period estimates in the LCDB and 17 asteroids which have rotation period estimates with $U \leq 2$. A description of how specific asteroids from this final target list were chosen for observation is provided in the following section.

3.1.3 Observation Strategy

The goal of this investigation was to obtain a minimum of 10 high quality asteroid lightcurves. As telescope time was limited, it was important to develop an observational strategy which would maximize productivity during the planned period of observations (November 2016 to June 2017). To start, using the JPL HORIZONS ephemerides web

service (<https://ssd.jpl.nasa.gov/horizons.cgi>), a Gantt-like (i.e. project schedule) chart was created for each of the three observatories showing which asteroids from the target list would be available for viewing at a given time. An example of such an “Aster-Gantt” chart is shown in Figure 20. This chart shows the “windows” of visibility for each of the target asteroids observable from CTIO. Each bar includes a data point and value which indicates the time and associated apparent magnitude (m) of brightest appearance. Using this chart, asteroid observations could be optimally planned in coordination with available telescope time.

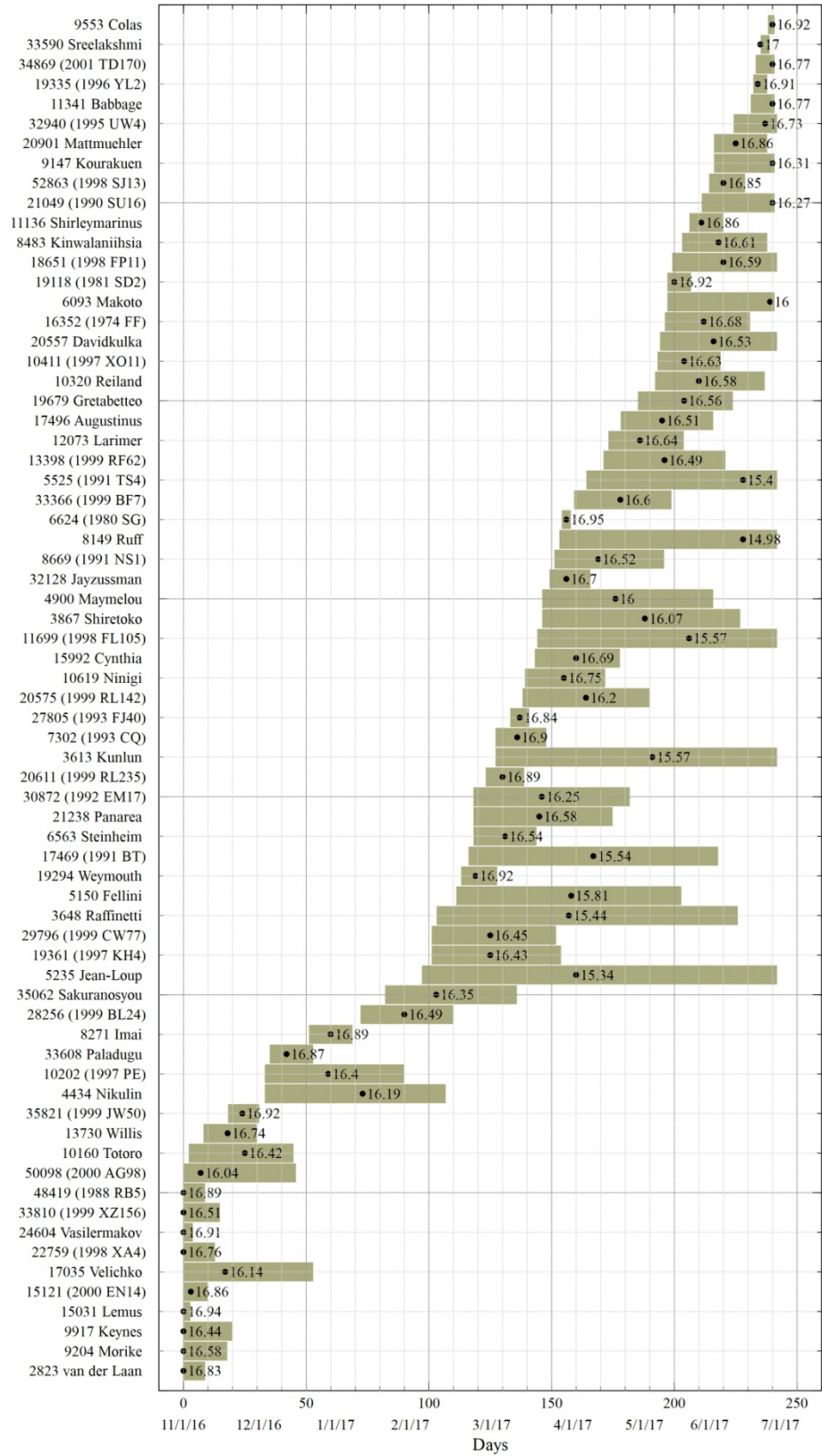


Figure 20. Aster-Gantt Observation Planning Chart (CTIO)

In addition to this scheduling tool, a Java-based application was developed to provide more detailed observing information as the planned date of observation approached. Using the JPL HORIZONS ephemeris service, this tool provides information describing the target coordinates, duration of availability, elevation range, phase angle, as well as the phase of the moon, angular distance from the moon, and the angular distance from the galactic plane. An example of this output is shown in Figure 21. In general, targets within 30° of the moon (Moon Phase Angle) were excluded in order to minimize background sky brightness for these relatively faint objects. In addition, targets within 20° of the galactic plane (Galactic Latitude) were excluded in order to avoid dense star fields which can make accurate asteroid aperture photometry difficult.

```

3613 Kunlun (1982 VJ11):
    06/01/2017 @ 00:00 for 8.5 hours.
    RA/DEC (transit) = 15:02:11.64 -13:41:08.4.
    Magnitude = 16.09. Min/Max Elev. = 30.7786/73.4986 deg. Phase Angle = 9.9968 deg.
    Max. Magnitude = 15.57 on 05/11/2017 (Moon Phase Angle = 1.232 deg, Moon Illumination = 99.7%).
    Moon Phase Angle = 73.5 deg. Moon Illumination = 44.1%.
    Galactic Latitude = 38.287798 deg.
3648 Raffinetti (1957 HK):
    06/01/2017 @ 00:00 for 6.8 hours.
    RA/DEC (transit) = 12:43:01.17 -03:20:42.9.
    Magnitude = 16.75. Min/Max Elev. = 31.2137/63.2595 deg. Phase Angle = 23.5641 deg.
    Max. Magnitude = 15.44 on 04/07/2017 (Moon Phase Angle = 50.0 deg, Moon Illumination = 82.8%).
    Moon Phase Angle = 37.7 deg. Moon Illumination = 44.1%.
    Galactic Latitude = 59.456863 deg.
3867 Shiretoko (1988 HG):
    06/01/2017 @ 00:00 for 8.5 hours.
    RA/DEC (transit) = 14:50:29.46 -11:45:45.1.
    Magnitude = 16.63. Min/Max Elev. = 30.3117/71.6339 deg. Phase Angle = 10.7904 deg.
    Max. Magnitude = 16.07 on 05/08/2017 (Moon Phase Angle = 32.3 deg, Moon Illumination = 92.9%).
    Moon Phase Angle = 70.2 deg. Moon Illumination = 44.1%.
    Galactic Latitude = 41.542527 deg.
4900 Maymelou (1988 ME):
    06/01/2017 @ 00:00 for 8.0 hours.
    RA/DEC (transit) = 13:50:18.57 -08:28:26.4.
    Magnitude = 16.93. Min/Max Elev. = 31.8445/68.3638 deg. Phase Angle = 17.3982 deg.
    Max. Magnitude = 16.0 on 04/26/2017 (Moon Phase Angle = 172.4 deg, Moon Illumination = 0.5%).
    Moon Phase Angle = 55.1 deg. Moon Illumination = 44.1%.
    Galactic Latitude = 51.636438 deg.
5235 Jean-Loup (1990 SA1):

```

Figure 21. Daily Observation Planning Tool (June 1, 2017 @ CTIO)

Once a target was identified for observation, a preliminary measurement was obtained in order to determine the exposure time required to achieve a minimum signal-to-noise ratio (SNR) of 30. A signal-to-noise ratio of 30 is equivalent to an uncertainty in magnitude of approximately 0.035. This SNR goal was determined based on the capabilities of the available telescopes, the typical brightness of the asteroids in the target list, and “rules of thumb” expressed in Brian Warner’s “A Practical Guide to Lightcurve Photometry and Analysis” (Warner, 2006).

The limitations of time and available resources for this study, combined with the objective to obtain 10 or more asteroid lightcurves, effectively excluded measurements of long period rotators ($P > 10$ hours). This bias is common in lightcurve studies; and as a result, the population of slow rotators is generally poorly constrained. For this study, in order to distinguish long period rotators, measurements were obtained over a duration of approximately 3 hours the first night a given target was observed. If the resulting lightcurve did not display any recognizable features (e.g. “peaks” or “valleys”) during this period, the target was set aside and the next target pursued. The potential impact of these excluded targets will be discussed in Chapter 4.

3.2 Data Reduction

This section describes the reduction of the raw asteroid images to produce lightcurves. This process includes image calibration, plate-solving, photometry, and lightcurve alignment and period determination. The software applications used to perform these steps are also identified.

3.2.1 Calibration

Before a photometric analysis can be applied, the asteroid images obtained from the telescopes must be calibrated. These calibrations include the application of bias, dark, and flat frames. A bias frame is used to correct for signal in the image which is derived solely from the CCD electronics. A bias frame is typically a zero-length exposure taken with the camera shutter closed. In some cases, such as for SEO, the CCD is not capable of zero-length exposures and instead uses the shortest exposure time permitted by the camera (for SEO, this is 0.1 seconds). Typically, 50-100 individual bias frames are averaged to create a master bias calibration frame.

A dark frame is used to correct an image for signal produced by thermal effects (i.e. electrons generated by atomic collisions). While the telescope cameras are mechanically cooled to reduce these effects, the dark signal remains a significant source of error that must be corrected. Dark calibration is dependent on CCD temperature and exposure time. Both the dark and asteroid image frames should be taken at the same CCD temperature. In addition, the dark frame exposure time should ideally match the exposure time of the asteroid image. However, in most cases, a master dark frame is created with an exposure time close to the “typical” asteroid image exposure time and is scaled appropriately.

A flat frame is used to correct for pixel-to-pixel differences in the sensitivity of the CCD, vignetting effects, as well as artifacts present in the optical path (e.g., dust, etc.). The flat frames used in this study were obtained at dusk using the twilight sky as a light source and were normalized before being used to scale the asteroid image. Flat frames

should be taken using the same filter as that used for asteroid imaging (“Clear” or “Open” for this study).

The bias, dark, and flat frames were applied to the raw asteroid images using a custom Python script which employed the *ccdproc* package (<http://ccdproc.readthedocs.io/en/latest/>) of astropy (<http://www.astropy.org/>), the popular Python library for astronomy. This script allowed for easy, efficient calibration of the large number (> 100) of asteroid images typically required to produce a lightcurve. The calibration process is described by the equation shown below:

$$calibrated = \frac{(raw - bias - scale * (dark - bias))}{flat} \quad (6)$$

where *scale* represents the ratio of the exposure times of the *raw* image and *dark* frame. In Equation 6, the *flat* frame has already been bias and dark corrected in a similar fashion to that shown for the raw image.

3.2.2 Plate-Solving (WCS)

The determination of an asteroid lightcurve from a set of time-lapsed asteroid images requires that the location of the asteroid in the image be precisely known. The location of a given image in the sky is typically defined by World Coordinate System (WCS) parameters embedded in the header of the associated FITS (Flexible Image Transport System) image file. This “plate-solving” process is done automatically by the image pipeline employed by Skynet telescopes (PROMPT and Yerkes) used in this study. However, the images obtained using the Stone Edge Observatory required post-processing. The WCS solutions for these images were calculated using a custom Python

script which was integrated with a local copy of astrometry.net’s “solve-field” application (<http://astrometry.net/downloads/>). The “solve-field” application uses a repository of star “plates” (index files) to precisely determine the celestial coordinates of a given FITS image.

3.2.3 Photometry

Photometry is the process of estimating the light flux of a given object from a telescopic image. For asteroid lightcurves, both the brightness of the asteroid (the target) and the surrounding stars (standards of comparison) is determined using photometry. This section describes the differential aperture photometry method applied in this study.

3.2.3.1 Differential Photometry

In differential photometry, the light flux of a given object is expressed in terms of a difference relative to the flux of some other object (or objects) in the same field of view. For asteroid photometry, this reference flux is associated with a *comparison* star or with the average of several comparison stars in the same field of view. This difference, sometimes called the delta magnitude, can be expressed as follows:

$$\Delta m = -2.5 \log_{10} \frac{I_{asteroid}}{I_{comp}} \quad (7)$$

where I represents an instrumental flux, corresponding to the number of electrons recorded by the CCD for a given object. The quantity, $I_{asteroid}$, is the instrumental flux of the asteroid, and I_{comp} is the instrumental flux of the comparison star (or an average of comparison stars).

This approach is particularly applicable to cases in which the flux variations relative to the reference are fairly small, as is typically the case for asteroid light curves. By using comparison stars in the same field of view (and hence at the same approximate airmass as the asteroid), first order atmospheric extinction effects are effectively cancelled. Furthermore, if comparison stars are selected which are similar in color to the asteroid (e.g. similar in color to the Sun), second order extinction effects (i.e. color-dependent atmospheric effects) can be mostly ignored as well. Restricting observations to elevations greater than 30° also helps to keep these second order extinction effects to a minimum.

The main disadvantage of this technique is that there is no common flux reference which is defined across different “sessions”. A session, in this case, is defined as a set of observations which shares the same imaging settings and the same set of comparison stars. A new session, for instance, would be required for a new night of observations, but also could be needed after a “meridian flip” of a German equatorial mount-style (GEM) telescope, or if the target asteroid moves out of the telescope field of view. The problem of integrating differential photometric data from different sessions is handled using a manually-specified offset known as a “delta comp” (Warner, 2006). This offset is applied during the lightcurve analysis to align the data from different sessions. More information about this process is provided in Section 3.2.4. As a general rule, when using differential photometry for asteroid lightcurves, it’s best to obtain as much data as possible in as short a time as possible. Hence, in an ideal case, sufficient data to resolve the complete lightcurve of a given asteroid would be obtained in a single session. These

factors were the primary rationale for selecting target asteroids which have nightly availability of 5 hours or more (refer to Section 3.1.2).

3.2.3.2 Aperture Photometry

In this study, the flux from a given object (asteroid or comparison star) was estimated using the aperture photometry technique. This technique is illustrated in Figure 22. To determine an object's brightness using this method, an aperture (usually a circle) is "drawn" around the object and the CCD electron counts are summed for all pixels inside. A second, larger, concentric aperture defines the "inner annulus". This region represents a transition between the object and the background sky, and the values inside this annulus (the "dead zone") are ignored. Finally, the largest concentric aperture (or "sky annulus") defines the outer annulus. The electron values within the outer annulus are averaged to estimate the brightness of the background sky. This per-pixel average value is then multiplied by the number of pixels in the object aperture and subtracted from the aperture sum in order to estimate the brightness of the object.

The most significant parameters for aperture photometry are the radii of the object aperture, inner annulus, and outer annulus. The object aperture is typically chosen based on the effective seeing, represented by the full-width-at-half-maximum (FWHM) of the object's radial flux profile (a Gaussian curve). Howell (2006) determined that most of the flux of a point source of light is contained within a circle with a diameter of three times the FWHM ($3 * \text{FWHM}$). Hence, for this study, object aperture diameters were typically chosen to be 2-3 times the average FWHM. The size of the sky annulus is an important parameter as well. Warner (2006) states, "In general, a larger sky annulus is

better than a smaller one...”, with the rationale being that a larger sky annulus is less sensitive to small inhomogeneities in the selected portion of the background sky. If the sky annulus diameter grows too large, however, there is an increasing chance that it will intersect another nearby bright object. This study followed the Warner (2006) recommendation of a sky annulus *thickness* equivalent to the diameter of the object aperture.

The aperture photometry method is most applicable to fields of stars which are relatively sparse. In the case of dense star fields, the apertures can intersect other bright objects. Avoiding this possibility was the primary rationale for ensuring that targets were a relatively large distance away from the galactic plane (refer to Section 3.1.2).

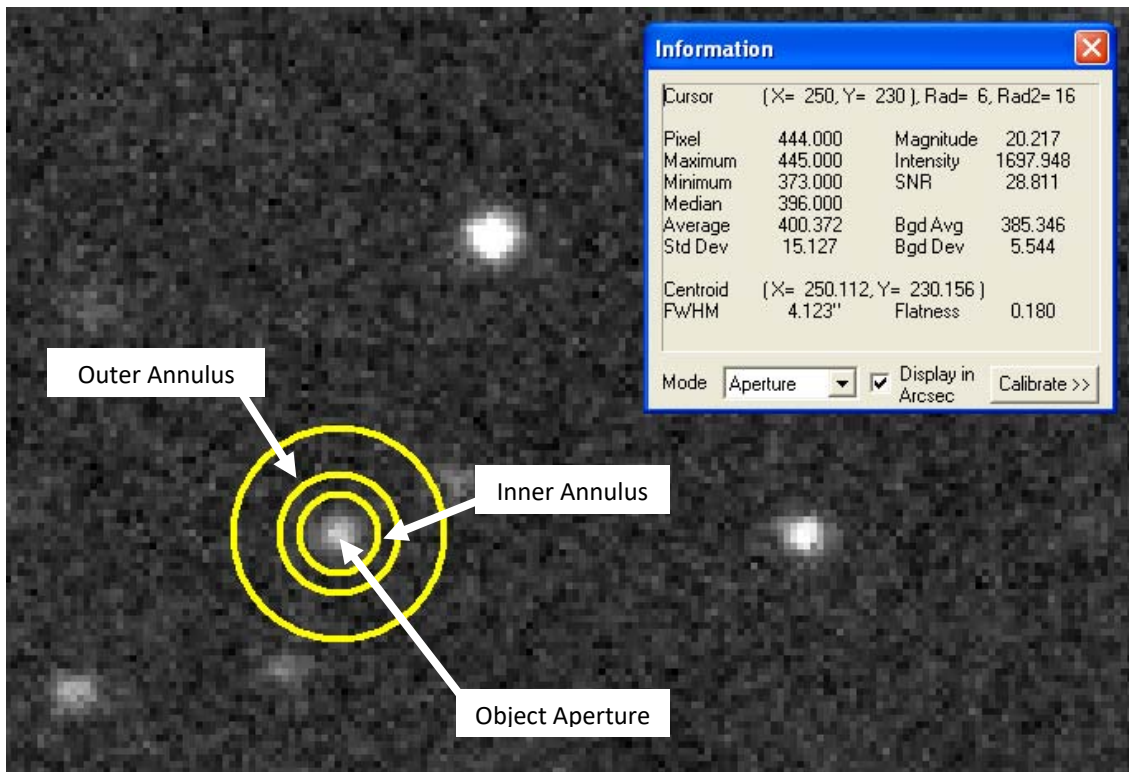


Figure 22. Aperture Photometry Method (Maxim-DL; Gary, 2005)

3.2.4 *MPO Canopus*

The MPO Canopus software application was used in this investigation to perform the full range of data reduction and analysis tasks, including star catalog matching, asteroid astrometry, differential aperture photometry, and lightcurve analysis. MPO Canopus, written by Brian Warner, is a commonly used commercial software package for asteroid lightcurve photometry.

MPO is a Windows (only) software application and is documented extensively in the MPO Canopus User's and Reference Guides (Warner, 2012, 2011). In addition to the capabilities mentioned above, MPO Canopus features a StarBGone! (Alard and Lupton, 1998) algorithm that aids in "removing" background stars which may overlap with the target asteroid as it moves across the field of view. This feature employs user-defined reference stars to form a model which can be scaled to effectively remove the flux added to an asteroid measurement by a nearby background star. This feature was applied with success during this investigation to "salvage" segments of measurements that would have otherwise been unusable in the lightcurve analysis.

The primary feature of MPO Canopus that distinguishes it from other photometry packages used for asteroid lightcurve work is its built-in lightcurve analysis routine. This routine is based on the Fourier Analysis LightCurve (FALC) program first applied by Harris et al. (1989). This algorithm performs phasing of the different segments of the lightcurve (from the same and/or different sessions) and calculates potential period solutions as a function of RMS error. This so-called "Period Search", depicted in Figure 23, highlights potential solutions where the RMS error reaches a minimum. The search

parameters (range of periods, resolution, etc.) can be set by the user. In addition, the “delta comp” value can be adjusted by the user in order to align lightcurve data from different sessions.

Although the lightcurve analysis capabilities of MPO are extensive, finding the period of an asteroid based on partial or segmented lightcurve data can be challenging and often requires a bit of “strategy”. This effort is made somewhat more complicated by the extra degree of freedom represented by the user-defined “delta comp” value, especially when the shape of the lightcurve does not include any distinctive features. In many cases, using the default MPO “Period Search” settings (e.g., wide range of sample periods) will result in the prediction of a rotational period near the high end of the sampled range. The MPO algorithms are sensitive and the presence of noise in the data can cause the “Period Search” to identify (what should be) overlapping lightcurve features as unique. In these cases, testing periods which are half (or even a quarter) of the predicted period is prudent. This technique is described by Warner (2006). If ambiguities persist, a bimodal lightcurve shape (refer to Section 2.2) is typically assumed.

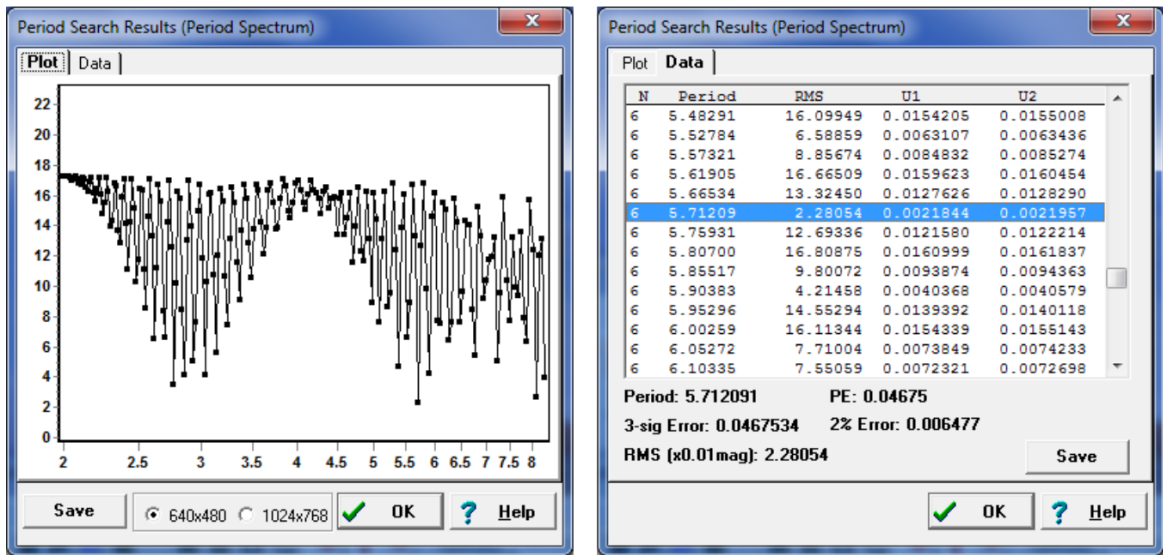


Figure 23. MPO Canopus Period Search(Warner, 2011)

CHAPTER 4

RESULTS AND ANALYSIS

In this chapter, the lightcurve photometric measurements for a set of 10 V_p -type asteroids are presented. The results for each asteroid are described in detail. In addition, the data from this study are analyzed in the context of other main belt asteroids in order to look for possible trends. Particular attention is devoted to exploring how these measurements compare to existing data in the literature for the V-type (and V_p -type) asteroid population (e.g., Hasegawa et al., 2014; Ryan et al., 2004).

4.1 Target Asteroids

Lightcurve photometric measurements were obtained for the following 10 V_p -type asteroids: (3648) Raffinetti, (5235) Jean-Loup, (9223) Leifandersson, (11699) 1998 FL105, (12073) Larimer, (15121) 2000 EN14, (16452) Goldfinger, (20557) Davidkulka, (29796) 1999 CW77, and (35821) 1999 JW50. Select physical and orbital data for these target asteroids are presented in Table 5.

The diameter (D) and albedo (p_V) values in Table 5 are taken from WISE measurements, except where noted. The average diameter of the target asteroids is approximately 4.8 km, and the average albedo is 0.32. The average absolute magnitude (H) is 13.7.

Two of the asteroids, (9223) Leifandersson and (35821) 1999 JW50, have previous lightcurve measurements available in the LCDB. For these two objects, the estimated rotational period (P), lightcurve amplitude (A), and quality code (U) are provided. Also, where available, the dynamical family assigned by Nesvorny (2010) is presented in Table 5. A total of five of the ten target V_p -type asteroids are associated with the Nesvorny (2010) Vesta dynamical family.

Table 5. Summary of V_p -Type Target Asteroids

#	Name	a (AU)	i (°)	e	H	D (km)	P_v	LCDB P(hr)/A(mag)/U	FAMILY
3648	Raffinetti	2.42	7.90	0.11	13	5.31	0.6087		
5235	Jean-Loup	2.30	4.85	0.14	12.7	7.39	0.3007		Flora
9223	Leifandersson	2.30	3.41	0.07	13.5	4.50	0.381	3.7584 / 0.33 / 2	
11699	1998 FL105	2.40	5.08	0.08	13.1	6.71	0.2268		Vesta
12073	Larimer	2.42	6.24	0.09	14	2.95	0.4647		Vesta
15121	2000 EN14	2.35	3.57	0.16	15	3.55	0.1687		
16452	Goldfinger	2.41	6.29	0.08	13.4	4.33	0.344		Vesta
20557	Davidkulka	2.38	6.27	0.10	14.1	3.95	0.1793		Vesta
29796	1999 CW77	2.34	7.87	0.07	13.9	4.85	0.2484		
35821	1999 JW50	2.48	5.95	0.13	14.3	3.28*	0.3*	4.9314 / 0.54 / 2	Vesta

*Diameter calculated based on H and an assumed value of albedo of 0.3 (Pravec and Harris, 2007).

A graphical illustration of the orbital characteristics of the ten target asteroids is provided in Figure 24 and Figure 25. In Figure 24, the orbital inclination angle (i) is plotted as a function of semi-major axis (a). In Figure 25, the orbital eccentricity (e) is plotted as a function of semimajor axis (a). In both graphs, the grey points represent main belt asteroids, the blue points are members of the Vesta dynamical family (Nesvorny, 2010), and the red triangles represent the ten target asteroids. The asteroid (4) Vesta is represented by a black circle.

From Figure 24, it can be seen that four asteroids, (5235) Jean-Loup, (9223) Leifandersson, (15121) 2000 EN14, and (11699) 1998 FL105, have smaller inclination

angles than the typical Vesta dynamical family, as well as the other target asteroids. In addition, the first three of these asteroids are not members of the Vesta dynamical family (Nesvorný, 2010) and hence are possible Vestoid “interlopers” in these regions.

From Figure 24, it can also be seen that the asteroid (35821) 1999 JW50 ($a = 2.48$ AU) is very near to the 3:1 mean motion resonance ($a = 2.5$ AU) with Jupiter. Binzel and Xu (1993) used visible spectroscopic measurements to identify such potential Vesta impact fragments which were ejected towards the 3:1 resonance. The 3:1 resonance increases the eccentricity of the asteroid’s orbit such that it may become Earth-crossing. This dynamic mechanism is believed to be an important potential source of HED meteorites. It follows that the eccentricity (0.13) of (35821) 1999 JW50 is higher than the average eccentricity of the Vesta family (~ 0.10) (refer to Figure 25).

From Figure 25, it can be seen that two of the “lower inclination” asteroids mentioned previously, (5235) Jean-Loup and (15121) 2000 EN14, also have a higher eccentricity than most Vesta dynamical family members and the highest eccentricity of the ten target asteroids. Roig et al. (2011) and Carruba et al. (2005) used numerical simulations to show how the Yarkovsky effect, chaotic diffusion, and interactions with non-linear secular resonances can create such “fugitives” from the Vesta family over long periods of time (~ 1.2 Gy). These studies have helped to set a lower limit on the age of the impact which likely created the Vesta asteroid family.

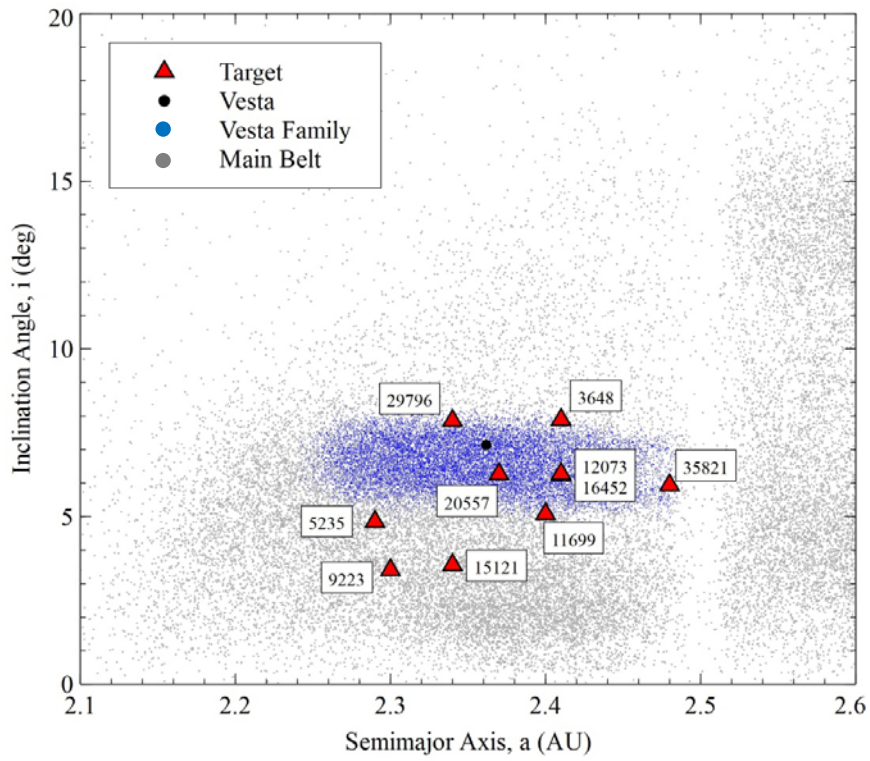


Figure 24. Target Asteroids: Inclination Angle (i) vs. Semimajor Axis (a)

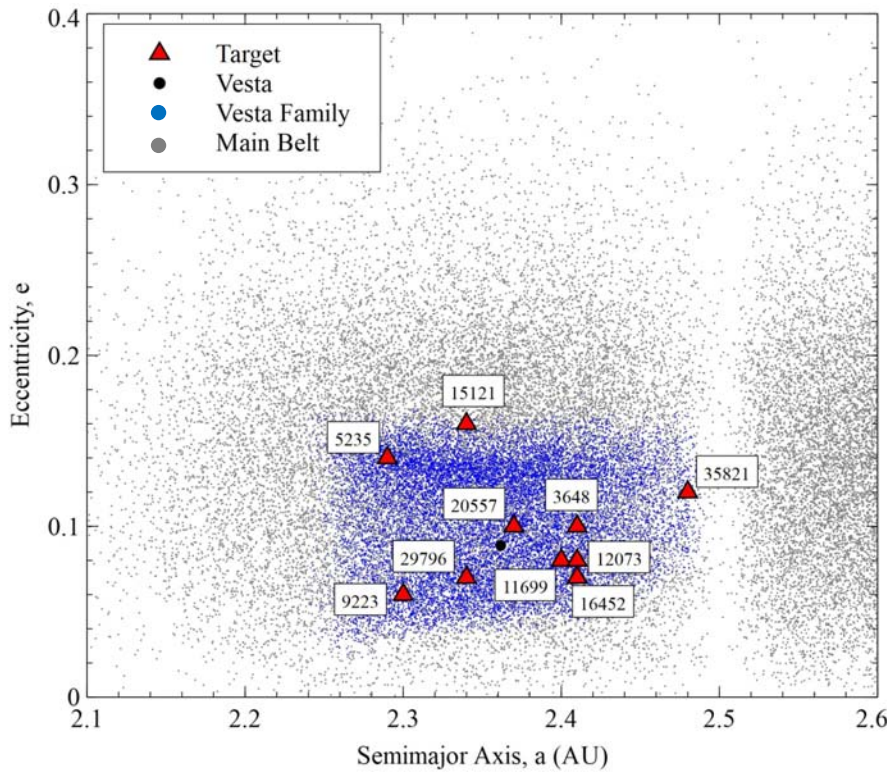


Figure 25. Target Asteroids: Eccentricity (e) vs. Semimajor Axis (a)

4.2 Asteroid Lightcurve Measurements

The target asteroid lightcurve measurements are summarized in Table 5. These observations were conducted over the period from November 2016 to June 2017. Measurements were collected using the PROMPT1, PROMPT3, and PROMPT6 telescopes at the Cerro Tololo Inter-American Observatory in La Serena, Chile; the Stone Edge Observatory (SEO) in Sonoma, CA; and the Yerkes-41 telescope at the Yerkes Observatory in Williams Bay, WI. Table 6 also includes the phase angles ("Sun-Target-Observer") at the time of observation, as well as the final calculated rotational periods and lightcurve amplitudes. The lightcurve measurements for each of the ten target asteroids are described in more detail in the following sections.

Table 6. Summary of V_p -Type Target Lightcurve Measurements

#	Name	Telescope	Date	Phase, α ($^\circ$)	Lightcurve	
					Period, P (hr)	Amp., A (mag)
3648	Raffinetti	PROMPT6	4/3/2017, 4/6/2017	2.9, 1.5	5.1756	0.16
5235	Jean-Loup	PROMPT6	3/30/2017, 4/2/2017	6.9, 5.5	2.4521	0.11
9223	Leifandersson	SEO PROMPT6	11/29/2016 12/19/2016-12/22/2016	2.2, 11.5-12.8	3.7583	0.33
11699	1998 FL105	PROMPT3	6/19/2017-6/20/2017	11.8-12.7	4.0990	0.58
12073	Larimer	PROMPT6	4/27/2017-4/28/2017	5.9-5.3	9.4873	0.35
15121	2000 EN14	PROMPT6	11/5/2016-11/6/2016, 11/9/2016	2.8-2.9, 3.9	5.5816	0.72
16452	Goldfinger	PROMPT6	12/27/2016, 12/29/2016, 1/2/2017	16.2, 15.5, 13.8	3.8838	0.31
20557	Davidkulka	PROMPT6 PROMPT1	6/2/2017 6/29/2017	5.9 13.1	5.6878	0.28
29796	1999 CW77	PROMPT6 YERKES-41	3/6/2017-3/7/2017 3/9/2017	4.41-4.38, 4.5	6.4716	0.19
35821	1999 JW50	PROMPT6	11/29/2016, 11/30/2016, 12/03/2016	4.3, 4.5, 5.6	4.9293	0.74

4.2.1 (3648) *Raffinetti*

The asteroid (3648) *Raffinetti* was discovered in 1957 at the La Plata Observatory near Buenos Aires, Argentina. The asteroid was named after Virgilio *Raffinetti* (1869–1946), the observatory’s director from 1889 to 1905. During this study, *Raffinetti* was observed on April 3, 2017 and April 6, 2017 using the PROMPT6 telescope. Over these two nights, photometric measurements were obtained for a total of approximately 15 hours using individual exposure times of 120 seconds. The resulting lightcurve for *Raffinetti* is shown in Figure 26.

Raffinetti is not a member of the Vesta dynamical family defined by Nesvorný (2010). It has an orbit inclination of 7.9° , larger than most Vesta family members (average of $\sim 6.5^\circ$) and the highest of the ten target asteroids. Based on WISE measurements, the diameter of the asteroid is 5.31 km and its albedo is 0.609, the highest of all of the target asteroids. The average albedo of the Vesta family of asteroids is approximately 0.35 (Mainzer et al., 2011b). Despite these discrepancies, *Raffinetti* is still likely a Vestoid. Hardersen (2017) cited unpublished near-infrared spectroscopic observations of *Raffinetti* which displayed “deep pyroxene features” and a “likely basaltic” composition. In addition, high albedo features (up to 0.67) were detected on Vesta’s surface by the Dawn mission (Reddy et al., 2012).

There were no previous lightcurve measurements available in the LCDB for *Raffinetti*. The measurements and analysis (using MPO Canopus) conducted by this study estimate a rotational period of 5.1756 ± 0.0007 hours and a lightcurve amplitude of 0.16 ± 0.007 magnitudes. The period error is calculated automatically by the Fourier

Analysis LightCurve (FALC) algorithm (Harris et al., 1989) used in MPO Canopus. The amplitude error is calculated based on an average of the photometric error of the individual observations. Raffinetti's lightcurve is dual-lobed and representative of a typical ellipsoid shaped asteroid rotating about its principal axis of maximum inertia. The difference in the depths of the two lightcurve minima suggests that the asteroid is somewhat narrower at one end of the ellipsoid than the other.

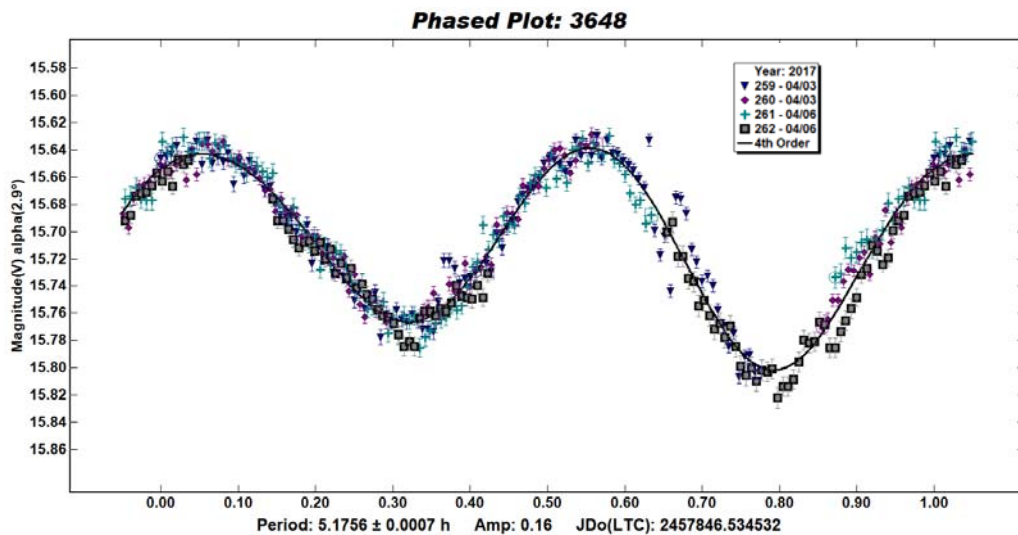


Figure 26. (3648) Raffinetti Lightcurve

4.2.2 (5235) Jean-Loup

The asteroid (5235) Jean-Loup was discovered in 1990 at the Palomar Observatory near San Diego, CA. The asteroid was named after French astronaut, Jean-Loup Jacques Marie Chrétien (Born 1938). For this investigation, Jean-Loup was observed on March 30, 2017 and April 2, 2017 using the PROMPT6. Over these two nights, measurements were obtained for a total of approximately 9.5 hours using individual exposure times of 120 seconds. The resulting lightcurve for Jean-Loup is shown in Figure 29.

From WISE measurements, the diameter of the asteroid is estimated to be 7.39 km and its albedo is 0.3. Jean-Loup is not a member of the Vesta dynamical family, but instead was identified by Nesvorný (2010) as a member of the neighboring Flora family (refer to Figure 27). As mentioned previously, Jean-Loup has a lower inclination angle than most of the Vesta family asteroids, but is likely an interloper in the Flora family.

This hypothesis is supported by spectroscopic measurements aimed at quantifying the surface composition of the asteroid. Jean-Loup was among the V_p -type targets included in a spectroscopic study of potential basaltic asteroids in the main belt performed by Hardersen et al. (2014). As shown by the near-infrared reflectance spectrum presented in Figure 28, Jean-Loup is characterized by absorption features near 1.0 μm and 2.0 μm that are typical of basaltic material, specifically pyroxene. Using calibrations derived from laboratory analyses of the Vesta-derived HED meteorites, Hardersen et al. (2014) demonstrated that the material covering the surface of Jean-Loup most closely resembles the Howardite meteorites. Howardites are regolith breccias of Vesta's eucrite (crustal) and diogenite (upper mantle) materials and typical of the debris which would result from an impact on Vesta's surface.

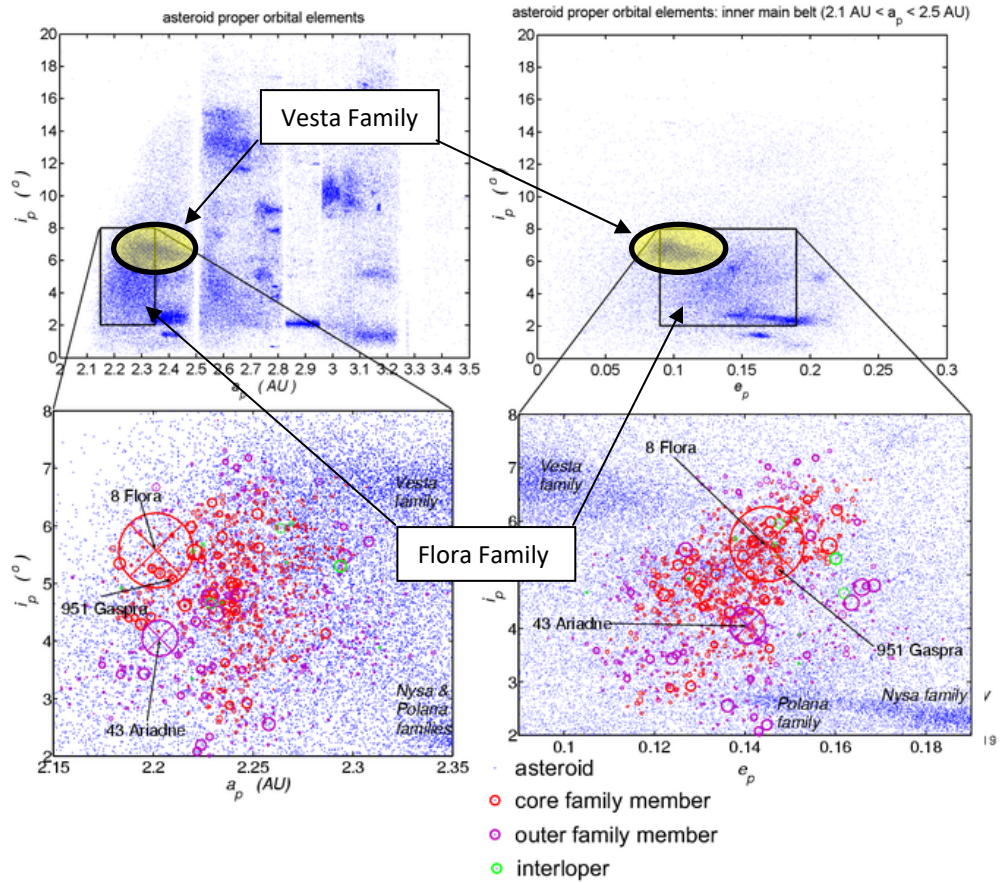


Figure 27. Flora Asteroid Family. The Flora family is indicated by the black square outlines and zoomed views. The nearby Vesta family is indicated by the yellow shaded oval regions (https://en.wikipedia.org/wiki/Flora_family).

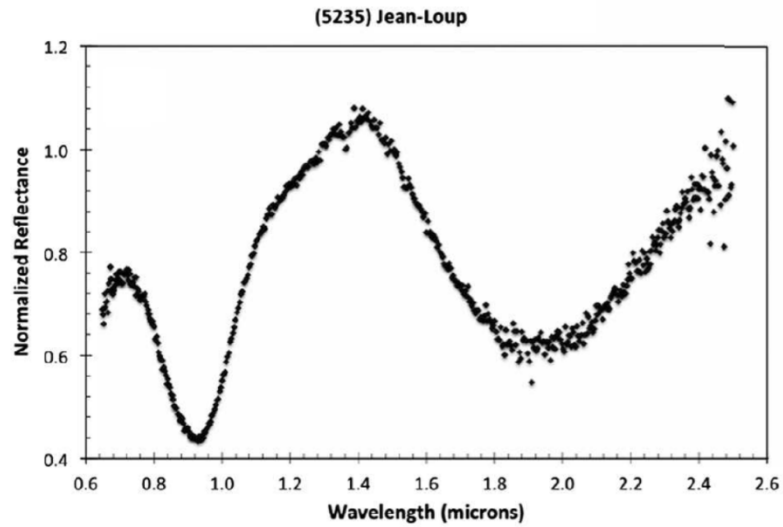


Figure 28. Near-Infrared Reflectance Spectrum of (5235) Jean-Loup (Hardersen et al., 2014a)

Jean-Loup was observed by Albers et al. (2010) in April 2010, but there was no reported lightcurve period in the LCDB. However, a lightcurve amplitude of 0.09 magnitudes was provided. Using data collected by this investigation, a rotational period for Jean-Loup of 2.4521 ± 0.0004 hours and a lightcurve amplitude of 0.11 ± 0.006 magnitudes were estimated. The shape of Jean-Loup’s lightcurve exhibits deviations from the typical dual-lobed sinusoidal curve. These differences could be attributed to variegations on the asteroid surface or geometric features inconsistent with a classic triaxial ellipsoid.

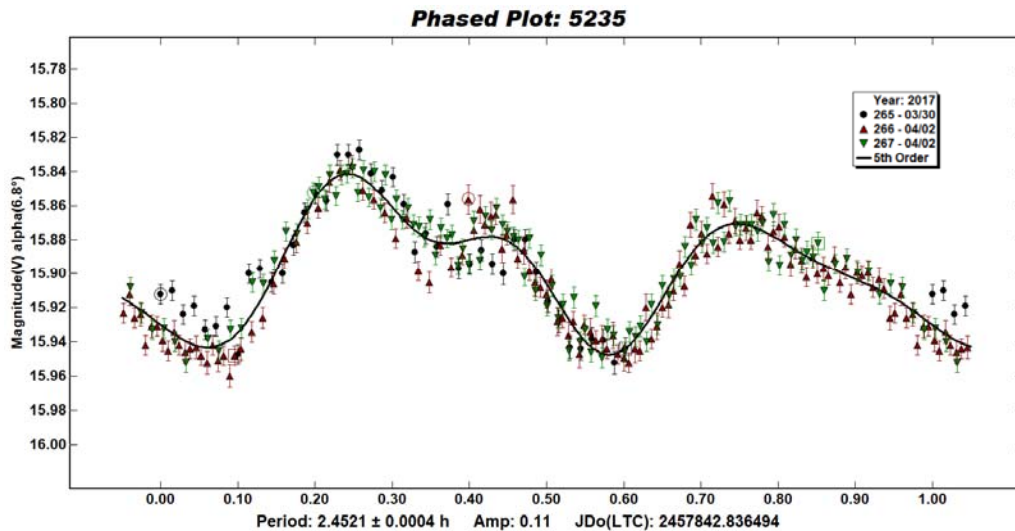


Figure 29. (5235) Jean-Loup Lightcurve

4.2.3 (9223) Leifandersson

The asteroid (9223) Leifandersson was discovered in 1995 by the University of Arizona’s SPACEWATCH group at the Kitt Peak National Observatory, AZ. The asteroid was named after Swedish astronomer, Leif Erland Andersson (1943–1979), who calculated the pole orientation of the planet Pluto. For this study, Leifandersson was observed on November 29, 2016 using SEO and from December 19 to December 22,

2016 using the PROMPT6 telescope. Over these five nights, measurements were obtained for a total of approximately 23 hours using individual exposure times of 120 (SEO) and 180 (PROMPT6) seconds. The resulting lightcurve for Leifandersson is shown in Figure 30.

Based on WISE measurements, the diameter of the asteroid is estimated to be 4.50 km and its albedo is 0.381. Leifandersson is not a member of the Vesta dynamical family (Nesvorny , 2010). Its orbit inclination (3.41°) is the lowest of all the target asteroids. As described in Section 4.1, Leifandersson, along with (5235) Jean-Loup and (15121) 2000 EN14, were likely scattered by thermal and gravitational effects over the past 1Gy or more. Further support for Leifandersson's Vesta origins is provided by a work to be published by Hardersen et al. (2018), which obtained near-infrared spectroscopic observations displaying characteristic basaltic absorption features near $1.0 \mu\text{m}$ and $2.0 \mu\text{m}$.

Leifandersson was observed in February 2011 by Waszczak et al. (2015) as part of the Palomar Transient Factory Survey, which used "sparse photometry" to obtain "reliable" lightcurves for approximately 8,000 asteroids. Waszczak et al. (2015) calculated a rotational period of 3.758 hours and a lightcurve amplitude of 0.33 magnitudes. In the LCDB, these measurements were assigned a quality rating, U, of 2 (out of 3). The measurements and analysis conducted by this study support the data of Waszczak et al. (2015), giving an identical rotational period of 3.7583 ± 0.0001 hours and lightcurve amplitude of 0.33 ± 0.028 magnitudes.

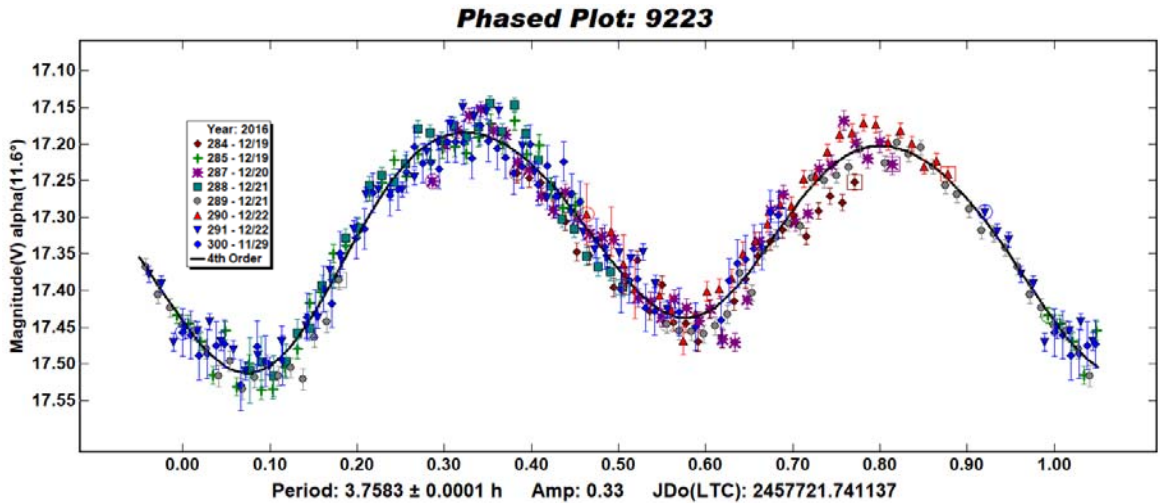


Figure 30. (9223) Leifandersson Lightcurve

4.2.4 (11699) 1998 FL105

The asteroid (11699) 1998 FL105 was discovered in 1998 by MIT’s Lincoln Near Earth Asteroid Research (LINEAR) program in Socorro, NM. For this investigation, (11699) 1998 FL105 was observed on April 26, 2017 using the PROMPT6 telescope and from June 19 to June 20, 2017 using the PROMPT3 telescope. Over these three nights, measurements were obtained for a total of approximately 15 hours using individual exposure times of 30 (PROMPT3) and 80 (PROMPT6) seconds. The resulting lightcurve for (11699) 1998 FL105 is shown in Figure 31.

Based on WISE measurements, the diameter of the (11699) 1998 FL105 is estimated to be 6.71 km and its albedo is 0.2268. The asteroid (11699) 1998 FL105 is a member of the Vesta dynamical family (Nesvorný , 2010). However, near-infrared spectroscopy measurements by Hardersen et al. (2018) revealed a “featureless spectrum” (Hardersen, 2017), indicating that (11699) 1998 FL105 is likely not derived from Vesta.

There were no previous lightcurve measurements available in the LCDB for (11699) 1998 FL105. The lightcurve measurements conducted by this study estimate a rotational period of 4.0990 ± 0.0007 hours and an amplitude of 0.58 ± 0.042 magnitudes. The lightcurve of (11699) 1998 FL105 is dual-lobed and symmetrical, typical of an ellipsoid shaped asteroid in principal axis rotation.

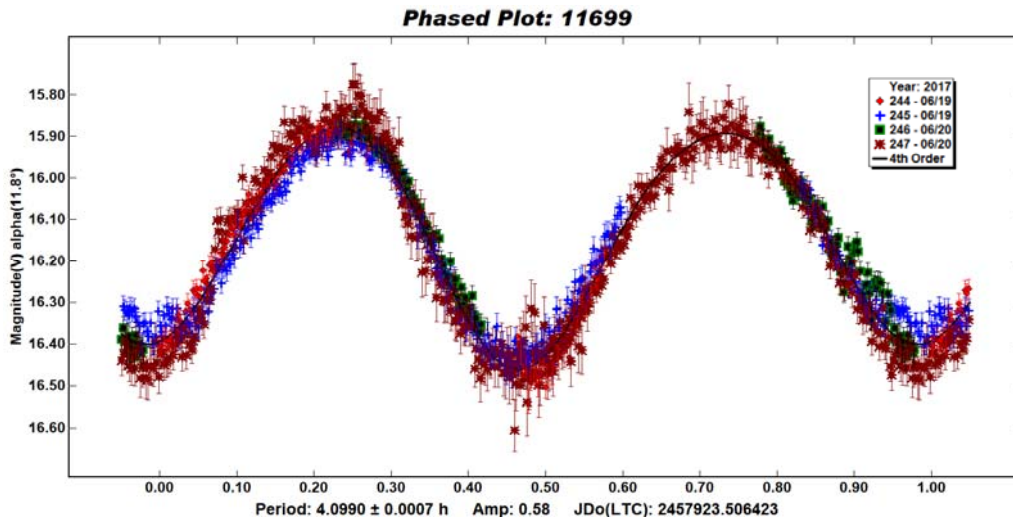


Figure 31. (11699) 1998 FL105 Lightcurve

4.2.5 (12073) Larimer

The asteroid (12073) Larimer was discovered in 1998 by LINEAR. The asteroid was named after Curtis James Larimer (Born 1986), a 2002 awardee of the Intel International Science and Engineering Fair (ISEF). For this study, Larimer was observed from April 27 to April 28, 2017 using the PROMPT6 telescope. Over these two nights, measurements were obtained for a total of approximately 11 hours using individual exposure times of 120 seconds. The resulting lightcurve for Larimer is shown in Figure 32.

Larimer is a member of the Vesta dynamical family (Nesvorny, 2010). Additional support for Larimer's Vesta lineage is provided by a work to be published by Hardersen

et al. (2018), which obtained near-infrared spectroscopic observations characterizing Larimer’s surface as similar in composition to the Howardite meteorites. The Howardite meteorites are believed to be an impact breccia of Vesta’s crustal and upper mantle materials.

Based on WISE measurements, the diameter of the asteroid is estimated to be 2.95 km, the smallest of the ten target asteroids, and its albedo is 0.4647. There were no previous lightcurve measurements available in the LCDB for Larimer. The lightcurve measurements conducted by this study estimate a rotational period of 9.4873 ± 0.0062 hours, the slowest rotator of the ten target asteroids. The lightcurve amplitude for Larimer is 0.35 ± 0.019 magnitudes.

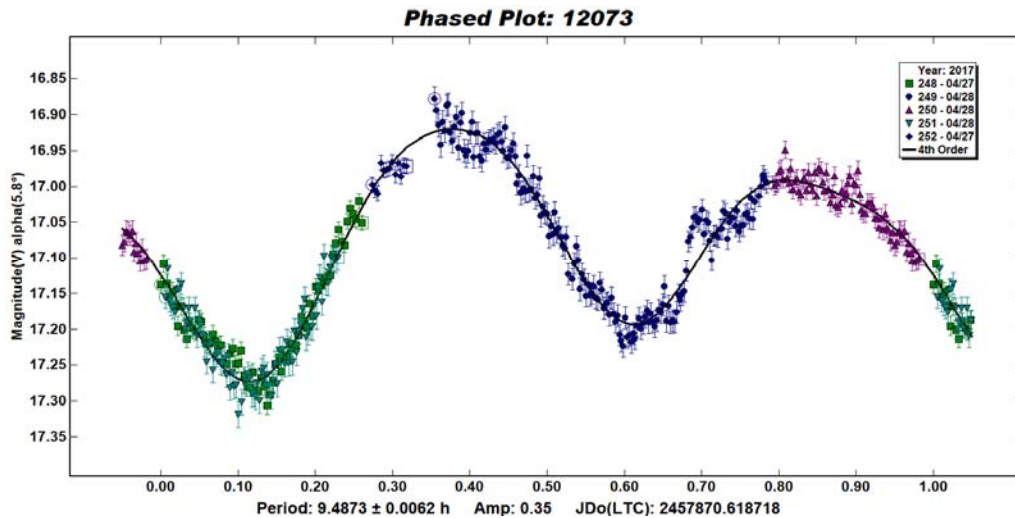


Figure 32. (12073) Larimer Lightcurve

4.2.6 (15121) 2000 EN14

The asteroid (15121) 2000 EN14 was discovered in 2000 by Korado Korlević at the Višnjan Observatory in Croatia. For this investigation, (15121) 2000 EN14 was observed on November 5, 6 and 9, 2017 using the PROMPT6 telescope. Over these three nights,

measurements were obtained for a total of approximately 15 hours using individual exposure times of 120 seconds. The resulting lightcurve for (15121) 2000 EN14 is shown in Figure 33.

The asteroid (15121) 2000 EN14 is not a member of the Vesta dynamical family (Nesvorny , 2010). As mentioned previously, its orbit eccentricity ($e = 0.16$) is the highest of all the target asteroids. Based on WISE measurements, the diameter of the asteroid is estimated to be 3.55 km and its albedo is 0.1687, the least reflective of the ten target asteroids.

There were no previous lightcurve measurements available in the LCDB for (15121) 2000 EN14. The lightcurve measurements conducted by this study estimate a rotational period of 5.5816 ± 0.0004 hours and an amplitude of 0.72 ± 0.020 magnitudes. It is interesting to note that the shape of this lightcurve is a departure from the typical sinusoidal curves associated with ellipsoid shaped objects. Instead, the lightcurve of (15121) 2000 EN14, with its “rounded” peaks and “sharp” valleys, is more representative of a highly elongated, non-convex (e.g., dumbbell-shaped) object, like 217 Kleopatra (Descamps, 2015).

Another possible explanation for the unique shape of this lightcurve is that (15121) 2000 EN14 is a synchronous binary asteroid system. In such a system, a secondary asteroid revolves about the primary asteroid at a rate equivalent to the primary’s rotational speed. As shown in Figure 34, the resulting lightcurve is a superposition of the lightcurve associated with rotation (e.g., a sinusoidal shape) and the lightcurve associated with an eclipsing event (e.g., flat with sharp valleys). This combination

produces distinctive “shoulders” to each side of the lightcurve peaks. These features, although very subtle, are indeed evident in the lightcurve of (15121) 2000 EN14, as illustrated in Figure 33 (bottom). Several binary systems have been identified in the Vesta family, including 854 Frostia (Behrend et al., 2006), 809 Lundia (Kryszczyńska, A. et al., 2009), and 3782 Celle (Ryan et al., 2004)

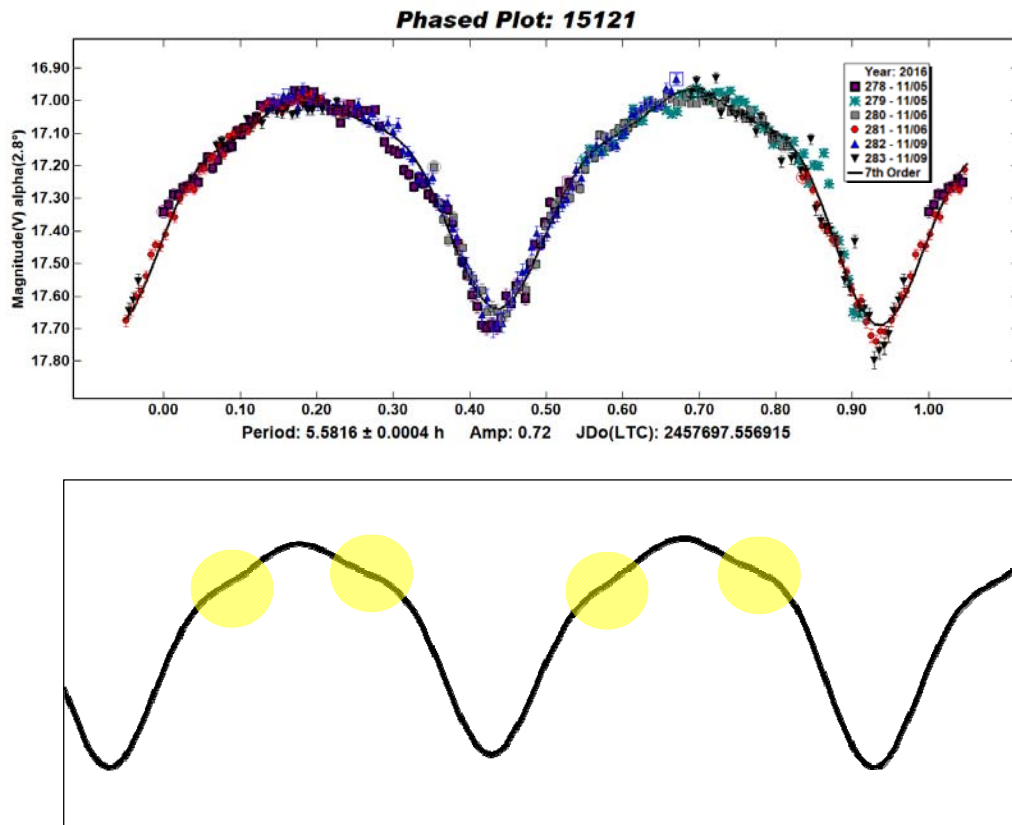


Figure 33. (15121) 2000 EN14 Lightcurve (top). Fourier curve fit (bottom) to lightcurve data. The so-called “shoulders” of the lightcurve, features typically associated with synchronous binary systems, are highlighted in yellow.

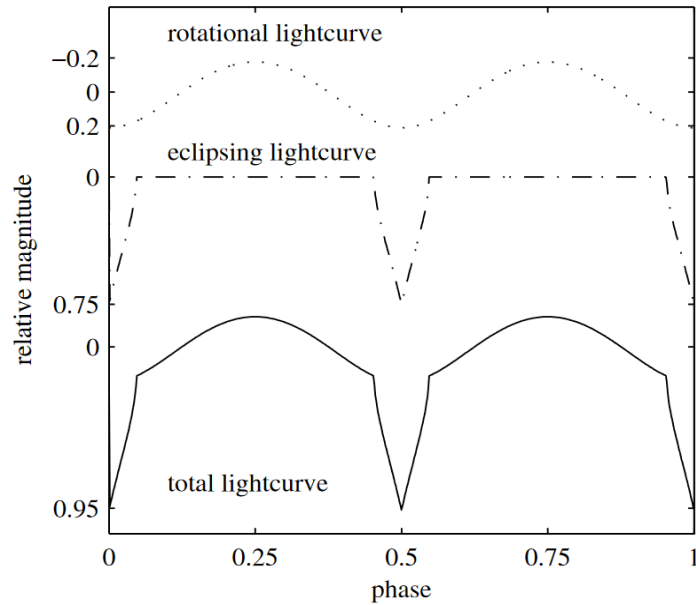


Figure 34. Synchronous Binary Asteroid Lightcurve (Behrend et al., 2006)

4.2.7 (16452) Goldfinger

The asteroid (16452) Goldfinger was discovered in 1998 by Carolyn Shoemaker at the Palomar Observatory near San Diego, CA. The asteroid was named after Pauline J. ("PJ") Goldfinger, an adaptive-optics operator at the observatory who helped to organize the glass plate archive of the observatory's famous Schmidt Oschin telescope. During this investigation, Goldfinger was observed on December 27 and 29, 2016, January 2, 2017, and February 27, 2017 using the PROMPT6 telescope. Over these four nights, measurements were obtained for a total of approximately 14 hours using individual exposure times of 120 (on February 27, 2017) and 180 seconds. The resulting lightcurve for Goldfinger is shown in Figure 35.

Goldfinger is a member of the Vesta dynamical family (Nesvorný, 2010). Based on WISE measurements, the diameter of the asteroid is estimated to be 4.33 km and its albedo is 0.344. There were no previous lightcurve measurements available in the LCDB

for Goldfinger. The measurements conducted by this study estimate a rotational period of 3.8838 ± 0.0003 hours and a lightcurve amplitude of 0.31 ± 0.014 magnitudes. The shape of Goldfinger's lightcurve exhibits deviations from the typical dual-lobed sinusoidal curve. These differences could be attributed to geometric features inconsistent with a classic triaxial ellipsoid.

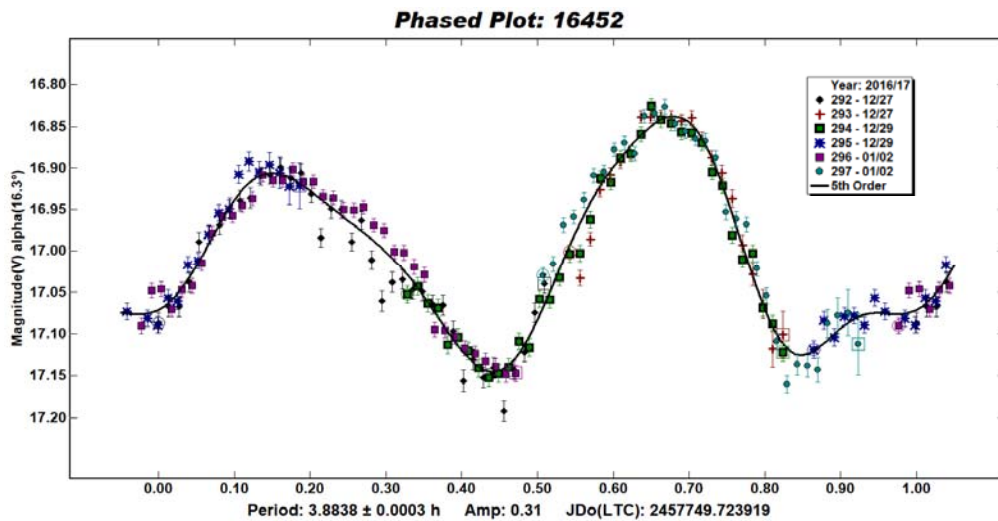


Figure 35. (16452) Goldfinger Lightcurve

4.2.8 (20557) Davidkulka

The asteroid (20557) Davidkulka was discovered in 1999 by LINEAR. The asteroid was named after David Kulka, a mentor at the 2004 Discovery Channel Young Scientist Challenge (DCYSC). During this investigation, Davidkulka was observed on May 30, 2017 and June 2, 2017 using the PROMPT6 telescope and on June 29, 2017 using the PROMPT1 telescope. Over these three nights, measurements were obtained for a total of approximately 16 hours using exposure times of 35 (PROMPT1) and 120 (PROMPT6) seconds. The resulting lightcurve for Davidkulka is shown in Figure 36.

Davidkulka is a member of the Vesta dynamical family (Nesvorny, 2010). Based on WISE measurements, the diameter of the asteroid is estimated to be 3.95 km and its albedo is 0.1793, the lowest albedo of ten target asteroids. There were no previous lightcurve measurements available in the LCDB for (20557) Davidkulka. The lightcurve measurements conducted by this study estimate a rotational period of 5.6878 ± 0.0002 hours and an amplitude of 0.28 ± 0.028 magnitudes.

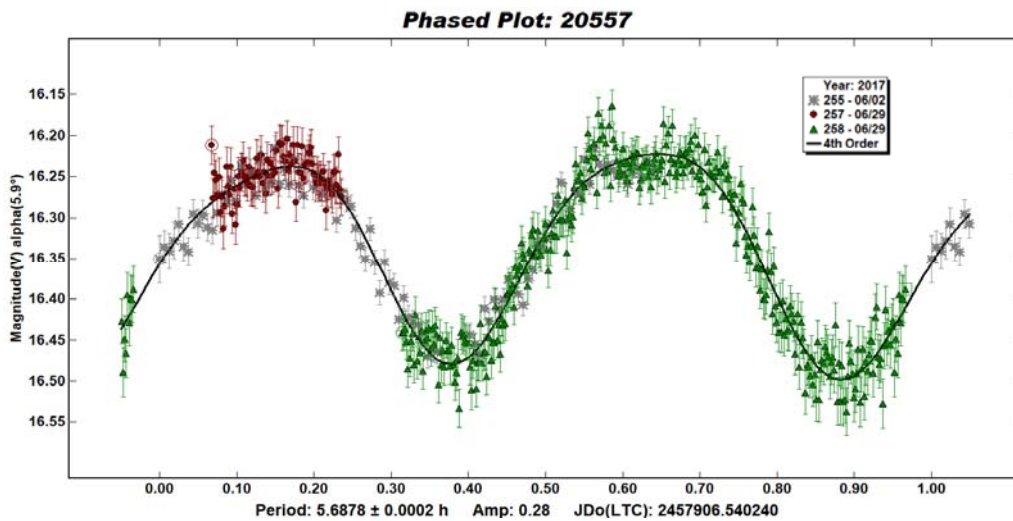


Figure 36. (20557) Davidkulka Lightcurve

4.2.9 (29796) 1999 CW

The asteroid (29796) 1999 CW was discovered in 1999 by LINEAR. During this investigation, (29796) 1999 CW was observed on March 6 and 7, 2017 using the PROMPT6 telescope and March 9, 2017 using the Yerkes-41 telescope at the Yerkes Observatory in Williams Bay, WI. Over these three nights, measurements were obtained for a total of approximately 16 hours using exposure times of 120 seconds. The resulting lightcurve for (29796) 1999 CW is shown in Figure 38.

Based on WISE measurements, the diameter of (29796) 1999 CW is estimated to be 4.85 km and its albedo is 0.2484. The asteroid is not a member of the Vesta dynamical family (Nesvorný, 2010). However, near-infrared spectroscopic measurements conducted by Hardersen et al. (2014) indicate a Vesta-like basaltic surface composition. As shown in Figure 37, (29796) 1999 CW is characterized by pyroxene absorption features near 1.0 μm and 2.0 μm . Using meteorite calibrations, Hardersen et al. (2014) demonstrated that the material covering the surface of (29796) 1999 CW most closely resembles the Howardite meteorites, a breccia of Vesta's crustal and upper mantle materials.

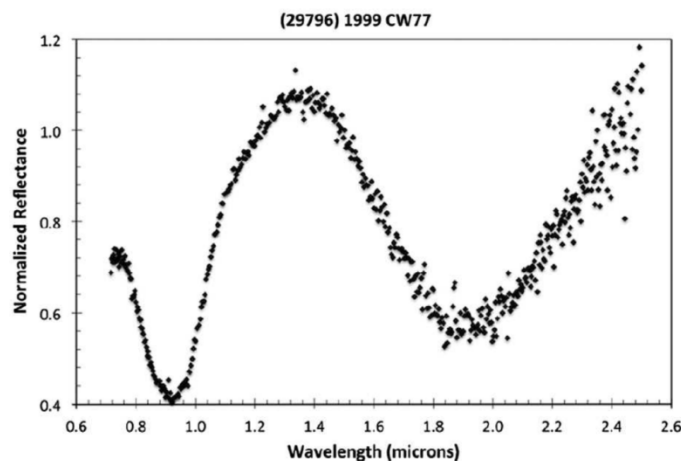


Figure 37. Near-Infrared Reflectance Spectrum of (29796) 1999 CW77 (Hardersen et al., 2014a)

There were no previous lightcurve measurements available in the LCDB for (29796) 1999 CW77. The lightcurve measurements conducted by this study estimate a rotational period of 6.4716 ± 0.0021 hours and an amplitude of 0.19 ± 0.013 magnitudes.

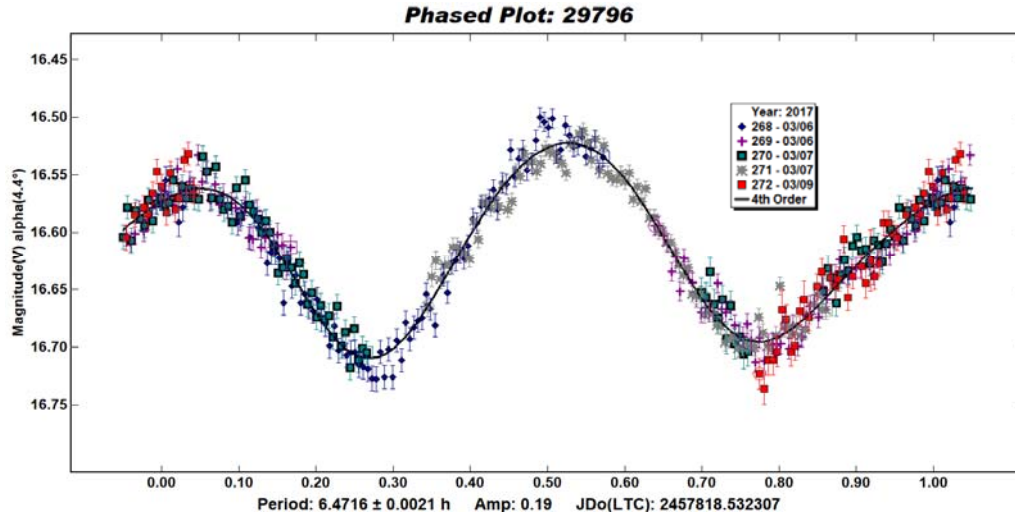


Figure 38. (29796) 1999 CW77 Lightcurve

4.2.10 (35821) 1999 JW50

The asteroid (35821) 1999 JW50 was discovered in 1999 by LINEAR. For this study, (35821) 1999 JW50 was observed on November 29 and 30, 2016 and December 3, 2016 using the PROMPT6 telescope. Over these three nights, measurements were obtained for a total of approximately 14 hours using exposure times of 120 and 80 (on December 3, 2016) seconds. The resulting lightcurve is shown in Figure 39.

The asteroid (35821) 1999 JW50 is a member of the Vesta dynamical family (Nesvorny, 2010). WISE measurements were not available for this asteroid. Instead, the diameter of the asteroid was estimated to be 3.28 km based on its absolute magnitude (14.3) and an assumed albedo of 0.3 (Pravec and Harris, 2007).

The asteroid (35821) 1999 JW50 was observed in April 2010 by Waszczak et al. (2015) as part of the Palomar Transient Factory Survey. Waszczak et al. (2015) calculated a rotational period of 4.931 ± 0.1177 hours and a lightcurve amplitude of 0.54 magnitudes. In the LCDB, these measurements were assigned a quality rating (U) of 2.

The photometric measurements obtained as part of this study support the rotational period calculated by Waszczak et al. (2015), providing a similar estimate of 4.9293 ± 0.0003 hours. The lightcurve amplitude estimated in this study is 0.74 ± 0.013 , larger than that measured by Waszczak et al. (2015). This difference is likely due to orientation of the asteroid’s rotational axis and the resulting changes in the viewing angle of the asteroid between the two studies. The longitude of the phase angle bisector (PAB), a measure of the orientation of the asteroid orbital position relative to the sun and Earth, was approximately 64° for this study and 169° for Waszczak et al. (2015).

The shape of (35821) 1999 JW50’s lightcurve is similar to that of (15121) 2000 EN14, exhibiting rounded maxima and steep minima. There is little if any evidence, however, of the “shoulder” features which would indicate a potential binary systems. Instead, (35821) 1999 JW50 is likely a highly elongated, non-convex object.

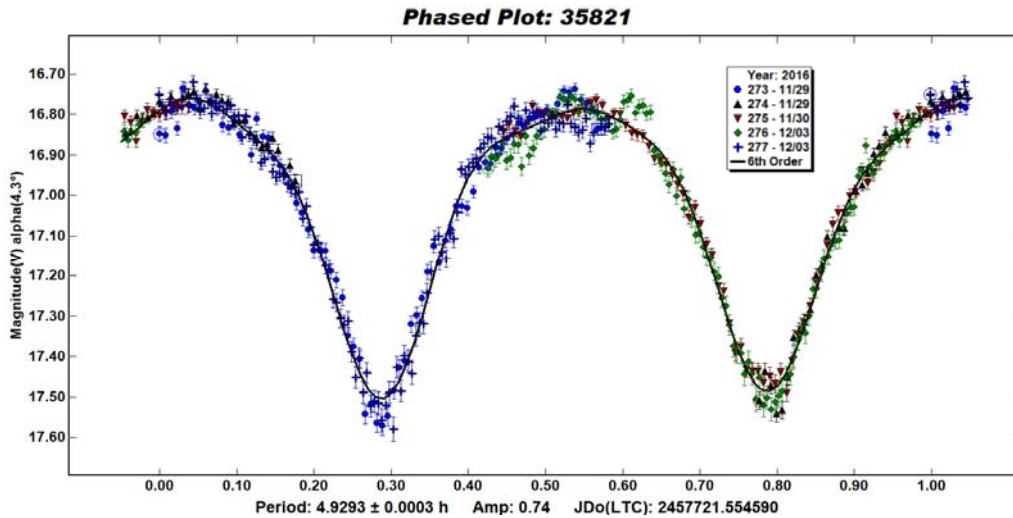


Figure 39. (35821) 1999 JW50 Lightcurve

4.3 Rotational Characteristics of V/V_p-type Asteroids

In this section, the lightcurve results from the previous section are compiled and analyzed to look for possible trends. Admittedly, the number of asteroids observed by this investigation (10) is relatively small. In addition, this study is characterized by the same biases which are typical of most lightcurve studies. Namely, short period and large amplitude lightcurves are preferentially represented. However, as described in Section 4.1, the asteroids targeted by this study are part of the larger “population” of V_p-type asteroids. Furthermore, the V_p-type asteroids have not generally been included in lightcurve studies of the Vesta family conducted to date (Hasegawa et al., 2014; Ryan et al., 2004).

The V_p-type taxonomic classification represents a group of potential Vesta family members that are distinct from other V-type asteroids. Specifically, due to the capabilities of SDSS, the V_p-type asteroids identified by Carvano et al. (2010) tend to be fainter, and hence generally smaller in diameter, than their V-type counterparts. This difference in the brightness of these two sets of asteroids is illustrated in terms of absolute magnitude (H) in Figure 40. In this histogram, the V-type asteroids (hatched blue) are taken from Hasegawa et al. (2014) and a compilation of asteroid taxonomic databases assembled by Neese (2010). The V-type histogram (solid green) peaks at an H of approximately 12.5. In contrast, the V_p-type histogram peaks at approximately 16.0. The 10 asteroids targeted by this study (solid red), a subset of the V_p-type group, peak between 13 and 14.

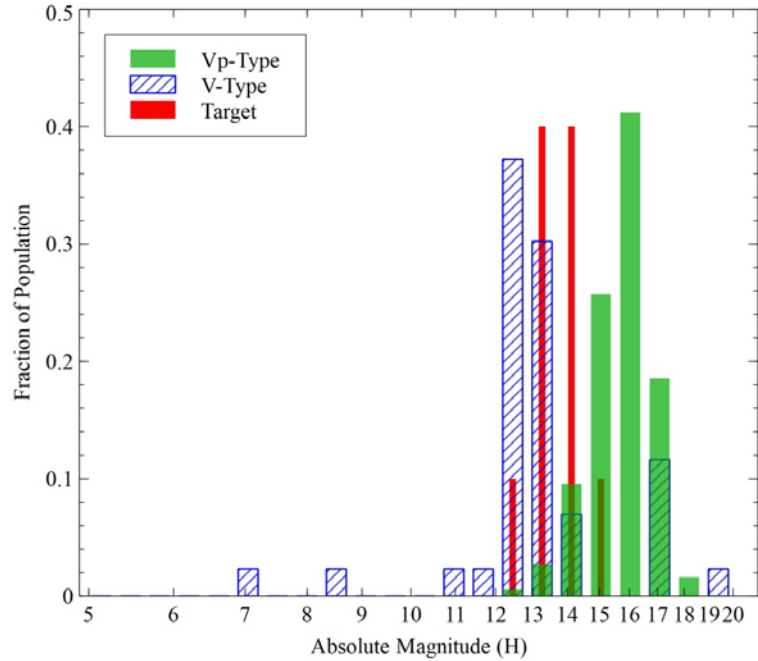


Figure 40. V/V_p-Type Absolute Magnitude (H) Histogram

A similar comparison is presented in Figure 41 in terms of asteroid diameter (D). In this histogram, the V-type group peaks at a diameter of approximately 6.5 km. The V_p-type diameter histogram peaks at approximately 2.5 km. The peak diameter of the ten target asteroids is between 3 km and 4 km.

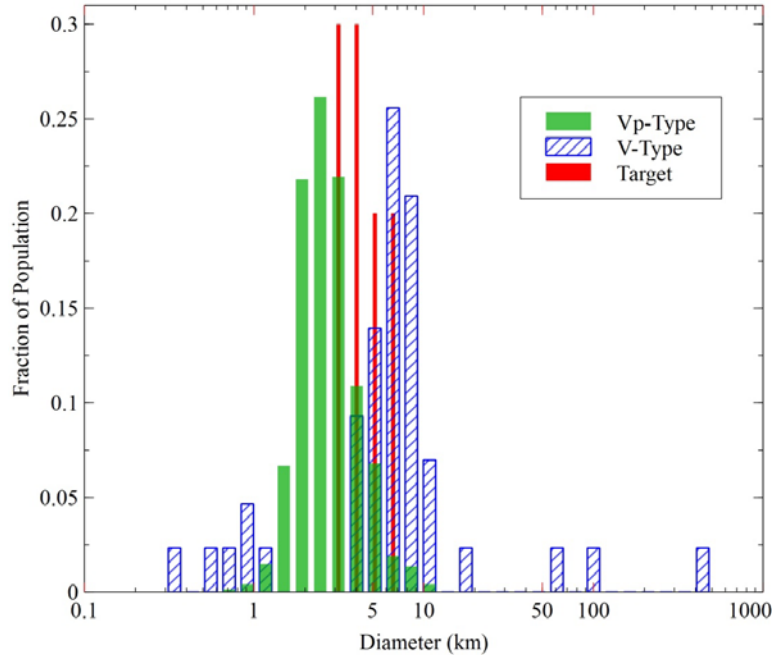


Figure 41. V/V_p-Type Asteroid Diameter (D) Histogram

Combining the lightcurve measurements obtained during this study with previously observed V_p-type asteroids, it is possible to investigate how the rotational characteristics of smaller diameter Vesta family members may differ from those studied to date. The rotation of smaller asteroids, for instance, is typically more significantly affected by the re-radiation of the sun’s thermal energy (e.g., the YORP effect). The YORP timescale is inversely related to the square of the asteroid radius (Bottke et al., 2002). Hence, smaller asteroids will typically “spin up” faster.

In addition, an asteroid’s size could imply information about its tensile strength. Namely, asteroids which are intact, monolithic bodies would generally be expected to be smaller remnants of the impact which created the asteroid family. Larger asteroids are mostly “rubble pile” assemblies, held together by self-gravity. The asteroid’s

makeup is an important determinant of its maximum rotational rate (i.e. the so-called “spin barrier”).

Finally, including V_p -type asteroids in such a rotational analysis of the Vesta family substantially increases the number of objects being considered. The analysis of Hasegawa et al. (2014) considered only 59 V-type asteroids. Adding the lightcurve measurements of this study’s ten target asteroids and existing LCDB measurements of other V_p -type asteroids results in a sample set of 208 potential Vesta family members. This larger sample set is more statistically significant and can provide more representative information about the rotational characteristics of the Vesta family of asteroids.

In the following sections, the rotational characteristics of this set of 208 V/V_p -type asteroids are analyzed. In Section 4.3.1, the distribution of rotational period of V/V_p -type asteroids as a function of asteroid diameter is investigated. In Section 4.3.2, the lightcurve amplitude of V/V_p -type asteroids as a function of spin rate is described. Finally, in Section 4.3.3, the distribution of rotational periods for this set of asteroids is compared with a Maxwellian distribution in order to learn more about the collisional history of Vesta.

4.3.1 Lightcurve Period vs. Diameter

In Figure 42, the asteroid lightcurve period is plotted as a function of asteroid diameter. The main belt and near-Earth asteroids (Warner et al., 2009) are shown as grey circles. The V-type asteroids (Hasegawa et al., 2014; Neese, 2010) are shown as green squares, and the V_p -type asteroids (Carvano et al., 2010) are shown as blue

circles. The ten target asteroids are represented by red triangles and are individually labeled in the key window to the right. The yellow line represents the “spin barrier”, a limit to the rotational speed of nearly spherical, strengthless bodies with bulk densities greater than 2.5 g/cm^3 .

Past studies (Pravec et al., 2002; Waszczak et al., 2015) have noted a general trend towards increasing rotational speed (decreasing lightcurve period) with decreasing asteroid diameter. In Figure 40, this trend is evident in the distribution of the main belt and near-Earth asteroid population (grey circles), but not clearly represented in the sampled V/V_p -type asteroid population (which has a more vertical distribution). The V -type asteroids have lightcurve periods ranging from approximately 2.5 to 19 hours, with the majority concentrated near 5.5 hours and greater than 10 hours. The V_p -type asteroids extend across a similar period range, but are predominantly distributed between 2.5 and 10 hours. Two of the V_p -type asteroids extend past the “spin barrier” ($< \text{approximately } 2.2 \text{ hours}$) and may be monolithic assemblages. Generally, the larger V_p -type data set provides improved resolution for the rotational period distribution of asteroids potentially derived from Vesta. This is particularly true for rotational rates less than 5 hours, where relatively little data were available previously.

The target asteroids from this study are mostly centered between rotational periods of 4 and 6 hours. Interestingly, the target asteroid with the largest diameter (7.4 km), (5235) Jean-Loup, has the shortest period (2.4 h). In addition, the target asteroid with the smallest diameter (2.95 km) has the longest period (9.49 h). This behavior runs

contrary to aforementioned trend, but is likely a coincidence related to the relatively small sample size.

In Figure 42, it can be seen that (5235) Jean-Loup is very close the “spin barrier” (~2.2 hr). Furthermore, recalling the dynamic and spectroscopic evidence presented in Section 4.1 and Section 4.2.2, respectively, it is very likely that (5235) Jean-Loup is a Vestoid “interloper” in the Flora asteroid family. It follows that Yarkovsky-YORP effects probably played an important role in its orbital migration and are also likely responsible for its relatively high spin rate.

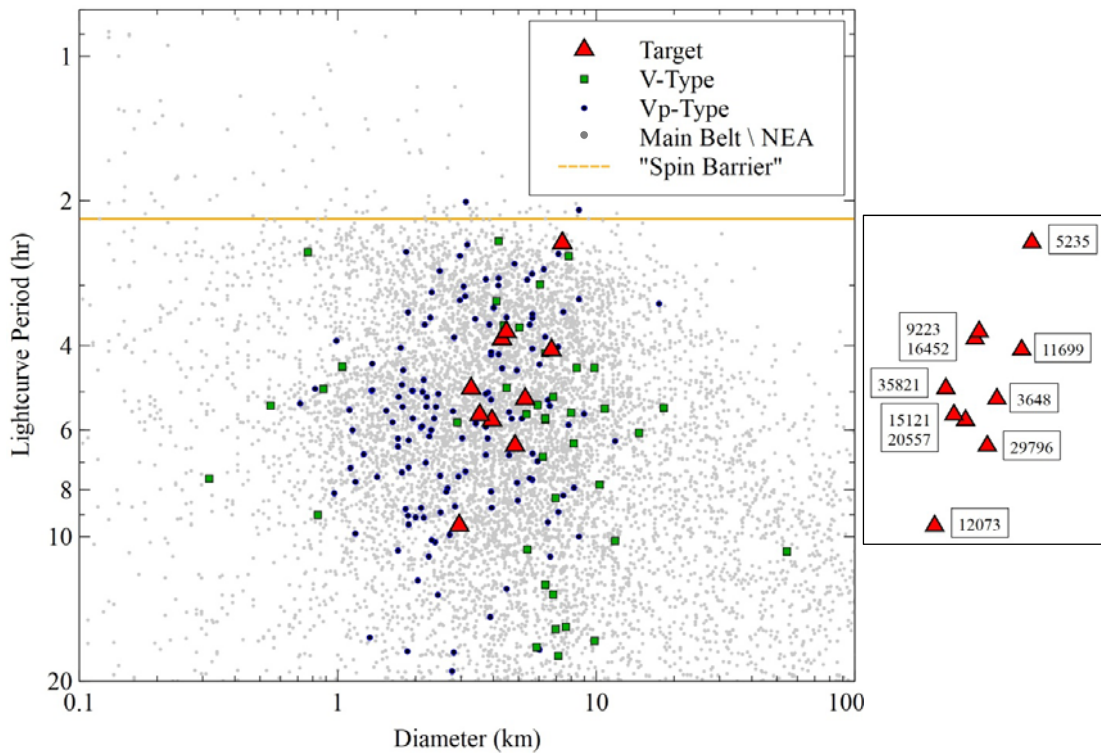


Figure 42. Asteroid Lightcurve Period vs. Diameter

4.3.2 Lightcurve Amplitude vs. Spin Rate

In Figure 43, the lightcurve amplitude is plotted as a function of spin rate. The main belt and near-Earth asteroids (Warner et al., 2009) are shown as grey circles. The V-type

asteroids (Hasegawa et al., 2014; Neese, 2010) are shown as green squares, and the V_p -type asteroids (Carvano et al., 2010) are shown as blue circles. The ten target asteroids are represented by red triangles and individually labeled in the key window to the right. The three dashed curves approximate upper limits of spin rates of objects held together by self-gravity only for bulk densities typical of asteroids (1 g/cm^3 , 2 g/cm^3 , and 3 g/cm^3) (Pravec and Harris, 2000).

Pravec et al. (2002) and Waszczak et al. (2015) demonstrated that lightcurve amplitudes generally decrease with increasing spin rate. This is behavior commonly attributed to the idea that most asteroids are loose aggregates and hence tend to assume a more spherical shape as their rotational rate increases. This trend is clearly evident in the main belt and near-Earth asteroid dataset (grey circles), but somewhat less apparent for the V_p -type asteroids. This behavior is not well represented in the V -type asteroid population, but this is likely due to the small size of the sample set.

The V -type asteroids are distributed over a wide range of lightcurve amplitudes from 0.1 to 1.2 magnitudes. The V_p -type asteroids are distributed over a similar range, but provide substantially improved fidelity in the region of small amplitude, fast rotators (lightcurve amplitude < 0.25 magnitudes and spin rates > 6 rev/day). One of the target asteroids, (5235) Jean-Loup, lies along the line of maximum spin rate for a bulk density of 2.0 g/cm^3 . Additionally, the lightcurve amplitude (0.11) for (5235) Jean-Loup is the smallest of all the target asteroids. It is likely that (5235) Jean-Loup is a “rubble pile” asteroid which has been “spun up” by the YORP effect and has assumed a more spherical shape. In addition to (5235) Jean-Loup, near-infrared spectroscopic studies

(Hardersen et al., 2014a; Hardersen, 2018, 2017) identified four other asteroids, including (3648) Raffinetti, (9223) Leifandersson, (12073) Larimer, and (29796) 1999 CW, as having a Vesta-like basaltic surface composition. As is highlighted by the yellow circle in Figure 43, it is interesting to note that all of these asteroids are in a region defined by faster rotation and smaller lightcurve amplitude. Hence, it seems likely that many of the Vesta family of asteroids are loose aggregates.

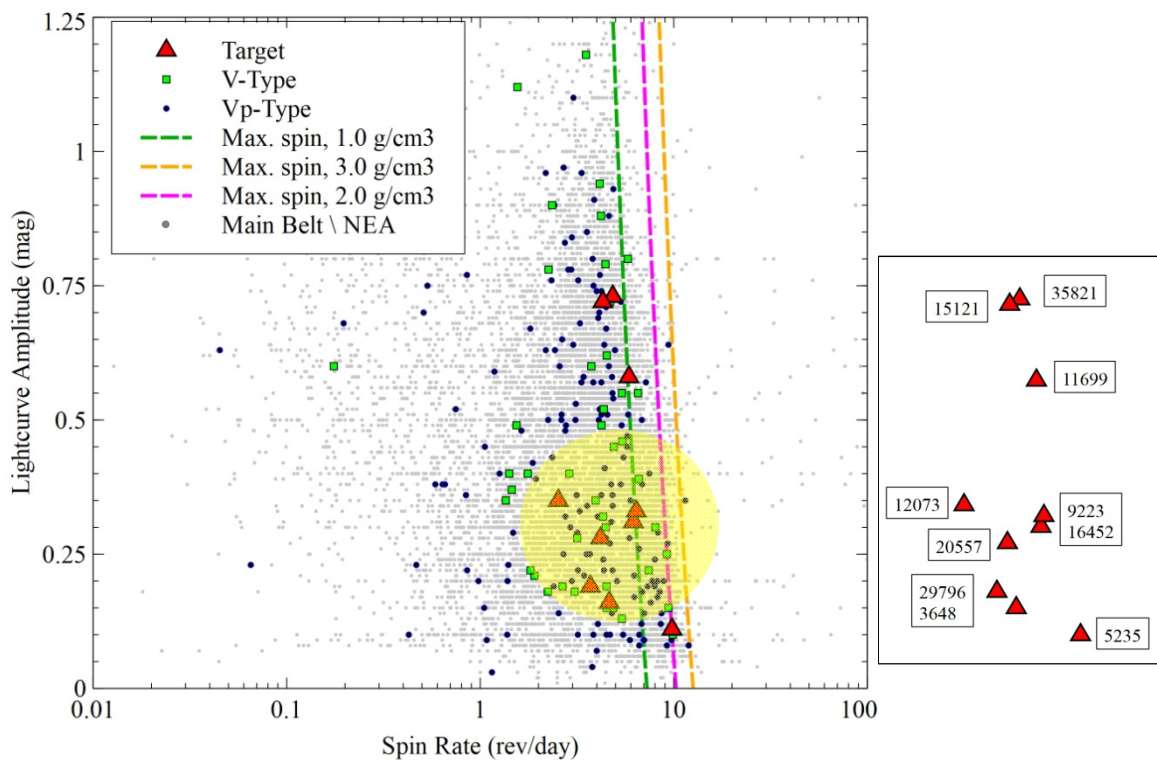


Figure 43. Lightcurve Amplitude vs. Spin Rate. The yellow circle encloses the five asteroids (3648, 5235, 9223, 12073, and 29796) that have Vesta-like basaltic surfaces confirmed by near-infrared spectroscopic measurements.

4.3.3 Maxwellian Distributions

As described in Section 2.3.2, it has been proposed that a Maxwellian distribution describes the distribution of asteroid rotation rates which would result if an asteroid population is purely collisionally evolved (Salo, 1987). Pravec et al. (2002) demonstrated

that for larger asteroids ($D > 40$ km), asteroid spin rates can very nearly be described by a Maxwellian distribution. Smaller asteroids, for which effects like YORP are more influential, typically are not distributed according to a Maxwellian curve.

Maxwellian analyses have also been applied to specific asteroid families. Binzel (1988), for instance, showed that the spin rates of Eos family of asteroids follow a Maxwellian distribution, “implying a collisionally evolved population” and suggesting that the larger members of the Eos family “may still remember their parent-body rotation rates.” Hasegawa et al. (2014) performed a similar analysis of the Vesta family using a set of approximately 60 V-type asteroids, including 13 asteroid lightcurves obtained as part of the investigation. Hasegawa et al. (2014) concluded that the distribution of rotational rates of this set of asteroids did not follow a Maxwellian distribution. Hasegawa et al. (2014) state, “...it is probable that the rotational rate distribution of V-type asteroids can be explained based on long-term modifications by the YORP torques.”

An updated histogram of the rotational periods known for V-type asteroids is shown in Figure 44. This asteroid set is drawn from Hasegawa et al. (2014) and Neese (2010) and does not include any V_p -type asteroids. The black dotted line represents the corresponding Maxwellian distribution. Visually, it is clear that the distribution of these V-type asteroid spin rates is not a good fit to the Maxwellian curve. Statistically, a Chi Square Goodness of Fit test reveals that the Maxwellian distribution can be rejected with a high level of confidence ($> 99\%$). These results agree with those of Hasegawa et al. (2014).

The asteroid distribution shown in Figure 45 is a combination of the V-type and V_p -type asteroid lightcurve data, including the 10 asteroids targeted by this study. As discussed in previous sections, the addition of the V_p -type data helps to de-bias the V-type (only) dataset by including a population of smaller diameter asteroids. Comparing Figure 44 and Figure 45, the addition of V_p -type asteroids with spin rates between 2 and 4 rev/day is apparent. Visually, this produces a distribution which appears to be closer to the Maxwellian distribution. However, a Chi Square Goodness of Fit test reveals that the Maxwellian distribution can still be rejected with a high level of confidence (> 99%).

The lack of agreement of the V/ V_p -type spin frequency distribution with the Maxwellian distribution is most likely due to the significant “excesses” near the slow (< 1 rev/day) and fast (> 7 rev/day) spin rate ranges. The latter range represents the same group of fast rotating asteroids highlighted in Section 4.3.2. These fast rotations are the likely result of radiative forces, like YORP. Pravec and Harris (2000) focused on these so-called “fast-rotating asteroids (FRAs)”, with spin rates between 7 and 11 rev/day, stating that these asteroids “are mostly loosely bound, gravity-dominated aggregates with negligible tensile strength (“rubble piles”)”. Figure 45 does not show any asteroids at the “spin barrier” (11 rev/day), but does show two V_p -type asteroids beyond the barrier. Pravec and Harris (2000) predict that such asteroids are typically very small ($D < 200$ m) and likely monolithic. However, these two V_p -type asteroids, (2704) Julian Loewe and (10750) 1989 PT, have diameters of 5.199km and 2.93 km, respectively. It is possible that the lightcurve periods reported for these asteroids (Warner et al., 2009) are

inaccurate. The quality scores (U) for (2704) Julian Loewe and (10750) 1989 PT are (only) 2+ and 1, respectively.

The dynamics of very slow rotating asteroids (< 1 rev/day) are less well understood. Pravec and Harris (2000) suggest different physical mechanisms including YORP, tidal effects, and non-principal rotation (very long damping scales). Additionally, this population of asteroids is under-represented in the V/V_p -type distribution shown here and in the asteroid population overall. Lightcurve studies of slowly rotating asteroids are time consuming and hence more difficult to complete. It is expected that the Maxwellian “excess” for slow rotators (< 1 rev/day) shown in Figure 45 will only increase with additional lightcurve studies focused on long period rotators.

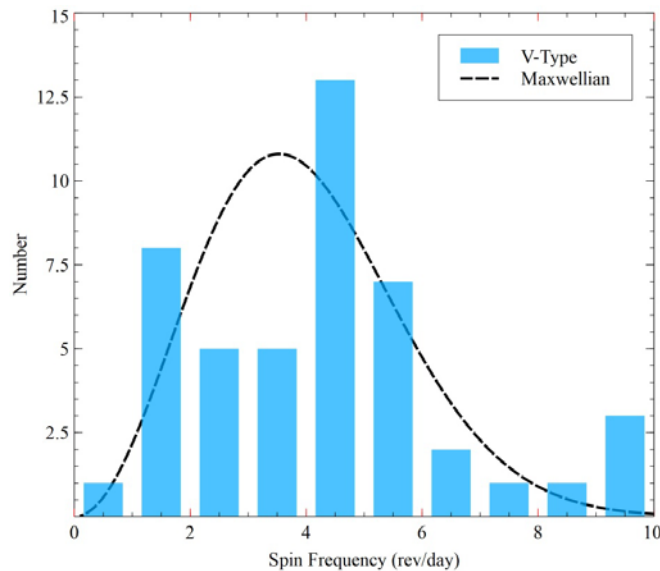


Figure 44. Spin Frequency Distribution: V-Type Asteroids

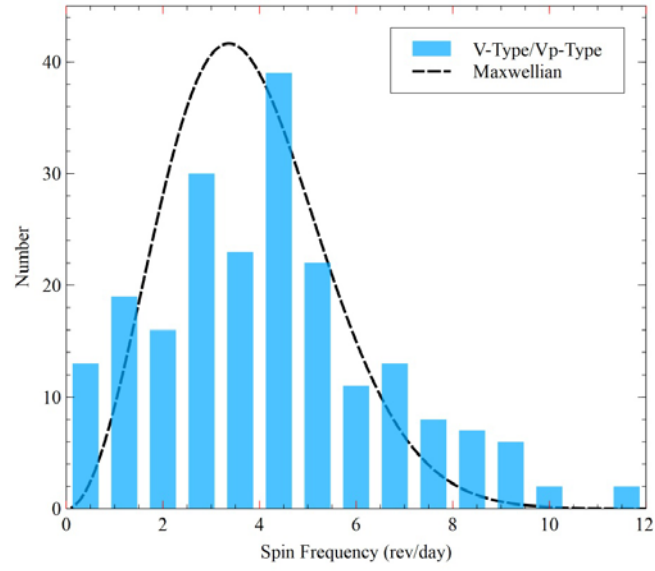


Figure 45. Spin Frequency Distribution: All V/V_p-Type Asteroids

CHAPTER 5

SUMMARY AND CONCLUSIONS

This study used lightcurve photometry to measure the spin rates of 10 V_p -type asteroids. The overall objective of this effort was to improve our understanding of the rotational characteristics of the Vesta family of asteroids (the “Vestoids”). The spin properties of these asteroids contain important clues about the impact event (or events) which created the family, as well as the mechanisms which injected its members into Earth-crossing orbits and eventually delivered meteorites (HED) to the Earth’s surface.

The targets for this study were drawn from the Carvano et al. (2010) V_p -type asteroid taxonomic classification, which is based on the SDSS MOC4. The V_p -type classification samples a set of potential “Vestoids” which are generally smaller in diameter than those which have been used in previous rotational studies of the Vesta family (Hasegawa et al., 2014; Ryan et al., 2004). In addition, including V_p -type asteroids in such studies produces a more statistically significant sample set and better facilitates an analysis of population trends and distributions.

The measurements for this study were obtained using five different telescopes located at three observatories: (1) Stone Edge Observatory (G52) in Sonoma, CA; (2) the Yerkes Observatory (754) in Williams Bay, WI; and (3) Cerro Tololo Inter-American Observatory (807) in La Serena, Chile. The ten target asteroids were drawn from a

subset of V_p -type asteroids which had no known or highly uncertain rotation rates in the LCDB. In addition, priority was given to those objects which had been part of a near-infrared spectroscopic compositional survey of V_p -type asteroids (Hardersen, 2016; Hardersen et al., 2013, 2014a, 2015b; Hardersen, 2016).

The target V_p -type asteroids for this study were (3648) Raffinetti, (5235) Jean-Loup, (9223) Leifandersson, (11699) 1998 FL105, (12073) Larimer, (15121) 2000 EN14, (16452) Goldfinger, (20557) Davidkulka, (29796) 1999 CW77, and (35821) 1999 JW50. Of these, five asteroids are members of the Vesta dynamical family (Nesvorny, 2010), one ((5235) Jean-Loup) is a member of the Flora dynamical family, and four have no known dynamical family association. In Section 4.1, it was noted that (5235) Jean-Loup is very close to the 3:1 mean-motion resonance with Jupiter, whose gravitational effects on (5235) Jean-Loup's orbit are likely responsible for the making the asteroid a "fugitive" in the Flora family (Roig et al., 2011).

Of the ten target asteroids, only two asteroids, (9223) Leifandersson and (35821) 1999 JW50, had lightcurve period estimates available in the LCDB. Five of the ten target asteroids, (3648) Raffinetti, (5235) Jean-Loup, (9223) Leifandersson, (11699) 1998 FL105, and (29796) 1999 CW77, were included in aforementioned near-infrared spectroscopy study (Hardersen, 2016; Hardersen et al., 2013, 2014a, 2015b; Hardersen, 2016). Of these, only (11699) 1998 FL105 did not exhibit Vesta-like basaltic absorption features near 1.0 μm and 2.0 μm . The other four asteroids have surface compositions very similar to Vesta and hence are likely to be "Vestoids".

Lightcurves for the ten target asteroids were generated from the photometric measurements using the MPO Canopus software (Warner, 2012, 2011). An estimation of the asteroid lightcurve amplitude and period was calculated using the “Period Search” feature of MPO Canopus (Harris et al., 1989). The individual asteroid lightcurve analyses were presented in Section 4.2. Most of the lightcurves exhibit the typical dual-lobed lightcurve shapes associated with triaxial ellipsoid-shaped asteroids. However, two asteroids, (15121) 2000 EN14 and (35821) 1999 JW50, have lightcurves with “rounded” peaks and “sharp” valleys, representative of more highly elongated, non-convex shapes (e.g., dumbbell-shaped). Alternatively, the asteroid (15121) 2000 EN14, with its “shoulder”-like lightcurve peak features, may in fact be a synchronous binary system.

Section 4.3 combined the lightcurve data obtained from this effort with that available in the literature for V/V_p -type asteroids (Hasegawa et al., 2014; Neese, 2010; Warner et al., 2009). An analysis was conducted to identify potential correlations between rotational period, lightcurve amplitude, and asteroid diameter. Perhaps the most interesting results from this study were for (5235) Jean-Loup, located close to the 3:1 mean motion resonance. In Figure 44 and Figure 44, it was shown that (5235) Jean-Loup has the shortest rotational period (2.45 hr) of the ten target asteroids and is very close to the so-called “spin barrier”. The asteroid also happens to have the smallest lightcurve amplitude (0.11). It is likely that (5235) Jean-Loup is a loose aggregate (“rubble pile”) body of approximately spherical shape which migrated towards the 3:1 mean-motion resonance due to Yarkovsky effects, was effectively “spun up” due to the related YORP torques, and had its orbit gravitationally altered by Jupiter such that it

became an “interloper” in the neighboring Flora family. These dynamic mechanisms, combined with the compositional information provided by Hardersen et al. (2014a) indicating that the surface composition of (5235) Jean-Loup is similar to the Howardite meteorites, present a relatively complete picture of how fragments generated by an impact on Vesta could bring meteorites to the Earth’s surface. It is interesting to note that all of the asteroids with surface compositions confirmed to be Vesta-like are in the group of faster rotating, smaller lightcurve amplitude asteroids. This is an indication that many of the Vesta family members are “rubble piles” which have been strongly affected by Yarkovsky/YORP radiative effects.

This idea is further supported by the Maxwellian distribution comparisons presented in Section 4.3.3. A population of asteroids whose distribution of spin rates follows a Maxwellian distribution is considered to be one in which collisional dynamics are the predominant evolutionary factor (Salo, 1987). Departures from the Maxwellian distribution, therefore, indicate that other factors, like YORP effects, are important for determining the population’s spin rates. Using a lightcurve data from a combination of V-type and V_p -type asteroids, including the ten target asteroids, it was shown that the spin rate distribution was non-Maxwellian and characterized by excesses of both very slow and very fast rotators. This result is similar to that reported by Hasegawa et al. (2014). Together, these results support the idea that YORP torques have played an important part in the evolution of the Vesta asteroid family. The YORP effect is dependent on several quantities, including the asteroid size, shape, spin vector, and distance from the Sun. For the size ranges of the V/V_p -type asteroid population

considered here (approximately 1 to 10 km in diameter), Rubincam (2000) predicts a doubling of spin rate due to YORP effects over a time span on the order of 10 to 100 million years. This is compatible with the approximately 1 billion year age estimate of the collision which is believed to have created the Vesta family (Carruba et al., 2005; Marchi et al., 2012; Nesvorný et al., 2008).

REFERENCES

- Alard, C., Lupton, R.H., 1998. A Method for Optimal Image Subtraction. *\apj* 503, 325–331. <https://doi.org/10.1086/305984>
- Albers, K., Kragh, K., Monnier, A., Pligge, Z., Stolze, K., West, J., Yim, A., Ditteon, R., 2010. Asteroid Lightcurve Analysis at the Oakley Southern Sky Observatory: 2009 October thru 2010 April. *Minor Planet Bull.* 37, 152–158.
- Alvarez, W., Asaro, F., 1990. An extraterrestrial impact. *Sci. Am.* 263, 78–84.
- Alvarez-Candal, A., Duffard, R., Angeli, C.A., Lazzaro, D., Fernández, S., 2004. Rotational lightcurves of asteroids belonging to families. *Icarus* 172, 388–401. <https://doi.org/10.1016/j.icarus.2004.06.008>
- Asphaug, E., 1997. Impact origin of the Vesta family. *Meteorit. Planet. Sci.* 32, 965–980.
- Asphaug, E., Ryan, E.V., Zuber, M.T., 2002. Asteroid Interiors, in: Bottke, W.F., Jr., Cellino, A., Paolicchi, P., Binzel, R.P. (Eds.), *Asteroids III*. pp. 463–484.
- Behrend, R., 2017. Courbes de rotation d’astéroïdes et de comètes, CdR [WWW Document]. *Courbes Rotat. Astéroïdes Comètes CdR*.
- Behrend, R., Bernasconi, L., Roy, R., Klotz, A., Colas, F., Antonini, P., Aoun, R., Augustesen, K., Barbotin, E., Berger, N., Berrouachdi, H., Brochard, E., Cazenave, A., Cavadore, C., Coloma, J., Cotrez, V., Deconihout, S., Demeautis, C., Dorseuil, J., Dubos, G., Durkee, R., Frappa, E., Hormuth, F., Itkonen, T., Jacques, C., Kurtze, L., Laffont, A., Lavayssière, M., Lecacheux, J., Leroy, A., Manzini, F., Masi, G., Matter, D., Michelsen, R., Nomen, J., Oksanen, A., Pääkkönen, P., Peyrot, A., Pimentel, E., Pray, D., Rinner, C., Sanchez, S., Sonnenberg, K., Sposetti, S., Starkey, D., Stoss, R., Teng, J.-P., Vignand, M., Waelchli, N., 2006. Four new binary minor planets: (854) Frostia, (1089) Tama, (1313) Berna, (4492) Debussy. *\aap* 446, 1177–1184. <https://doi.org/10.1051/0004-6361:20053709>
- Bell, J.F., 1988. An Earth-Crossing Source Body for the Basaltic Achondrites: Vesta’s Son or Vesta’s Nephew?, in: *Lunar and Planetary Science Conference, Lunar and Planetary Science Conference*. p. 55.

- Bell, J.F., Owensby, P.D., Hawke, B.R., Brown, R.H., Cruikshank, D., Hartmann, W.K., 1995. 52-color Asteroid Survey.
- Bell, J.F., Owensby, P.D., Hawke, B.R., Gaffey, M.J., 1988. The 52-Color Asteroid Survey: Final Results and Interpretation, in: Lunar and Planetary Science Conference, Lunar and Planetary Science Conference. p. 57.
- Binzel, R.P., 2012. A Golden Spike for Planetary Science. *Science* 338, 203–204.
<https://doi.org/10.1126/science.1228328>
- Binzel, R.P., 1988. Collisional evolution in the Eos and Koronis asteroid families: Observational and numerical results. *Icarus* 73, 303–313.
[https://doi.org/10.1016/0019-1035\(88\)90100-5](https://doi.org/10.1016/0019-1035(88)90100-5)
- Binzel, R.P., Farinella, P., Zappala, V., Cellino, A., 1989. Asteroid rotation rates - Distributions and statistics, in: Binzel, R.P., Gehrels, T., Matthews, M.S. (Eds.), *Asteroids II*. pp. 416–441.
- Binzel, R.P., Xu, S., 1993. Chips off of Asteroid 4 Vesta: Evidence for the Parent Body of Basaltic Achondrite Meteorites. *Science, New Series* 260, 186–191.
- Bottke, W.F., 2002. *Asteroids III*, Space Science Series. University of Arizona Press.
- Bottke, W.F., Durda, D.D., Nesvorný, D., Jedicke, R., Morbidelli, A., Vokrouhlický, D., Levison, H., 2005. The fossilized size distribution of the main asteroid belt. *Icarus* 175, 111–140. <https://doi.org/10.1016/j.icarus.2004.10.026>
- Bottke, W.F., Rubincam, D.P., Broz, M., 2002. The Effect of Yarkovsky Thermal Forces on the Dynamical Evolution of Asteroids and Meteoroids.
- Bottke, W.F., Vokrouhlický, D., Rubincam, D.P., Nesvorný, D., 2006. The Yarkovsky and YORP effects: Implications for asteroid dynamics. *Annu Rev Earth Planet Sci* 34, 157–191.
- Bowell, E., Chapman, C.R., Gradie, J.C., Morrison, D., Zellner, B., 1978. Taxonomy of asteroids. *Icarus* 35, 313–335.
- Bus, S., Binzel, R., 2002a. Phase II of the small main-belt asteroid spectroscopic survey: A feature-based taxonomy. *Icarus* 158, 146–177.
- Bus, S., Binzel, R., 2002b. Phase {II} of the Small Main-Belt Asteroid Spectroscopic Survey: The Observations. *Icarus* 158, 106–145.
<https://doi.org/http://dx.doi.org/10.1006/icar.2002.6857>

- Carruba, V., Michtchenko, T.A., Roig, F., Ferraz-Mello, S., Nesvorný, D., 2005. On the V-type asteroids outside the Vesta family. I. Interplay of nonlinear secular resonances and the Yarkovsky effect: The cases of 956 Elisa and 809 Lundia. *Astron. Astrophys.* 441, 819–829.
- Carvano, J., Hasselmann, P. H., Lazzaro, D., Mothé-Diniz, T., 2010. SDSS-based taxonomic classification and orbital distribution of main belt asteroids. *A&A* 510, A43. <https://doi.org/10.1051/0004-6361/200913322>
- Chamberlain, A., 2007. Asteroid Main-Belt Distribution - Kirkwood Gaps [WWW Document]. URL http://ssd.jpl.nasa.gov/images/ast_histo.ps
- Chang, C.-K., Ip, W.-H., Lin, H.-W., Cheng, Y.-C., Ngeow, C.-C., Yang, T.-C., Waszczak, A., Kulkarni, S.R., Levitan, D., Sesar, B., Laher, R., Surace, J., Prince, T.A., 2015. ASTEROID SPIN-RATE STUDY USING THE INTERMEDIATE PALOMAR TRANSIENT FACTORY. *Astrophys. J. Suppl. Ser.* 219, 27. <https://doi.org/10.1088/0067-0049/219/2/27>
- Chapman, C.R., Morrison, D., Zellner, B., 1975. Surface properties of asteroids: A synthesis of polarimetry, radiometry, and spectrophotometry. *Icarus* 25, 104–130.
- Cheng, A.F., 2002. Near Earth asteroid rendezvous: mission summary. *Asteroids III* 1, 351–366.
- Cruikshank, D.P., Tholen, D.J., Hartmann, W.K., Bell, J.F., Brown, R.H., 1991. Three basaltic earth-approaching asteroids and the source of the basaltic meteorites. *Icarus* 89, 1–13. [https://doi.org/http://dx.doi.org/10.1016/0019-1035\(91\)90083-6](https://doi.org/http://dx.doi.org/10.1016/0019-1035(91)90083-6)
- De Sanctis, M.C., Ammannito, E., Capria, M.T., Tosi, F., Capaccioni, F., Zambon, F., Carraro, F., Fonte, S., Frigeri, A., Jaumann, R., Magni, G., Marchi, S., McCord, T.B., McFadden, L.A., McSween, H.Y., Mittlefehldt, D.W., Nathues, A., Palomba, E., Pieters, C.M., Raymond, C.A., Russell, C.T., Toplis, M.J., Turrini, D., 2012. Spectroscopic Characterization of Mineralogy and Its Diversity Across Vesta. *Science, New Series* 336, 697–700. <https://doi.org/10.2307/41584790>
- DeMeo, F., Carry, B., 2014. Solar System evolution from compositional mapping of the asteroid belt. *ArXiv Prepr. ArXiv14082787*.
- DeMeo, F.E., Binzel, R.P., Slivan, S.M., Bus, S.J., 2009. An extension of the Bus asteroid taxonomy into the near-infrared. *Icarus* 202, 160–180. <https://doi.org/10.1016/j.icarus.2009.02.005>

- Descamps, P., 2015. Dumb-bell-shaped equilibrium figures for fiducial contact-binary asteroids and EKBOs. *Icarus* 245, 64–79.
<https://doi.org/https://doi.org/10.1016/j.icarus.2014.08.002>
- Deuar, P., 2006. Vesta Family [WWW Document]. URL
http://commons.wikimedia.org/wiki/File:Vesta_family.png
- Farinella, P., Paolicchi, P., Zappala, V., 1981. Analysis of the spin rate distribution of asteroids. *Astron. Astrophys.* 104, 159–165.
- Farinella, P., Vokrouhlický, D., Hartmann, W.K., 1998. Meteorite delivery via Yarkovsky orbital drift. *Icarus* 132, 378–387.
- Fodera, S., Manara, A., Sicoli, P., 2003. Giuseppe Piazzi and the Discovery of Ceres in Asteroids III, WF Bottke Jr. et al. eds 17–24.
- Fujiwara, A., Kawaguchi, J., Yeomans, D.K., Abe, M., Mukai, T., Okada, T., Saito, J., Yano, H., Yoshikawa, M., Scheeres, D.J., Barnouin-Jha, O., Cheng, A.F., Demura, H., Gaskell, R.W., Hirata, N., Ikeda, H., Kominato, T., Miyamoto, H., Nakamura, A.M., Nakamura, R., Sasaki, S., Uesugi, K., 2006. The Rubble-Pile Asteroid Itokawa as Observed by Hayabusa. *Science* 312, 1330–1334.
<https://doi.org/10.1126/science.1125841>
- Fulchignoni, M., Barucci, M.A., di Martino, M., Dotto, E., 1995. On the evolution of the asteroid spin. *JPL* 299, 929.
- Gaffey, M., 1983. The asteroid (4) Vesta: Rotational spectral variations, surface material heterogeneity, and implications for the origin of the basaltic achondrites. *LPI Contrib.* 497, 14–18.
- Gaffey, M.J., 1997. Surface Lithologic Heterogeneity of Asteroid 4 Vesta. *Icarus* 127, 130–157. <https://doi.org/10.1006/icar.1997.5680>
- Gaffey, M.J., Cloutis, E.A., Kelley, M.S., Reed, K.L., 2002. Mineralogy of asteroids. *Asteroids III* 183.
- Gary, B., 2005. PHOTOMETRY USING SIMPLIFIED MAGNETUDE EQUATIONS: QUICK START EXAMPLES [WWW Document]. *Photom. USING Simpl. MAGNETUDE EQATIONS QUICK START Ex.* URL
<http://brucegary.net/photometry/quickstart.html>
- Gladman, B.J., Davis, D.R., Neese, C., Jedicke, R., Williams, G., Kavelaars, J., Petit, J.-M., Scholl, H., Holman, M., Warrington, B., 2009. On the asteroid belt's orbital and size distribution. *Icarus* 202, 104–118.

- Gladman, B.J., Migliorini, F., Morbidelli, A., Zappala, V., Michel, P., Cellino, A., Froeschele, C., Levison, H.F., Bailey, M., Duncan, M., 1997. Dynamical lifetimes of objects injected into asteroid belt resonances. *Science* 277, 197+.
- Gradie, J.C., Tedesco, E.F., 1982. Compositional Structure of the Asteroid Belt. *Science* 216, 1405–1407. <https://doi.org/10.1126/science.216.4553.1405>
- Hardersen, P., 2016. Finding ancient lava flows: Continuing the effort to inventory basaltic asteroids in the main asteroid belt.
- Hardersen, P.S., TBD, 2018. To Be Published.
- Hardersen, P.S., 2017. E-mail correspondence.
- Hardersen, P.S., 2016. Eight is Enough, Episode 2 (to be published).
- Hardersen, P.S., 2015. Finding the lava: constraining the basaltic asteroid population in the main asteroid belt.
- Hardersen, P.S., Genet, R.M., Roberts, R., 2013. Near-IR Spectroscopy of V-type Asteroids. *Soc. Astron. Sci. Annu. Symp.* 32, 169–174.
- Hardersen, P.S., Reddy, V., Nowinski, M., Dievendorf, M., 2015a. NIR spectral and mineralogic studies of nine Vp-type asteroids: 7 likely Vestoids and 2 likely new outer belt basaltic asteroid candidates, in: AAS/Division for Planetary Sciences Meeting Abstracts, AAS/Division for Planetary Sciences Meeting Abstracts. p. 106.01.
- Hardersen, P.S., Reddy, V., Roberts, R., 2015b. The Dirty Dozen: NIR Spectral and Mineralogical Interpretations for 12 Vp-Type Asteroids as Candidate Vestoids, in: Lunar and Planetary Science Conference, Lunar and Planetary Science Conference. p. 1775.
- Hardersen, P.S., Reddy, V., Roberts, R., 2015c. Vestoids, Part II: The basaltic nature and HED meteorite analogs for eight Vp-type asteroids and their associations with (4) Vesta. *Astrophys. J. Suppl. Ser.* 221, 19. <https://doi.org/10.1088/0067-0049/221/1/19>
- Hardersen, P.S., Reddy, V., Roberts, R., Mainzer, A., 2014a. More chips off of Asteroid (4) Vesta: Characterization of eight Vestoids and their {HED} meteorite analogs. *Icarus* 242, 269–282. <https://doi.org/http://dx.doi.org/10.1016/j.icarus.2014.08.020>

- Hardersen, P.S., Reddy, V., Roberts, R., Mainzer, A., 2014b. Eight is enough: Identification of additional Vestoids via NIR spectral and mineralogical characterization, in: AAS/Division for Planetary Sciences Meeting Abstracts, AAS/Division for Planetary Sciences Meeting Abstracts. p. 500.01.
- Harris, A.W., 1994. Tumbling Asteroids. *Icarus* 107, 209–211.
<https://doi.org/http://dx.doi.org/10.1006/icar.1994.1017>
- Harris, A.W., Burns, J.A., 1979. Asteroid rotation. *Icarus* 40, 115–144.
[https://doi.org/http://dx.doi.org/10.1016/0019-1035\(79\)90058-7](https://doi.org/http://dx.doi.org/10.1016/0019-1035(79)90058-7)
- Harris, A.W., Pravec, P., Galád, A., Skiff, B.A., Warner, B.D., Világi, J., Gajdoš, Š., Carbognani, A., Hornoch, K., Kušnirák, P., others, 2014. On the maximum amplitude of harmonics of an asteroid lightcurve. *Icarus* 235, 55–59.
- Harris, A.W., Young, J.W., Bowell, E., Martin, L.J., Millis, R.L., Poutanen, M., Scaltriti, F., Zappala, V., Schober, H.J., Debehogne, H., Zeigler, K.W., 1989. Photoelectric observations of asteroids 3, 24, 60, 261, and 863. *Icarus* 77, 171–186.
[https://doi.org/10.1016/0019-1035\(89\)90015-8](https://doi.org/10.1016/0019-1035(89)90015-8)
- Hasegawa, S., Miyasaka, S., Mito, H., Sarugaku, Y., Ozawa, T., Kuroda, D., Nishihara, S., Harada, A., Yoshida, M., Yanagisawa, K., Shimizu, Y., Nagayama, S., Toda, H., Okita, K., Kawai, N., Mori, M., Sekiguchi, T., Ishiguro, M., Abe, T., Abe, M., 2014. Lightcurve survey of V-type asteroids in the inner asteroid belt. *Publ. Astron. Soc. Jpn.* 66, 54–54. <https://doi.org/10.1093/pasj/psu040>
- Hasselmann, P.H., Carvano, J.M., Lazzaro, D., 2012. SDSS-based Asteroid Taxonomy, EAR-A-I0035-5-SDSSTAX-V1.1.
- Holsapple, K., Glibin, I., Housen, K., Nakamura, A., Ryan, E., 2002. Asteroid Impacts: Laboratory Experiments and Scaling Laws, in: Bottke, W.F., Jr., Cellino, A., Paolicchi, P., Binzel, R.P. (Eds.), *Asteroids III*. pp. 443–462.
- Holsapple, K.A., Schmidt, R.M., 1982. On the scaling of crater dimensions. II - Impact processes. *J. Geophys. Res.* 87, 1849–1870.
<https://doi.org/10.1029/JB087iB03p01849>
- Howell, S.B., 2006. *Handbook of CCD Astronomy*, 2nd ed, Cambridge Observing Handbooks for Research Astronomers. Cambridge University Press.
<https://doi.org/10.1017/CBO9780511807909>
- Hudson, R.S., Ostro, S.J., 1995. Shape and Non-Principal Axis Spin State of Asteroid 4179 Toutatis. *Science* 270, 84–86. <https://doi.org/10.1126/science.270.5233.84>
- Hudson, S., Hamilton, C., 2013. Asteroid Toutatis [WWW Document]. Asteroid Toutatis. URL <http://solarviews.com/thumb/ast/toutat9.gif>

- Ivanov, B.A., Melosh, H.J., 2013. Two-dimensional numerical modeling of the Rheasilvia impact formation. *J. Geophys. Res. Planets* 118, 1545–1557. <https://doi.org/10.1002/jgre.20108>
- Ivezić, Ž., Jurić, M., Lupton, R., 2010. Sloan Digital Sky Survey (SDSS) Moving Object Catalog 4th Release, EAR-A-I0035-3-SDSSMOC-V3.0.
- Jedicke, R., Jedicke, P., 2006. Color is the key to understanding asteroid family histories. *Astron. Mag.* 6, 36–41.
- Jutzi, M., Asphaug, E., Gillet, P., Barrat, J.-A., Benz, W., 2013. The structure of the asteroid 4[Vesta] as revealed by models of planet-scale collisions. *Nature* 494, 207–210. <https://doi.org/10.1038/nature11892>
- Jutzi, M., Holsapple, K., Wünneman, K., Michel, P., 2015. Modeling asteroid collisions and impact processes. *ArXiv E-Prints*.
- Kaasalainen, M., 2001a. Optimization Methods for Asteroid Lightcurve Inversion I. Shape Determination. *Icarus* 153, 24–36. <https://doi.org/10.1006/icar.2001.6673>
- Kaasalainen, M., 2001b. Optimization Methods for Asteroid Lightcurve Inversion II. The Complete Inverse Problem. *Icarus* 153, 37–51. <https://doi.org/10.1006/icar.2001.6674>
- Kirkwood, D., 1888. *The Asteroids Or Minor Planets Between Mars and Jupiter*. J.B. Lippincott Company, Philadelphia, PA.
- Kozai, Y., 1994. Kiyotsugu Hirayama and his families of asteroids. Presented at the 75 Years of Hirayama Asteroid Families: The Role of Collisions in the Solar System History, p. 1.
- Kryszczyńska, A., 2013. Do Slivan states exist in the Flora family? . II. Fingerprints of the Yarkovsky and YORP effects. *A&A* 551, A102. <https://doi.org/10.1051/0004-6361/201220490>
- Kryszczyńska, A., Colas, F., Descamps, P., Bartczak, P., Polińska, M., Kwiatkowski, T., Lecacheux, J., Hirsch, R., Fagas, M., Kamiński, K., Michałowski, T., Marciniak, A., 2009. New binary asteroid 809 Lundia - I. Photometry and modelling. *A&A* 501, 769–776. <https://doi.org/10.1051/0004-6361/200809877>

- Kryszczyńska, A., Colas, F., Polińska, M., Hirsch, R., Ivanova, V., Apostolovska, G., Bilkina, B., Velichko, F.P., Kwiatkowski, T., Kankiewicz, P., Vachier, F., Umlenski, V., Michałowski, T., Marciniak, A., Maury, A., Kamiński, K., Fagas, M., Dimitrov, W., Borczyk, W., Sobkowiak, K., Lecacheux, J., Behrend, R., Klotz, A., Bernasconi, L., Crippa, R., Manzini, F., Poncy, R., Antonini, P., Oszkiewicz, D., Santana-Ros, T., 2012. Do Slivan states exist in the Flora family?. I. Photometric survey of the Flora region. *AAS* 546, A72. <https://doi.org/10.1051/0004-6361/201219199>
- Mainzer, a., Bauer, J., Grav, T., Masiero, J., Cutri, R.M., Dailey, J., Eisenhardt, P., McMillan, R.S., Wright, E., Walker, R., Jedicke, R., Spahr, T., Tholen, D., Alles, R., Beck, R., Brandenburg, H., Conrow, T., Evans, T., Fowler, J., Jarrett, T., Marsh, K., Masci, F., McCallon, H., Wheelock, S., Wittman, M., Wyatt, P., DeBaun, E., Elliott, G., Elsbury, D., Gautier, T., Gomillion, S., Leisawitz, D., Maleszewski, C., Micheli, M., Wilkins, a., 2011a. Preliminary Results From Neowise: an Enhancement To the Wide-Field Infrared Survey Explorer for Solar System Science. *Astrophys. J.* 731, 53. <https://doi.org/10.1088/0004-637X/731/1/53>
- Mainzer, a., Grav, T., Masiero, J., Hand, E., Bauer, J., Tholen, D., McMillan, R.S., Spahr, T., Cutri, R.M., Wright, E., Watkins, J., Mo, W., Maleszewski, C., 2011b. Neowise Studies of Spectrophotometrically Classified Asteroids: Preliminary Results. *Astrophys. J.* 741, 90. <https://doi.org/10.1088/0004-637X/741/2/90>
- Marchi, S., McSween, H.Y., O'Brien, D.P., Schenk, P., Sanctis, M.C.D., Gaskell, R., Jaumann, R., Mottola, S., Preusker, F., Raymond, C.A., Roatsch, T., Russell, C.T., 2012. The Violent Collisional History of Asteroid 4 Vesta. *Science, New Series* 336, 690–694. <https://doi.org/10.2307/41584788>
- Masiero, J., A. K. Mainzer, Grav, T., J. M. Bauer, R. M. Cutri, J. Dailey, P. R. M. Eisenhardt, R. S. McMillan, T. B. Spahr, M. F. Skrutskie, D. Tholen, R. G. Walker, E. L. Wright, E. DeBaun, D. Elsbury, T. Gautier IV, S. Gomillion, A. Wilkin, 2011. Main Belt Asteroids with WISE/NEOWISE. I. Preliminary Albedos and Diameters. *Astrophys. J.* 741, 68.
- Masiero, J.R., Mainzer, a K., Grav, T., Bauer, J.M., Cutri, R.M., Dailey, J., Eisenhardt, P.R.M., McMillan, R.S., Spahr, T.B., Skrutskie, M.F., Tholen, D., Walker, R.G., Wright, E.L., DeBaun, E., Elsbury, D., Gautier IV, T., Gomillion, S., Wilkins, a, 2011. Main Belt Asteroids with WISE/NEOWISE. I. Preliminary Albedos and Diameters. *Astrophys. J.* 741, 68. <https://doi.org/10.1088/0004-637X/741/2/68>
- McCord, T.B., Adams, J.B., Johnson, T.V., 1970. Asteroid Vesta: Spectral Reflectivity and Compositional Implications. *Science, New Series* 168, 1445–1447. <https://doi.org/10.2307/1730448>
- McSween, H.Y., 1999. *Meteorites and Their Parent Planets*, 2nd ed. Cambridge University Press.

- Meteoritical Bulletin Database [WWW Document], 2015. URL <http://www.lpi.usra.edu/meteor/>
- Migliorini, F., Morbidelli, A., Zappala, V., Gladman, B.J., Bailey, M.E., Cellino, A., 1997. Vesta fragments from v6 and 3: 1 resonances: Implications for V-type near-Earth asteroids and howardite, eucrite and diogenite meteorites. *Meteorit. Planet. Sci.* 32, 903–916.
- Minor Planet Center, 2016a. Distribution of the Minor Planets: Semimajor Axis [WWW Document]. *Distrib. Minor Planets Semimajor Axis*. URL <http://www.minorplanetcenter.net/iau/plot/OrbEls01.gif>
- Minor Planet Center, 2016b. Distribution of the Minor Planets: e vs i [WWW Document]. *Distrib. Minor Planets E Vs I*. URL <http://www.minorplanetcenter.net/iau/plot/OrbEls52.gif>
- Morbidelli, A., Brasser, R., Gomes, R., Levison, H.F., Tsiganis, K., 2010. Evidence from the Asteroid Belt for a Violent Past Evolution of Jupiter’s Orbit. *Astron. J.* 140, 1391–1401.
- Mueller, M., Delbo, M., Hora, J., Trilling, D., Bhattacharya, B., Bottke, W., Chesley, S., Emery, J., Fazio, G., Harris, A., 2011. ExploreNEOs. III. Physical characterization of 65 potential spacecraft target asteroids. *Astron. J.* 141, 109.
- Neese, C., 2010. Asteroid Taxonomy V6.0, EAR-A-5-DDR-TAXONOMY-V6.0.
- Nesvorný, D., 2010. Nesvorný HCM Asteroid Families V1.0. *NASA Planet. Data Syst.* 133.
- Nesvorný, D., Roig, F., Gladman, B., Lazzaro, D., Carruba, V., Mothé-Diniz, T., 2008. Fugitives from the Vesta family. *Icarus* 193, 85–95. <https://doi.org/10.1016/j.icarus.2007.08.034>
- Newton, E., 2014. The composition and architecture of the asteroid belt: from simple to complicated in just three decades [WWW Document]. *Compos. Archit. Asteroid Belt Simple Complicat. Just Three Decades*. URL <https://astrobites.org/2014/02/01/the-composition-and-architecture-of-the-asteroid-belt-from-simple-to-complicated-in-just-three-decades/>
- Öpik, E.J., 1951. Collision probabilities with the planets and the distribution of interplanetary matter. Presented at the Proceedings of the Royal Irish Academy. Section A: Mathematical and Physical Sciences, JSTOR, pp. 165–199.
- Paolicchi, P., Burns, J.A., Weidenschilling, S.J., 2002. Side effects of collisions: spin rate changes, tumbling rotation states, and binary asteroids. *Asteroids III* 1, 517–526.

- Pater, I. de, Palmer, P., Mitchell, D.L., Ostro, S.J., Yeomans, D.K., Snyder, L.E., 1994. Radar Aperture Synthesis Observations of Asteroids. *Icarus* 111, 489–502. <https://doi.org/10.1006/icar.1994.1159>
- Pravec, P., 2017. Ondrejov Asteroid Photometry Project [WWW Document]. Ondrejov Asteroid Photom. Proj. URL <http://www.asu.cas.cz/~ppravec/>
- Pravec, P., Harris, A.W., 2007. Binary asteroid population. 1. Angular momentum content. *Icarus* 190, 250–259. <https://doi.org/10.1016/j.icarus.2007.02.023>
- Pravec, P., Harris, A.W., 2000. Fast and Slow Rotation of Asteroids. *Icarus* 148, 12–20. <https://doi.org/10.1006/icar.2000.6482>
- Pravec, P., Harris, A.W., Michalowski, T., 2002. Asteroid rotations. *Asteroids III* 113.
- Prettyman, T.H., Mittlefehldt, D.W., Yamashita, N., Lawrence, D.J., Beck, A.W., Feldman, W.C., McCoy, T.J., McSween, H.Y., Toplis, M.J., Titus, T.N., Tricarico, P., Reedy, R.C., Hendricks, J.S., Forni, O., Le Corre, L., Li, J.-Y., Mizzon, H., Reddy, V., Raymond, C.A., Russell, C.T., 2012. Elemental Mapping by Dawn Reveals Exogenic H in Vesta's Regolith. *Science* 338, 242–246. <https://doi.org/10.1126/science.1225354>
- Reddy, V., Nathues, a., Le Corre, L., Sierks, H., Li, J.-Y., Gaskell, R., McCoy, T., Beck, a. W., Schroder, S.E., Pieters, C.M., Becker, K.J., Buratti, B.J., Denevi, B., Blewett, D.T., Christensen, U., Gaffey, M.J., Gutierrez-Marques, P., Hicks, M., Keller, H.U., Maue, T., Mottola, S., McFadden, L. a., McSween, H.Y., Mittlefehldt, D., O'Brien, D.P., Raymond, C., Russell, C., 2012. Color and Albedo Heterogeneity of Vesta from Dawn. *Science* 336, 700–704. <https://doi.org/10.1126/science.1219088>
- Roig, F., Folonier, H., Beaugé, C., Ribeiro, A.O., 2011. Dynamical origin of V-type asteroids outside the Vesta family. *Workshop Ser. Assoc. Argent. Astron.* 3, 307–317.
- Roig, F., Nesvorný, D., Gil-Hutton, R., Lazzaro, D., 2008. V-type asteroids in the middle main belt. *Icarus* 194, 125–136. <https://doi.org/10.1016/j.icarus.2007.10.004>
- Rubincam, D., 2000. Radiative Spin-up and Spin-down of Small Asteroids. *Icarus* 148, 2–11. <https://doi.org/10.1006/icar.2000.6485>
- Russell, C.T., Raymond, C.A., Coradini, A., McSween, H.Y., Zuber, M.T., Nathues, A., Sanctis, M.C.D., Jaumann, R., Konopliv, A.S., Preusker, F., Asmar, S.W., Park, R.S., Gaskell, R., Keller, H.U., Mottola, S., Roatsch, T., Scully, J.E.C., Smith, D.E., Tricarico, P., Toplis, M.J., Christensen, U.R., Feldman, W.C., Lawrence, D.J., McCoy, T.J., Prettyman, T.H., Reedy, R.C., Sykes, M.E., Titus, T.N., 2012. Dawn at Vesta: Testing the Protoplanetary Paradigm. *Science, New Series* 336, 684–686. <https://doi.org/10.2307/41584786>

- Ryan, E.V., Melosh, H.J., 1998. Impact Fragmentation: From the Laboratory to Asteroids. *icarus* 133, 1–24. <https://doi.org/10.1006/icar.1998.5915>
- Ryan, E.V., Ryan, W.H., 2007. Shapes and Multiplicities of Vesta Family Asteroids.
- Ryan, W.H., Ryan, E.V., Martinez, C.T., 2004. 3782 Celle: Discovery of a binary system within the Vesta family of asteroids. *Planet. Space Sci., Catastrophic Disruption of Small Solar System Bodies* 52, 1093–1101. <https://doi.org/10.1016/j.pss.2004.07.006>
- Ryan, W. H., Ryan, E.V., Martinez, C.T., 2004. Unusual Lightcurves in the Vesta Family of Asteroids. Presented at the Bulletin of the American Astronomical Society, p. 46.09.
- Salo, H., 1987. Numerical simulations of collisions between rotating particles. *icarus* 70, 37–51. [https://doi.org/10.1016/0019-1035\(87\)90073-X](https://doi.org/10.1016/0019-1035(87)90073-X)
- Scheeres, D.J., 2007. The dynamical evolution of uniformly rotating asteroids subject to YORP. *Icarus* 188, 430–450. <https://doi.org/10.1016/j.icarus.2006.12.015>
- Slivan, S.M., Binzel, R.P., Crespo da Silva, L.D., Kaasalainen, M., Lyndaker, M.M., Krčo, M., 2003. Spin vectors in the Koronis family: comprehensive results from two independent analyses of 213 rotation lightcurves. *icarus* 162, 285–307. [https://doi.org/10.1016/S0019-1035\(03\)00029-0](https://doi.org/10.1016/S0019-1035(03)00029-0)
- Tedesco, E.F., Desert, F.-X., 2002. The Infrared Space Observatory deep Asteroid Search. *Astron. J.* 123, 2070.
- Tholen, D.J., 1984. Asteroid taxonomy from cluster analysis of photometry. University of Arizona, Tucson.
- Thomas, P.C., Binzel, R.P., 1997. Impact excavation on Asteroid 4 Vesta: Hubble Space Telescope results. (Cover story). *Science* 277, 1492–1495.
- Thomas, P.C., Binzel, R.P., Gaffey, M.J., Zellner, B.H., Storrs, A.D., Wells, E., 1997. Vesta: Spin Pole, Size, and Shape from HST Images. *Icarus* 128, 88–94. <https://doi.org/10.1006/icar.1997.5736>
- Vokrouhlicky, D., Nesvorny, D., Bottke, W.F., 2003. The vector alignments of asteroid spins by thermal torques. *Nature* 425, 147–151. <https://doi.org/10.1038/nature01948>
- Warner, B., 2012. *The MPO User's Guide*, 10th ed. BDW Publishing.
- Warner, B., 2011. *MPO Canopus and PhotoRed Reference Guide*, 10th ed. BDW Publishing.

- Warner, B., 2006. A Practical Guide to Lightcurve Photometry and Analysis, Patrick Moore's Practical Astronomy Series. Springer.
- Warner, B.D., Harris, A.W., Pravec, P., 2009. The asteroid lightcurve database. *icarus* 202, 134–146. <https://doi.org/10.1016/j.icarus.2009.02.003>
- Waszczak, A., Chang, C.-K., Ofek, E.O., Laher, R., Masci, F., Levitan, D., Surace, J., Cheng, Y.-C., Ip, W.-H., Kinoshita, D., Helou, G., Prince, T.A., Kulkarni, S., 2015. Asteroid Light Curves from the Palomar Transient Factory Survey: Rotation Periods and Phase Functions from Sparse Photometry. *\aj* 150, 75. <https://doi.org/10.1088/0004-6256/150/3/75>
- Xu, S., Binzel, R.P., Burbine, T.H., Bus, S.J., 1995. Small main-belt asteroid spectroscopic survey: Initial results. *Icarus* 115, 1–35.
- Yeomans, D.K., 2015. JPL Small-Body Database Search Engine [WWW Document]. JPL Small-Body Database Search Engine.
- Yeomans, D.K., 2013. Near-Earth objects: finding them before they find us. Princeton University Press.
- Zappalà, V., Bendjoya, P., Cellino, A., Farinella, P., Froeschlé, C., 1995. Asteroid Families: Search of a 12,487-Asteroid Sample Using Two Different Clustering Techniques. *Icarus* 116, 291–314. <https://doi.org/10.1006/icar.1995.1127>
- Zellner, B., Tholen, D., Tedesco, E., 1985. The eight-color asteroid survey: Results for 589 minor planets. *Icarus* 61, 355–416.